$\mathcal{L}$|

INVERSE SEGREGATION IN Al-Cu ALLOYS

BY

BALASUBRAMANIAM PRABHAKAR

B.Sc., Osmania University, India, 1967

B.E. (Metallurgy), Indian Institute of Science, India, 1970

A THESIS SUBMITTED IN PARTIAL FULFILMENT OF THE

REQUIREMENTS FOR THE DEGREE OF

MASTER OF APPLIED SCIENCE

in the Department

of

METALLURGY

We accept this thesis as conforming to the

required standard

THE UNIVERSITY OF BRITISH COLUMBIA

April, 1973

In presenting this thesis in partial fulfilment of the requirements for an advanced degree at the University of British Columbia, I agree that the Library shall make it freely available for reference and study. I further agree that permission for extensive copying of this thesis for scholarly purposes may be granted by the Head of my Department or by his representatives. It is understood that copying or publication of this thesis for financial gain shall not be allowed without my written permission.

Department of ___Metallurgy___

The University of British Columbia
Vancouver 8, Canada

Date ___12th June 1973___

ABSTRACT

Inverse segregation has been studied in unidirectionally cast ingots as a function of alloy composition and casting conditions. Chill face segregation and the extent of segregation adjacent to the chill face has been examined in the Al-Cu and the Al-Ag systems, using radioactive copper (Cu^{64}) and radioactive silver (Ag^{110}) to measure the segregation. The results indicate that the observed segregation is markedly dependent on the alloy composition, melt superheat, thermal conductivity of the chill, temperature gradient in the casting, and other casting variables.

The results obtained are compared to those reported in the literature for the Al-Cu alloys, and to the values predicted theoretically.

TABLE OF CONTENTS

LIST OF FIGURES

LIST OF TABLES

ACKNOWLEDGEMENT

1. INTRODUCTION

Cast materials are used extensively, in a wide variety of appli-
cations. With the increasing sophistication of modern technology,
greater demands are being made on the quality and reliability of cast
products. In addition, competitive manufacturing processes and new
materials have resulted in efforts being made to increase the effic-
iency of the casting process. Accordingly, the production, structure
and properties of castings, in both ferrous and non-ferrous materials,
warrants continuing investigation.

The fundamental nature of the solidification of alloys, in which
solid of one composition forms from liquid of another composition,
makes it impossible to cast homogeneous materials with uniform struc-
ture and properties.

Inhomogeneities can occur both on a macroscopic and microscopic
scale in the solidified metal. On a macroscopic scale, macrosegrega-
tion can occur in three different forms, which may or may not occur
together. The three forms commonly observed can be classified as
follows:

1. Normal segregation: Solute is segregated in a manner pre-
dicted by the phase diagram, in which the alloy composition
increases with increasing distance from the chill face, for a
system in which the segregation coefficient is less than unity.

2. Gravity segregation: Solute segregates as a result of den-
sity differences in the constituents of the casting during

solidification. This process is most pronounced in slowly solidified large castings.

3. Inverse segregation: In this case, solute content decreases with increasing distance from the chill face, for a system with a segregation coefficient less than unity. It is most pronounced in a small region near the chill face.

The present investigation is primarily concerned with the last category, namely inverse segregation.

1.1 Inverse segregation: Reported experimental results and theories

Inverse segregation has been studied extensively, both theoretically and experimentally for many years, and many theories have been proposed to account for the apparently anomalous segregation behaviour. It is also of considerable interest commercially, particularly in nonferrous materials, since inverse segregation can be seriously detrimental to the surface quality of the cast product. Pell-Walpole[1] has reviewed in considerable detail the experimental evidence and theories presented prior to 1949, primarily in cast bronzes and other nonferrous alloys. A short summary of the theories will be presented below. More recently, Vosskuhler[2] has collected the results of further work, and has given a critical review of these results and the newer theories. He has also added experimental evidence which he obtained on a number of alloy systems with different types of equilibrium phase diagrams.

Since the review of Vosskuhler, more experimental results have been reported. In addition, theoretical models for macro-segregation, of which inverse segregation is a part, have been extended and refined, primarily by Flemings and his co-workers.[3,4,5]

1.1.1 Summary of the different theories of inverse segregation

These theories have been discussed in detail elsewhere[1,2,6]; as a result, only brief summaries will be presented here. The theories fall broadly into two groups. In the first group, it is assumed that there is a solute enrichment of the liquid next to the mold surface before solidification occurs, and that the composition stays enriched during the solidification process. In the second group, it is assumed that solidification proceeds as predicted by the equilibrium diagram. Inverse segregation results from inter-dendritic fluid flow during solidification. The second, and more recent group, is now considered to correctly describe the major processes occurring during inverse segregation.

The theories are briefly summarized as follows:

(a) The theory of mobile equilibrium: Le Chatelier's principle is assumed to be operative during solidification. The hypothesis is then put forward that, in order to retard solidification, the component of the alloy which would tend to lower the melting point segregates toward the mold surface.

(b) Benedicks' theory: The Ludwig-Soret effect, which involves the appearance of a concentration gradient under a temperature grad-ient, is the mechanism leading to inverse segregation at the chill

face.

(c) Undercooling of the alloy: The liquid undercools next to the mold face and therefore deposits solid richer in the solute element in this region.

(d) Theory of crystal migration: Depending on the density differences, there is a migration of primary crystals away from a suddenly chilled mold wall.

(e) Gas evolution theory: This theory was developed to explain the segregation in cast bronzes. The gas present in the cooling alloy becomes concentrated in the last region to solidify, and the evolution of the gas on cooling tends to force the enriched liquid into the interdendritic regions towards the outside of the casting, i.e., towards the mold face.

(f) Crystallization pressure theory: Crystallization pressure, or the pressure exerted on the liquid by the growing dendrites, is the driving force for transport of the enriched residual liquid towards the mold surface of the casting.

(g) Shell contraction pressure theory: A crystalline shell is formed surrounding the molten metal. On cooling, this shell contracts, and the resultant pressure set up in the liquid causes the shell to rupture and the liquid to flow to the outside.

(h) Interdendritic flow theory: This theory was first proposed in 1921, and, in a modified form, is now the accepted one. The solidification shrinkage of the primary dendrites is followed by interdendritic backflow of the enriched residual liquid. The

segregation depends on the growth rate and the direction of the primary dendrites, solute diffusion in the solid and the liquid, and the temperature dependence of the specific volume of the solid and liquid.

1.1.2 Quantitative predictions of inverse segregation

Scheil[7] was the first to derive an analytical expression to define the amount of segregation that could occur at the chill face of a binary alloy during unidirectional solidification, as a function of the composition of the alloy. The predictions made by the theory involve the knowledge of the specific volumes of the solid and the liquid, as a function of temperature near the melting point, and the equilibrium phase diagram of the constituents of the binary alloy.

The equations given by Scheil have been modified, and the theory has been extended by Kirkaldy and Youdelis[6,8] to predict the composition distribution along the longitudinal direction (the direction of heat removal) of the ingot away from the chill face.

1.1.2.1 Theoretical model for chill face segregation

The theoretical model for inverse segregation[9] makes the following assumptions:

(a) Surface exudations are absent on the chill face.

(b) There is negligible undercooling at the solid-liquid interface, i.e., at the interface, equilibrium conditions exist.

(c) There is no restriction on the backflow of liquid through the interdendritic regions.

(d) Gas levels in the ingot are low and no porosity exists.

(e) No significant solute diffusion occurs in the solid state, i.e., complete coring is assumed to be present in the solidified metal.

(f) There is no diffusion or liquid mixing in the liquid in a direction parallel to the growth direction. The concentration gradients in the liquid along this direction are assumed small. There is complete mixing in the liquid perpendicular to the growth direction.

(g) The distribution of the liquid and solid mass throughout the solid-liquid region can be estimated from temperature measurements during solidification and the equilibrium phase diagram.

The analysis uses a "control volume", a representative section of the system, and evaluates the mass and concentration balances for material entering and leaving this volume. With assumed or measured boundary conditions, the whole system is then defined, and the processes taking place during solidification are characterized. The control volume selected is shown in Figure 1(a), position A, adjacent to the chill. This volume is part of the solid-liquid region, drawn schematically in the Figure. The solute concentration in the liquid (x-x) as a function of the distance from the chill is shown in Figure 1(b).
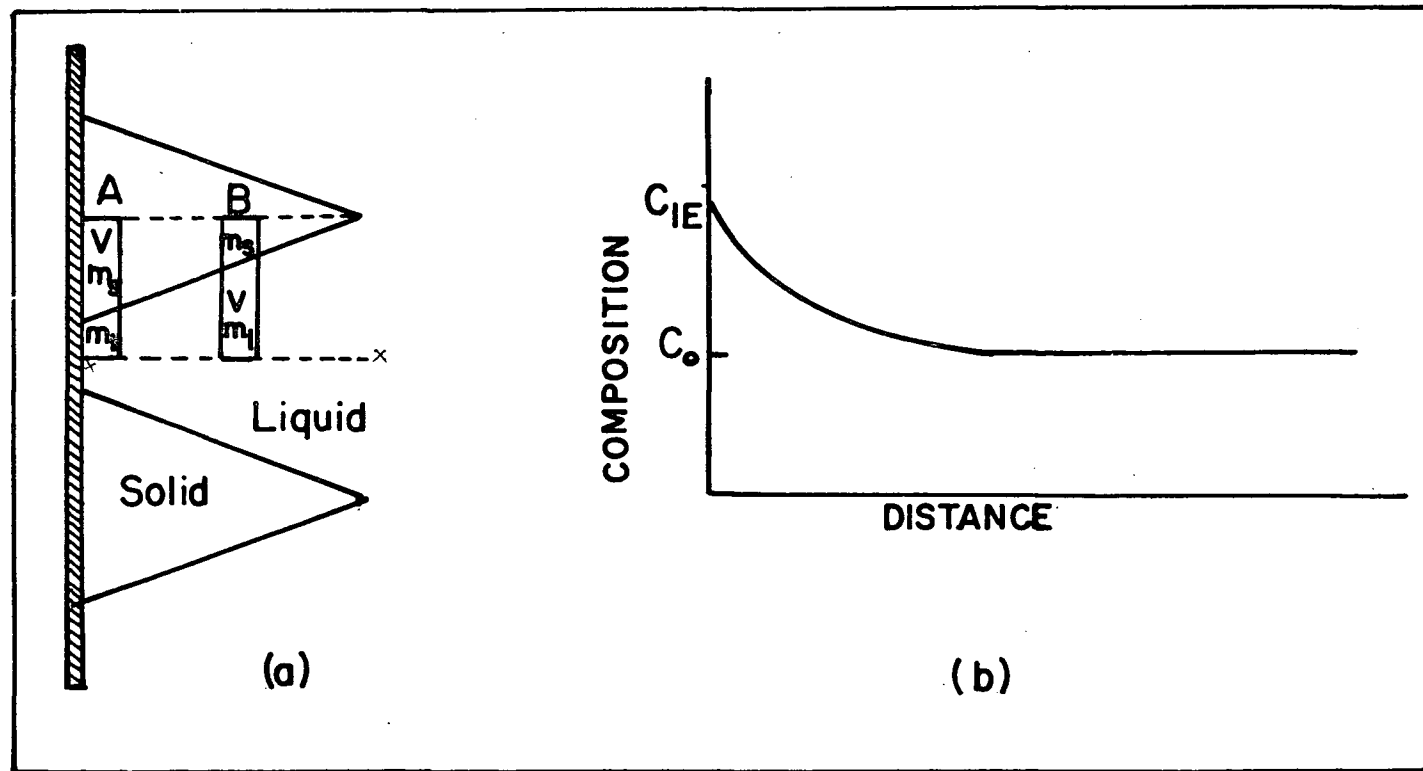
Fig. 1(a)   Schematic representation of the solid-liquid region near the chill face.

   (b)   Schematic liquid concentration distribution in this region.

Denoting solid by the subscript s and liquid by the subscript ℓ, the mean composition $\overline{C}$ of the volume element after solidification is given by

$$\overline{C} = \left[\frac{\dfrac{m_\ell\, C_\ell}{a} + m_s\, C_s}{\dfrac{m_\ell}{a} + m_s}\right] \qquad (1)$$

where $a = \left(\dfrac{v_s}{v_\ell}\right)$ $\qquad (2)$

v_s represents the specific volume of the solid, and v_ℓ the specific volume of the liquid, and m_ℓ, m_s represent the masses of the liquid and solid, respectively.

The segregation ΔC is given by

$$\Delta C = \overline{C} - Co \qquad (3)$$

where Co is the mean composition of the ingot.

For the binary eutectic alloy system, the solute concentration C is given by

$$\overline{C} = \left[\frac{\dfrac{m_{\ell E}\, C_{\ell E}}{a} + m_{sE}\, C_{sE}}{\dfrac{m_{\ell E}}{a} + m_{sE}}\right] \qquad (4)$$

where $m_{\ell E}$ and m_{sE} are the liquid and solid masses respectively in the representative volume at the eutectic temperature, $c_{\ell E}$ is the mean solute content in the liquid at the eutectic, and C_{sE} the mean solute

content in the cored crystals.

For the volume element at the chill face, there is flow only into the element, and the volume V of the element is given by

$$V = \nu_s \, m_s + \nu_\ell \, m_\ell \tag{5}$$

On solidification and on cooling, there is shrinkage in the volume element, and if this is completely filled by backflow of liquid, then

$$dV = 0 = \nu_\ell dm_\ell + \nu_s dm_s + m_\ell d\nu_\ell + m_s d\nu_s \tag{6}$$

If ν_s is considered to be constant, this gives

$$dm_\ell = -dm_s \left[\frac{\nu_s}{\nu_\ell} + \frac{m_\ell}{\nu_\ell} \frac{d\nu_\ell}{dm_s} \right] \tag{7}$$

or $\qquad dm_\ell = -b dm_s \tag{8}$

where $\qquad b = \left[\frac{\nu_s}{\nu_\ell} + \frac{m_\ell}{\nu_\ell} \frac{d\nu_\ell}{dm_s} \right] \tag{9}$

Considering mass balances in the volume element after some solidification, and assuming complete coring,

$$d(m_\ell C_\ell) = -C_s dm_s + \left[C_\ell dm_s \frac{(\nu_s - \nu_\ell)}{\nu_\ell} - C_\ell m_\ell \left(\frac{d\nu_\ell}{\nu_\ell} \right) \right] \tag{10}$$

where the right hand side of the equation is composed of terms considering the solute mass in the solidified region, the solute mass gained due to volume shrinkage in the elements, and the solute mass gained due to concentration change of the liquid. The solute mass added due to temperature change is considered to be negligible.

$$\frac{dv_\ell}{v_\ell} = -\left(\frac{dm_\ell}{m_\ell}\right) - \left(\frac{v_s}{v_\ell}\right) \tag{11}$$

from equation (9), and equation (10) reduces to

$$\frac{dm_\ell}{m_\ell} = \frac{bdC_\ell}{C_s - C_\ell} = -\frac{b}{A}\frac{dC_\ell}{C_\ell} \tag{12}$$

using,

$$\frac{C_\ell - C_s}{C_\ell} = 1-K = A \tag{13}$$

since both A and b vary with composition, stepwise integration becomes necessary, between the i and i+1th step.

$$\int_{m_{s_i}}^{m_{s_{i+1}}} dm_s = -\frac{1}{b} \int_{m_{\ell_i}}^{m_{\ell_{i+1}}} dm_\ell \tag{14}$$

gives $\quad m_{s_{i+1}} = m_{s_i} + \frac{1}{b_i}(m_{\ell_i} - m_{\ell_{i+1}}) \tag{15}$

and
$$\int_{i}^{i+1} \frac{dm_\ell}{m_\ell} = -\frac{b_i}{A_i} \int_{i}^{i+1} \frac{dC_\ell}{C_\ell} \tag{16}$$

given
$$m_{\ell_{i+1}} = m_{\ell_i} \left(\frac{C_{\ell_{i+1}}}{C_{\ell_i}}\right)^{\frac{-b_i}{A_i}} \tag{17}$$

The solute mass in the cored primary crystals is given by

$$d\,(m_s\,C_s) = C_s\,dm_s \tag{18}$$

The right hand side of the equation reduces to

$$C_s\,dm_s = \left(\frac{m_\ell}{A}\,dC_\ell - m_\ell\,dC_\ell\right)$$

and

$$\int_{i}^{i+1} d(m_s C_s) = \frac{1-A_i}{A_i} \int_{i}^{i+1} \left[m_{\ell_i}\left\{\frac{C_{\ell_{i+1}}}{C_{\ell_i}}\right\}^{\frac{-b_i}{A_i}} \right] dC_\ell \tag{19}$$

gives

$$m_{s_{i+1}}C_{s_{i+1}} = m_{s_i}C_{s_i} + \left\{\frac{1-A_i}{A_i-b_i}\right\} m_{\ell_i}C_{\ell_i}\left[\left(\frac{C_{\ell_{i+1}}}{C_{\ell_i}}\right)^{\frac{A_i-b_i}{A_i}} - 1\right] \tag{20}$$

Stepwise integration is carried out until $m_{sE}C_{sE}$ and $m_{\ell E}$ are reached. The values obtained are substituted into equation (4) and (3) to give the maximum chill face segregation.

1.1.2.2 Comparison with experimental results

For the Al-Cu system, the temperature dependence of the specific volumes of solid and liquid, and the equilibrium phase diagram are given in Figure 2. The specific volume data was obtained by Sauerwald[10]. Using this data, Scheil calculated values of the maximum segregation at the chill face for unidirectionally solidified alloys with compositions varying between 0 and 33% Cu, obtaining the solid line shown in Figure 3. The experimental results of the chill face segregation as determined by Scheil, Adams[11] and Kirkaldy and Youdelis[8] are also presented in the Figure.

Comparing the experimental values with the theoretical curve, it is apparent that there is excellent agreement between the experimental results and the theoretical curve for all three investigations over the entire composition range examined and for both slow and fast cool in the results of Kirkaldy and Youdelis.

Similar measurements and calculations of inverse segregation for the Bi-Sb, Al-Zn and Al-Si alloy systems were made. The specific volume and phase diagram data for the Bi-Sb system is given in Figure 4 and the corresponding theoretical curve and
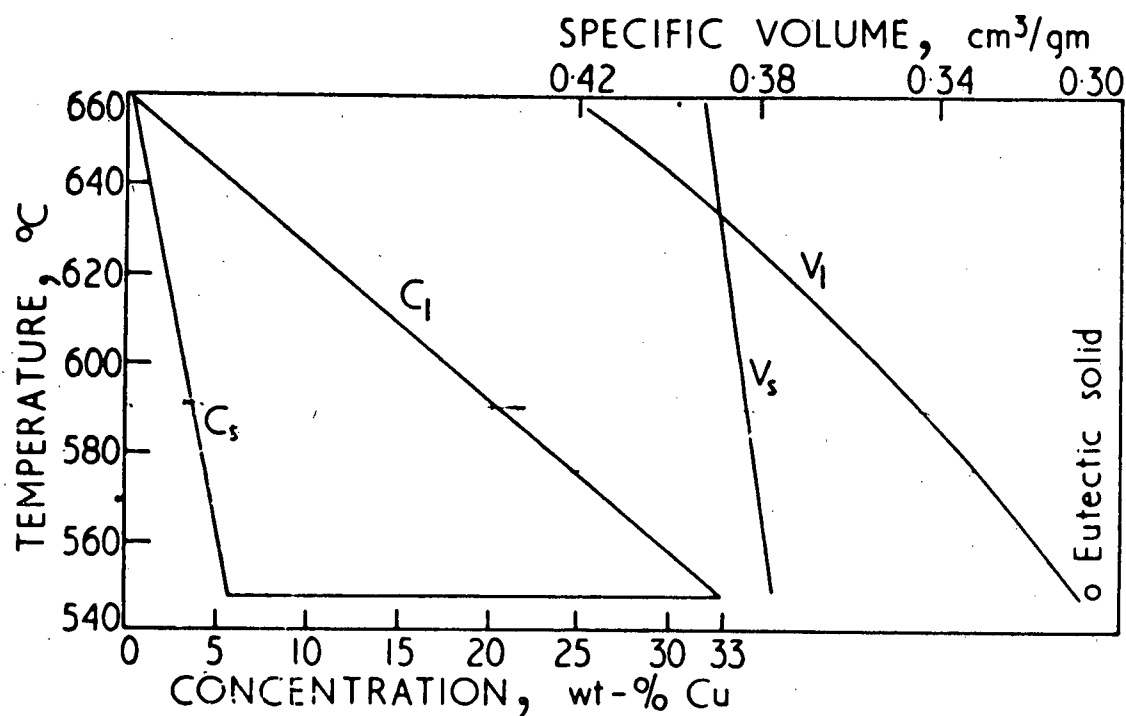
Fig. 2   Constitution diagram, and variation of the specific volumes of solid and liquid for Al-Cu alloys.
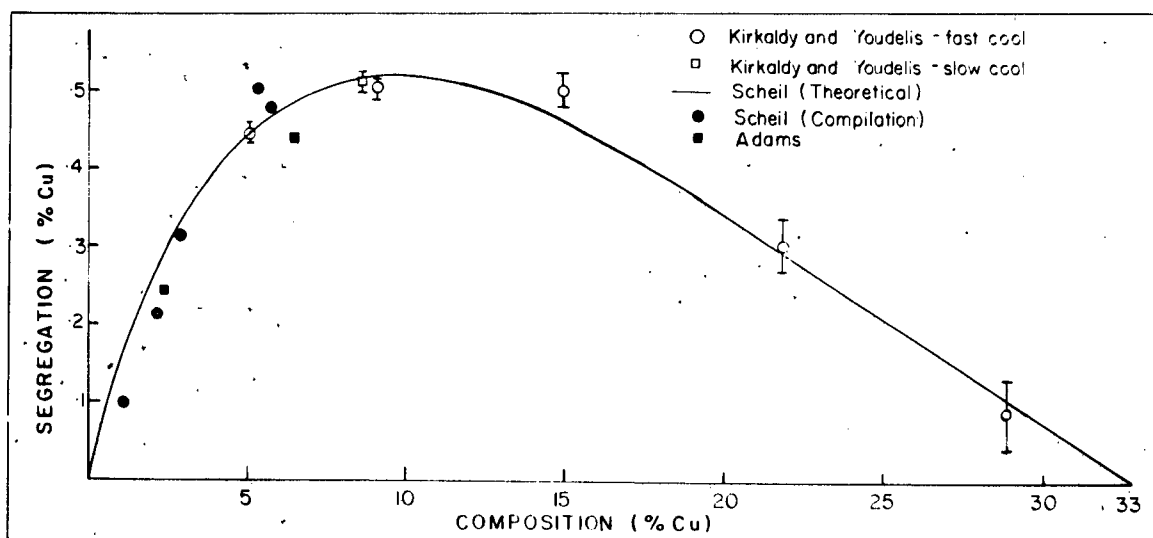
Fig. 3   Theoretical predictions and experimental results for maximum chill face segregation vs. alloy composition for the Al-Cu system[8].
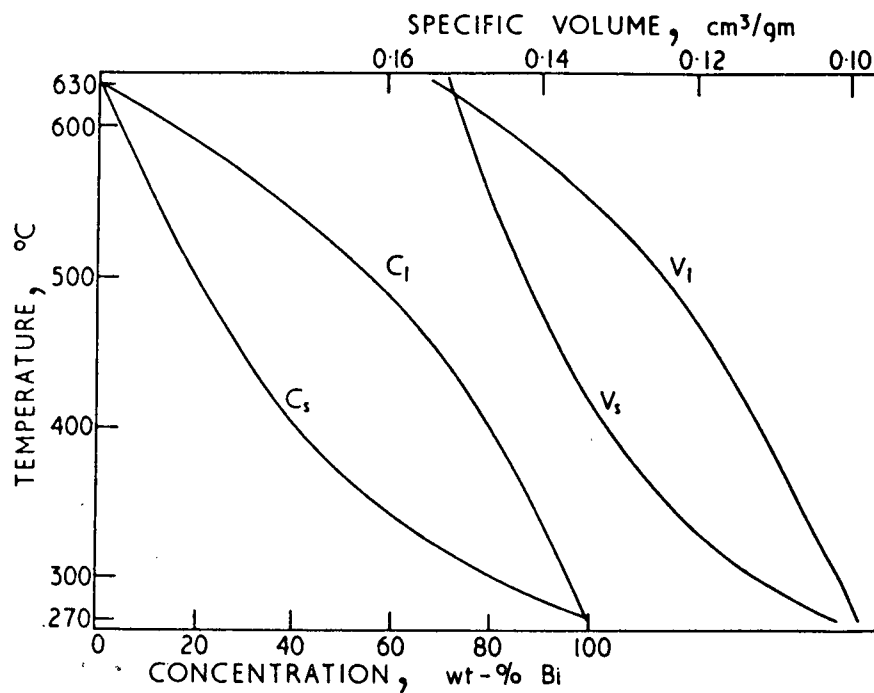
Fig. 4   Constitutional - specific volume diagram for the Bi-Sb system.
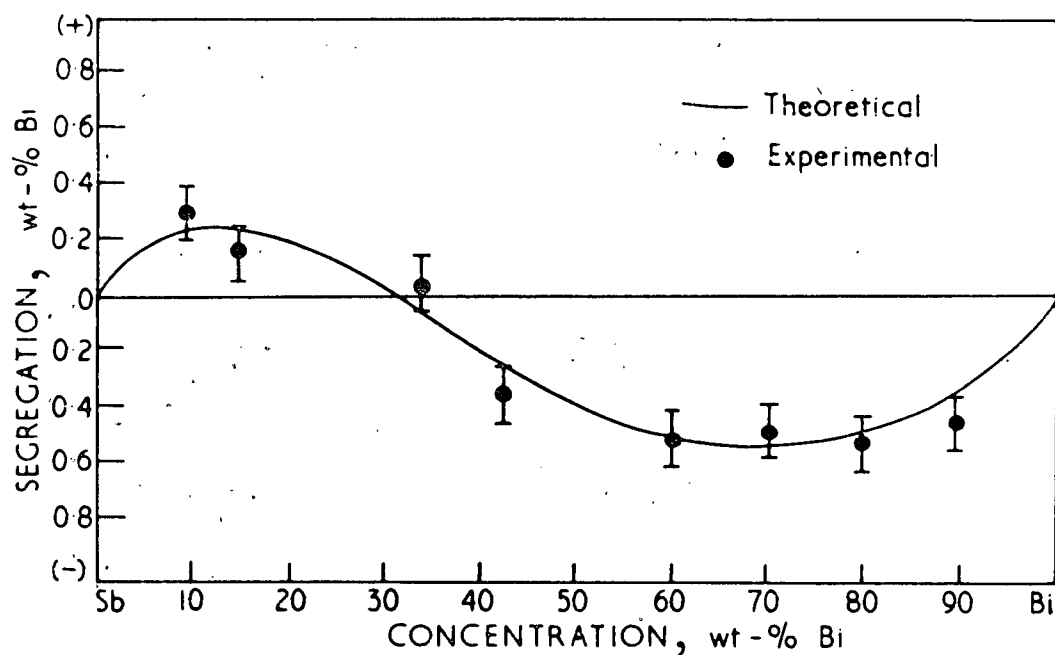
Fig. 5   Theoretical curve and experimental results for the maximum chill
face segregation vs. alloy composition for Bi-Sb alloys[9].

experimental points for the chill face segregation as reported by Youdelis[9] are given in Figure 5. This system is of particular interest since pure Bismuth expands on freezing. No volume shrinkage occurs and therefore no inverse segregation should occur for alloys high in Bismuth concentration. As shown in Figure 5, this is what is observed. Again, the fit between theory and experiment is excellent.

The specific volumes of the solid and liquid and the equilibrium phase diagrams for the Al-Zn system are shown in Figure 6, and the corresponding theoretical curve for chill face segregation, with experimental results[12] is shown in Figure 7. The experimental scatter (error bars) reported is much larger in this system, but using average values, there is still excellent agreement between theory and experiment.

The results for the Al-Si system have been reported recently by Ball and Youdelis[13] using the data of Figure 8. In this case, Figure 9, there is a large discrepancy between theory and experiment, the measured concentrations at the chill face being far below the calculated values.

1.1.2.3 Extensions of the theories to predict composition
        variations within the ingot, away from the chill face

Kirkaldy and Youdelis have extended the Scheil analysis to calculate the variation in the solute concentration with distance
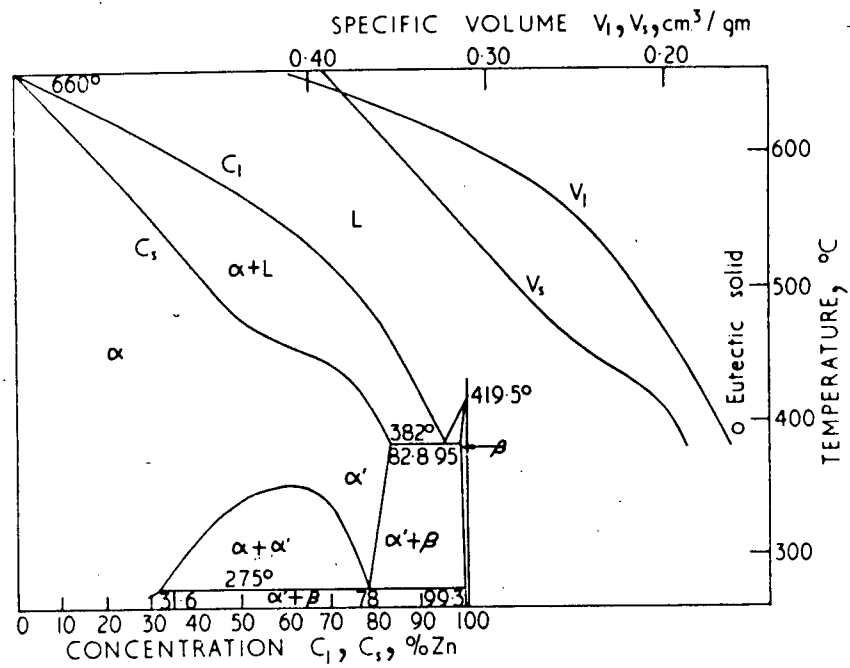
Fig. 6   Constitutional - specific volume diagram for the Al-Zn system.
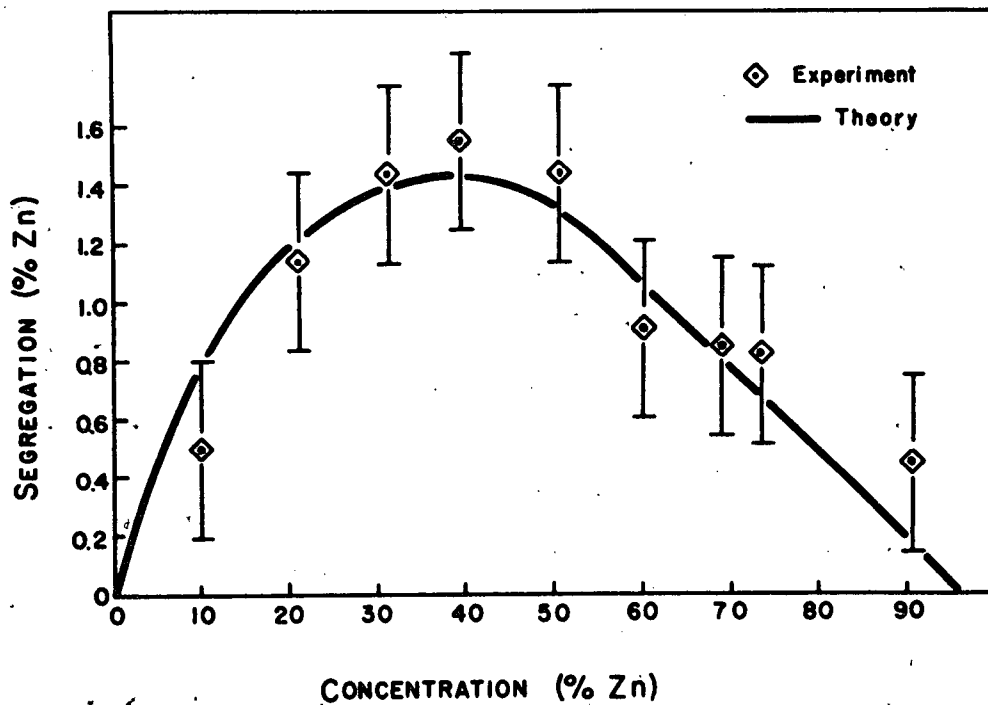
Fig. 7   Theoretical curve and experimental results for the chill face
segregation vs. alloy composition for Al-Zn alloys[12].
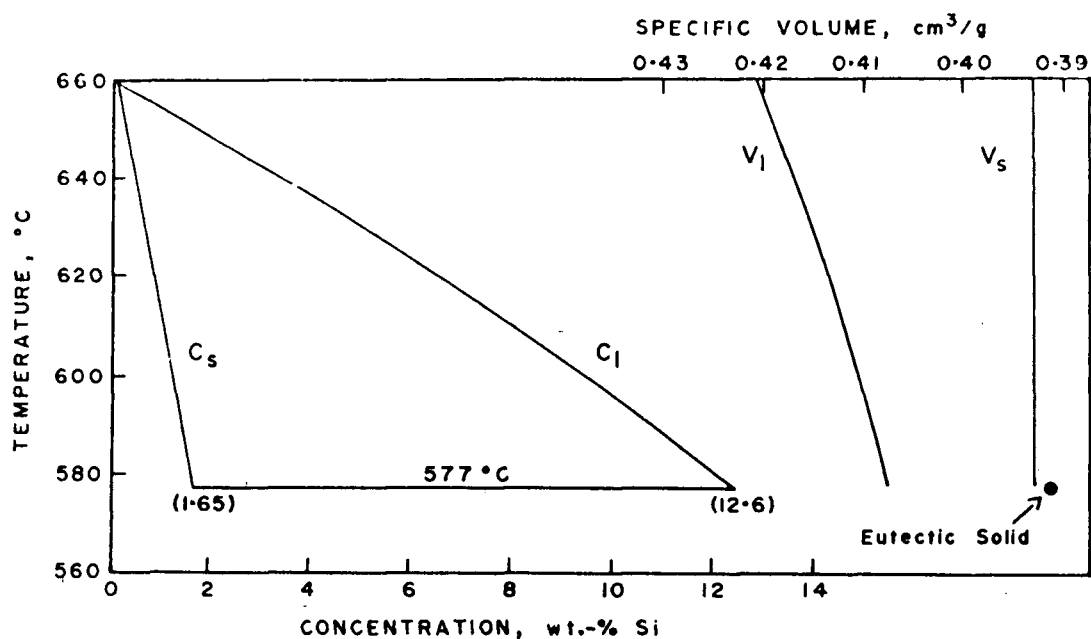
Fig. 8   Constitutional - specific volume relationships for the Al-Si system.
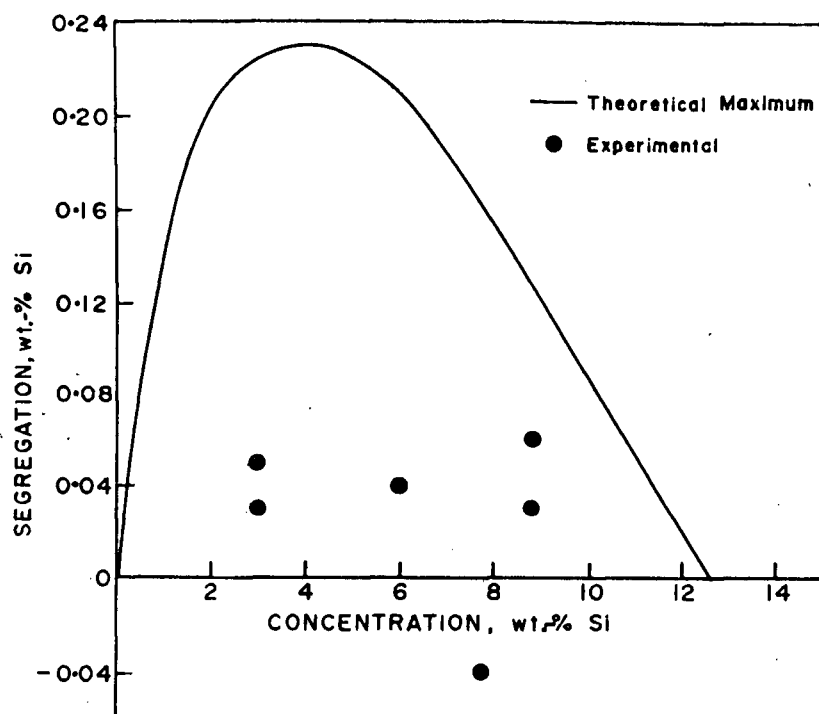
Fig. 9   Theoretical curve and experimental results for the chill face
segregation vs. alloy composition for Al-Si alloys[13].

from the chill face[6,8,9]. In this case, the control volume element is shifted away from the chill face to position B as shown in Figure 1. Solute transfer now occurs both into and out of the volume element, in order to feed the contraction to the left of the volume element.

The amount of the liquid (mass distribution of liquid) in the solid-liquid region is assumed to increase linearly with distance in the freezing direction from the completely solid interface. The length of the solid-liquid region is assumed to start from zero at the chill face, increases to a steady state value, and then decreases as solidification reaches the final part of the casting to freeze. The change in the length of the solid-liquid zone is shown schematically in Figure 10(a), and the corresponding slope of the liquid mass distributions in the casting at various stages of solidification is shown in Figure 10(b).

The theoretical predictions of the solute segregation in an Al-10% Cu alloy, using the data in Figure 2, is shown as the solid line in Figure 11. The corresponding experimental values are plotted and it is apparent that there is excellent fit between the experimental values and the theoretical curve over the entire casting. One point at about 0.2" is a little low; the remaining points coincide with or are very close to the theoretical curve. The corresponding curve and the experimental points for an Al-15% Cu alloy is shown in Figure 12, again showing excellent agreement
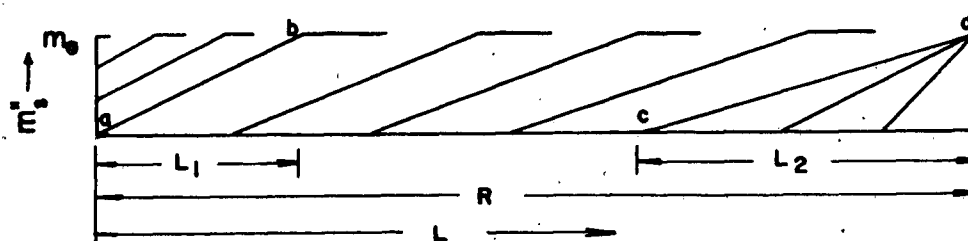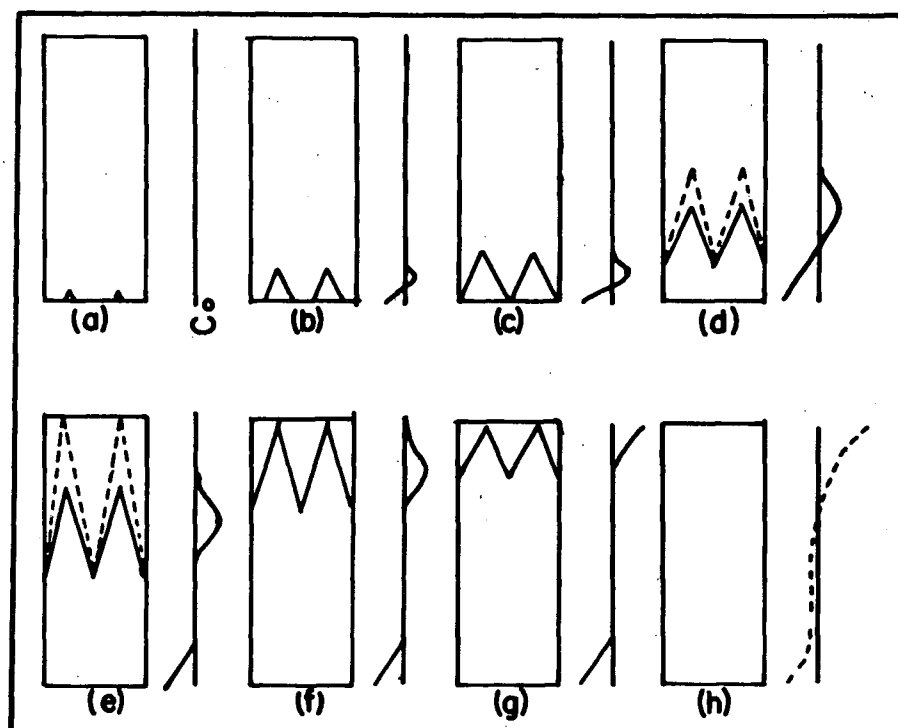
Fig. 10(a) Representation of crystal growth and accompanying concentration changes in an unidirectionally solidified ingot. (Dotted lines indicate constantly increasing length of the solid-liquid region till the ingot top is reached).

(b) Liquid mass distribution curves in the model ingot for representative times during solidification[6].
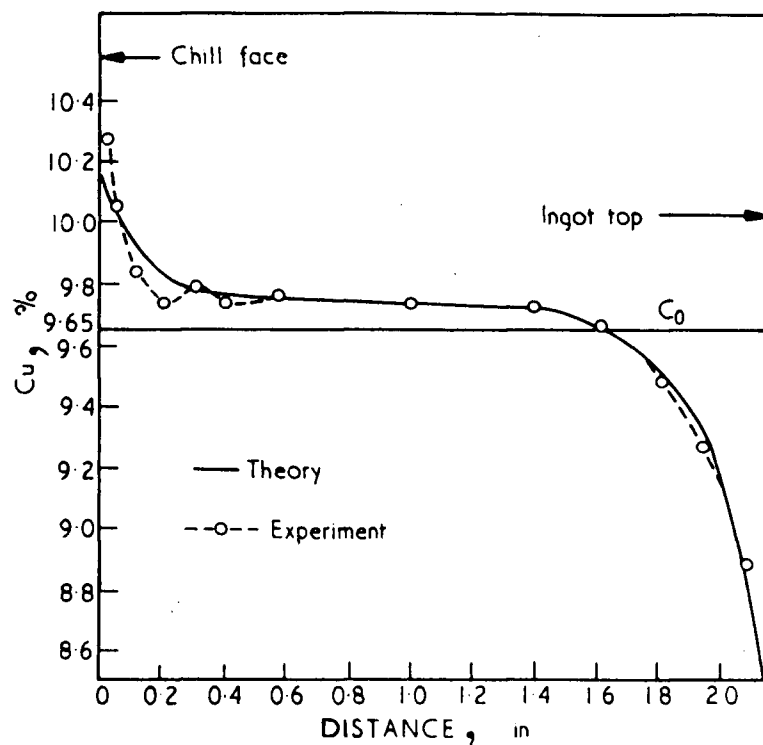
Fig. 11   Theoretical and experimental segregation curves for an Al-10% Cu ingot.
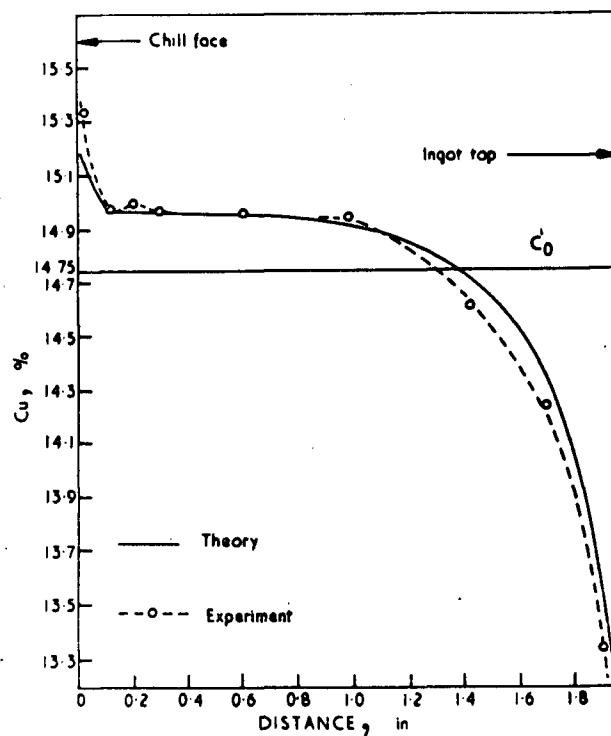
Fig. 12   Theoretical and experimental segregation curves for an Al-15% Cu ingot.[9]

between theory and experiment.

This excellent agreement in all of the results reported between theory and experiment (with the exception of the Al-Si system) is, on closer examination, somewhat surprising. The extensive results of inverse segregation measurements summar--zed by Pell-Walpole[1] where no attempt was made to compare experiments with theory, shows a very wide scatter of results. The theory of inverse segregation does not take into account the cast structure, the thermal conditions during solidification, exudations on the surface, dissolved gas and porosity, superheat, nucleation, or other variables in the casting process. In addition, the accuracy of the measured average concentrations seem remarkably good considering that all the castings have micro-segregation, and sampling to give highly reproducible results is difficult. In Figure 12, the difference between the average composition of the casting and the composition remote from the chill face is 0.2%, in an alloy of 14.75% Cu composition. This difference involves establishing the average composition of the casting, which is difficult, as well as locally measuring the composition accurately.

The values of the solute composition at the chill face are based on one point near the face, which is suspect due to the presence of the exudations on the chill face, or on extrapolation of two or three points showing scatter.

Some of the assumptions of the model, in particular, that there is complete mixing in the liquid perpendicular to the freezing direction, and no mixing parallel to the freezing direction, seems to be only a first approximation.

Flemings et al.[3,4,5] have adopted the volume element analysis to calculate the macrosegregation in an entire casting, with or without chill faces being present, and with solidification proceeding in three dimensions. The assumptions made are essentially the same as those used by Scheil. The general solutions as derived by Flemings et al., are stated to reduce to those derived by Scheil for inverse segregation at the chill face, using suitable boundary conditions related to casting directionally against a chill face.

The important contribution of the general treatment of Flemings et al. is the generality of their solutions which consider normal segregation, density effects, and inverse segregation concurrently. They give numerical examples of their analysis for the Al-4.5% Cu alloy and compare their calculations with their experimental measurements for unidirectionally solidified castings[5,23], in general, obtaining excellent agreement.

The maximum segregation at the chill face was calculated from the general solutions, as a part of this investigation, to test the applicability of the general theory to inverse segregation in Al-Cu alloys. The calculated segregation obtained is
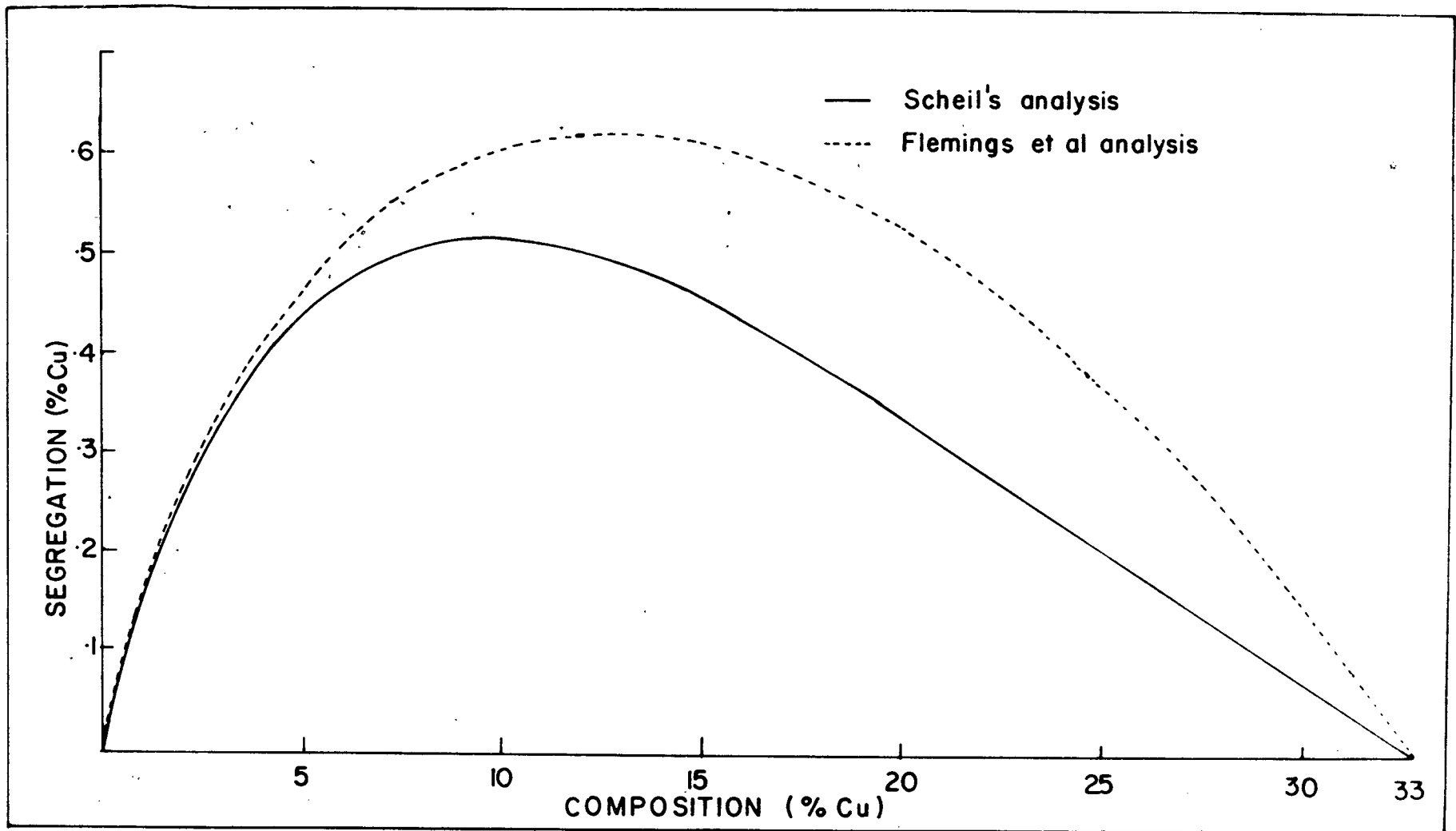
Fig. 13   Comparison of the theoretical predictions of the maximum chill face segregation in Al-Cu alloys.

shown in Figure 13 and compared to the values obtained from the
Scheil analysis. It is seen that the two calculations give
markedly different results, the Flemings analysis giving much
larger values than the Scheil analysis. The basic reason for
this difference is that simplifying assumptions are introduced
in the Flemings analysis in order to reduce the complex math-
ematical expressions to simpler analytical solutions in order
for the calculations to be made. Specifically, a constant
partition ratio ($k = 0.172$) is used as well as constant values
of the solid and liquid densities, yielding a constant value for
the solidification shrinkage ($\beta = 0.055$). The assumption of
constant liquid density is not justified in the Al-Cu system
since it is this variation that is the major factor leading to
the observed inverse segregation. It can be observed from the
Figure that the two theories predict maximum chill face segrega-
tion at different compositions, i.e., the maxima of the two curves
correspond to different compositions.

1.2 Exudations

Exudations on the surface of the ingot are not considered
part of the theoretical model of inverse segregation. However,
the presence of exudations is generally observed on the chill
face and is very important in the casting industry. This is
because exudations are normally eutectic material, and are often
hard, brittle, and abrasive. As a result, the surface layer of

ingots with exudations often has to be removed before further fabrication can be carried out. The formation of exudations is normally due to the partially solidified ingot drawing away from the mold wall due to solidification shrinkage, which causes a decrease in the rate of heat removal from the surface of the ingot. As a result, the solid shell of the ingot may reheat, due to the superheat normally present in the liquid portions of the casting. This in turn causes the flow of en-riched residual liquid through the partially remelted shell to the surface of the casting through interdendritic pipes. In addition to the formations of exudations on the surface, there may be a depletion of solute in the regions next to the chill face. Studies of this phenomenon have been carried out and models proposed for the quantitative prediction of this effect[14].

1.3 Aim of the present work

This investigation was undertaken to experimentally investi-gate the amount and extent of inverse segregation at the chill face and in the chill zone. By using radioactive tracer tech-niques, it was hoped to obtain a sufficient number of points in the region of the chill face to be able to extrapolate the values with confidence and compare measured chill face values with extrapolated values.

The effect of all the major casting variables would be con-sidered experimentally to determine their effect on inverse segregation. This would include the cast structure, the rate of

heat removal from the chill face, the superheat, the temperature gradient in the freezing direction in the liquid during solidification, the gas content of the liquid metal, as well as the alloy composition. Both chill face and the chill zone segregation would be examined.

Initial experiments were carried out on the Al-Ag system using Ag^{110} as the tracer. No significant inverse segregation was detected, contrary to what had been anticipated. However, a quantitative estimate of the chill face segregation could not be predicted from theory for this system since values of the specific volumes of the solid and the liquid as a function of composition and temperature could not be obtained from the literature. Accordingly, it was decided to revert to the Al-Cu system on which the bulk of the previous observations reported in literature had been made. Specific volume data is available for this system; this system is one of the best systems for the examination of inverse segregation; and preliminary measurements demonstrated that Cu^{64} could be successfully by used as tracer material, even though it has a short half life (12.8 hours).

The short half life of the copper permitted normal chemical analysis to be carried out on the same samples that were used to determine the activity variations along the ingot length. This was done by allowing the radiation in the samples to decay to a negligible level prior to analysis.

2.   EXPERIMENTAL PROCEDURE

2.1 Materials

Aluminium: Superpure Aluminium (99.995%) obtained from Alcan was used in the preparation of all the ingots.

Copper: Copper used in the preparation of the Aluminium-Copper ingots was of 99.999% purity and was obtained from the American Smelting and Refining Co., New Jersey.

Silver: High purity silver, obtained from Cominco Ltd., was used in the Aluminium-Silver ingots.

Radioactive Copper: Cu^{64} (half life 12.8 hours, $\beta+\gamma$). Specimens were irradiated in the form of sheet, 0.025 cm. thick, weighing 0.5 grams each. Irradiation was carried out by the International Nuclear and Chemical Corporation, Buffalo, New York.

Radioactive Silver: Ag^{110} (half life 253 days, $\beta+\gamma$). Silver wire of 0.1 cm. diameter was irradiated by International Nuclear and Chemical Corporation, Buffalo. Specimens were cut from the wire when required.

2.2 Alloy preparation

The alloys were melted in a graphite crucible (under an argon atmosphere), by induction, using an Inductotherm power supply. Weighed amounts of the pure constituents were added to the crucible to give an alloy of the desired composition. Melting occurred in about five minutes, using a power input of 10 Kw. After melting, the cover of the crucible was removed and the melt was vigorously stirred using a

graphite plunger with a perforated graphite disc at its end, the diameter of the disc being slightly smaller than the inside diameter of the crucible. Prior to casting, the melt temperature was measured with a bare chromel-alumel thermocouple and recorded on a Honeywell chart recorder. The pouring temperature was determined by extrapolating the falling temperature of the melt, just prior to pouring, to the start of pouring. Specific superheats at pouring were obtained by adjusting the time of pouring to the melt temperature and the cooling rate prior to pouring.

In general, the melt size was three hundred grams. For the Al-Cu alloys, approximately 0.5 grams of Cu^{64} having an activity of about 8 mC at the time of the test was added to each melt, giving a concentration of radioactive copper of about 1600 ppm. After the addition, the liquid was vigorously stirred, a sample was removed for the measurement of the melt composition, and the alloy cast as soon as the desired pouring temperature was attained.

A number of procedures were tried to obtain suitable samples for the measurement of the melt composition. In initial tests, liquid was drawn up into 0.32 cm I.D. Vycor tubing. This method was found to be unsatisfactory, since reproducible results were not obtained, as described in section 3.3. Subsequently, the method adopted was to scoop some of the well mixed melt into a graphite cup and pour the liquid into a copper chill mold, giving cylindrical samples 2 cm. in diameter and 2.5 cm. long. These samples proved to be satisfactory for subsequent sectioning and counting, and gave reproducible values for the melt composition.

2.3 Casting

Two different casting procedures were used. In one case, (a), the melt was heated in a furnace and solidified in situ by water cooling a chill adjacent to the melt. In the second case, (b), the melt was poured into a preheated fibrefrax mold against a water cooled chill. Details of these procedures are given below.

The furnace used in procedure (a) is shown in Figure 14. The liquid metal was cast into a graphite sleeve with either a copper or stainless steel chill in the bottom of the sleeve. The graphite sleeve and the chill were surrounded by a graphite core, heated by two 750 watt elements, the graphite core serving to provide a uniform temperature in the centre of the furnace prior to casting. A chromel-alumel thermocouple inserted in the core was used to monitor the temperature of the furnace. With power supplied independently to each half of the furnace through two variacs, the temperature of the furnace could be brought up to $700^{\circ}C$ in about 0.5 hours.

The copper and stainless steel chills were used in order to obtain different cooling rates. The surface of the chill was polished and then coated with Aquadag (a colloidal suspension of graphite in a volatile medium), to prevent the liquid metal from alloying with the top surface of the chill on casting. A stream of argon was passed through the furnace prior to casting to reduce oxidation during casting, and also to prevent the oxidation of the Aquadag coating on the chill. This gas stream, by displacing the air in the furnace, also served to minimize the burning away of the graphite sleeve.
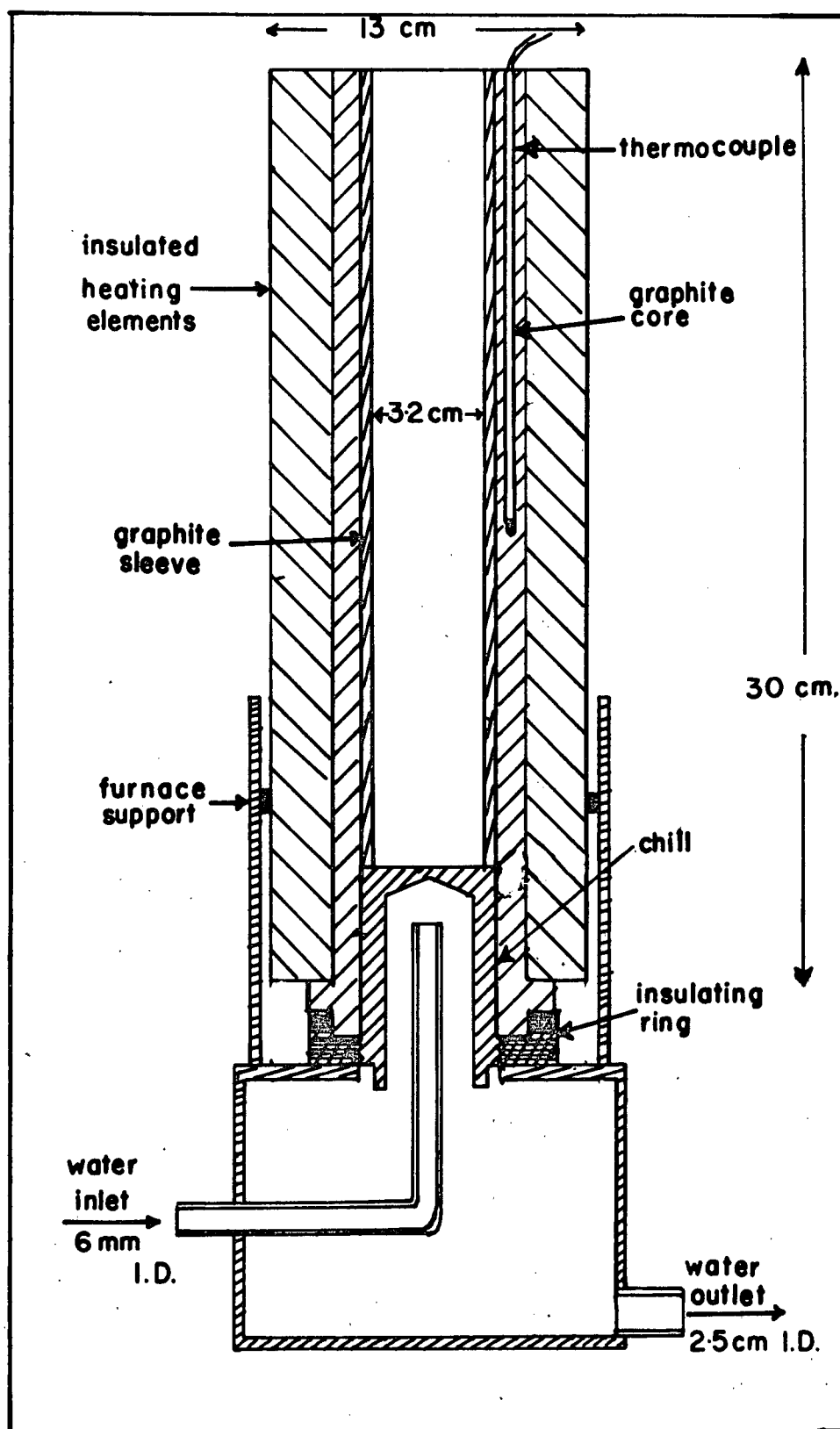
Fig. 14 Schematic representation of the casting arrangement for casting procedure (a).
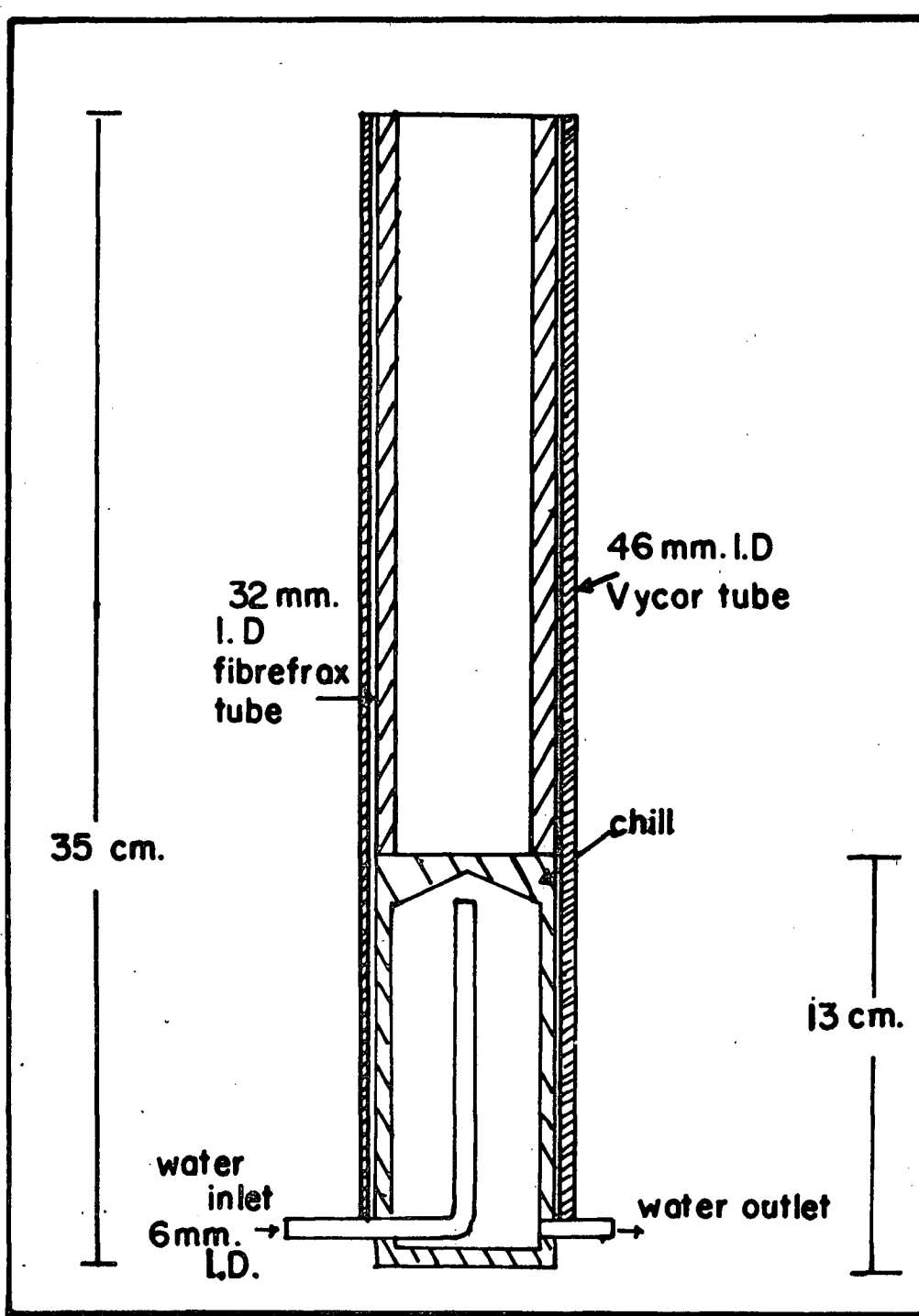
Fig. 15   Schematic representation of the casting arrangement for casting procedure (b).

To cast, the liquid melt was poured into the preheated furnace and the temperature of the liquid monitored. When the required super-heat was reached, the power to the furnace was turned off and the water flow to the chill was turned on, causing the liquid metal to solidify progressively from the chill.

In the second casting procedure, as illustrated in Figure 15, a preheated fibrefrax tube was inserted into a 46 mm. I.D. Vycor tube, the metal solidifying progressively from the water cooled metal chill. The tube was inclined slightly to the vertical to obtain an even flow of liquid onto the chill during the initial stages of pouring. Pour-ing into a vertical tube with a cold chill was found to cause local, irregular initial solidification. The fibrefrax tubing was normally preheated to between $800^{\circ}C$ and $900^{\circ}C$ in a resistance furnace. The water flow to the chill was turned on just prior to casting, to elim-inate condensation on the chill. Both copper and stainless steel chills, coated with Aquadag, were used, as in procedure (a).

The ingots obtained were about 3 cm. in diameter and about 12.5 cm. in length. Shrinkage pipes were absent in all the ingots.

2.4 Metallography and Autoradiography

The macrostructure of the castings was determined by sectioning the casting longitudinally, mechanically polishing the exposed sur-faces, and then etching in a modified Kellers reagent consisting of HF, HNO_3, HCl and water in the proportion 2:3:5:25, followed immediately by immersion in concentrated HNO_3 to remove the layer formed on the

surface due to the etching.

Ingots containing Cu^{64} were sectioned and autoradiographed to determine whether the radioactive material was distributed reasonably uniformly throughout the ingot, i.e., to establish that the liquid was well mixed before casting. After the material adjacent to the chill face was removed for analysis, transverse and longitudinal sections were cut from the ingot. These were mechanically polished, and then placed on Kodak Contrast Process Ortho film, backed by a glass plate. The exposure time required for the autoradiographs varied from 15 to 50 hours depending on the activity of the tracer in the section. The darkening of any region of the film was taken as directly related to the concentration of Cu^{64} adjacent to the film in that region.

Transverse sections, 1 cm. from the chill face, were taken from the ingots used for the temperature measurements (section 2.7), to obtain the average dendrite spacings. These samples, after being mechanically polished for metallographic examination, were etched in the Kellers reagent, diluted with water in the proportion 1:9. The washing of the sample with concentrated HNO_3 was dispensed with. Dendrite spacings were measured from enlarged photographs of the polished and etched sections.

2.5 Measurement of the variation of the solute concentration

2.5.1 Radioactive Tracer method

The cast ingot was placed in a lathe and layers 500μ thick parallel

to the chill face were progressively machined from the ingot, the cuttings from each layer being caught in a box enclosing the cutting tool and the ingot. Before these layers were cut, the outside surface of the ingot in the longitudinal direction was removed, so that the layers in contact with the mold would not affect the analysis. Cuttings from each layer, to make approximately one gram of material, were packed in 3 dram stoppered vials. The weight of the cuttings was determined from the measured weight of each vial before and after the cuttings were introduced into them.

The activity of the cuttings in each vial was measured with a Picker Nuclear Twinscaler II automatic scintillation counter. One hundred samples at a time were loaded into the automatic changer device of the instrument and the activity of each sample was counted in turn over a 0.2 minute interval by two detectors simultaneously. The output of the scalers was automatically printed on a teletype, and a punched tape output was also generated on a papertape punch machine coupled to the teletype. The printout information included the sample number (as loaded on the machine), the counts per sample for each scaler, and the counting time. The average background count, as determined by manually measuring the background level a number of times at the start of counting, was set on the machine and was automatically subtracted from each reading. The symmetrical design of the sample tray ensured a constant background level at the detectors, independent of the position of the samples.

The counter was calibrated with a Cesium[137] standard source prior to counting. In counting the samples containing Cu^{64}, the energy range of the gamma activity detected by the scalers was adjusted to be between 400 KeV and 1 MeV, since the activity peak for Cu^{64} is about 500 KeV. (Figure 16). For Ag^{110} the energy range over which measurements were made was 50 KeV to 1 MeV.

All the samples from the ingots were counted at least three times each, to ensure that counting or machine errors would be detected. In addition, by having repeat counts made over a two day period, saturation effects associated with high counting rates could be detected. For the samples cut from the chill cast buttons (cast to obtain the initial liquid composition), counts were made at least ten times over at least four half lives, and decay curves were drawn from this information. The half life obtained from these curves, when compared with the published value for Cu^{64}, further established the stability and reliability of the counting system.

The information on the punched tapes from the counters was read and stored on magnetic tape at the U.B.C. Computing Centre. The weight of each sample was recorded on Fortran Coding sheets, and added to the tape information. A correction was made to the activity measurement for each sample to allow for decay from the time of the start of counting.for each set of 100 samples.

Since the amount of data handled per set of experiments was quite large (about 2,000 readings), the data was processed with the IBM 360/67 computer at the U.B.C. Computing Centre. After applying the corrections
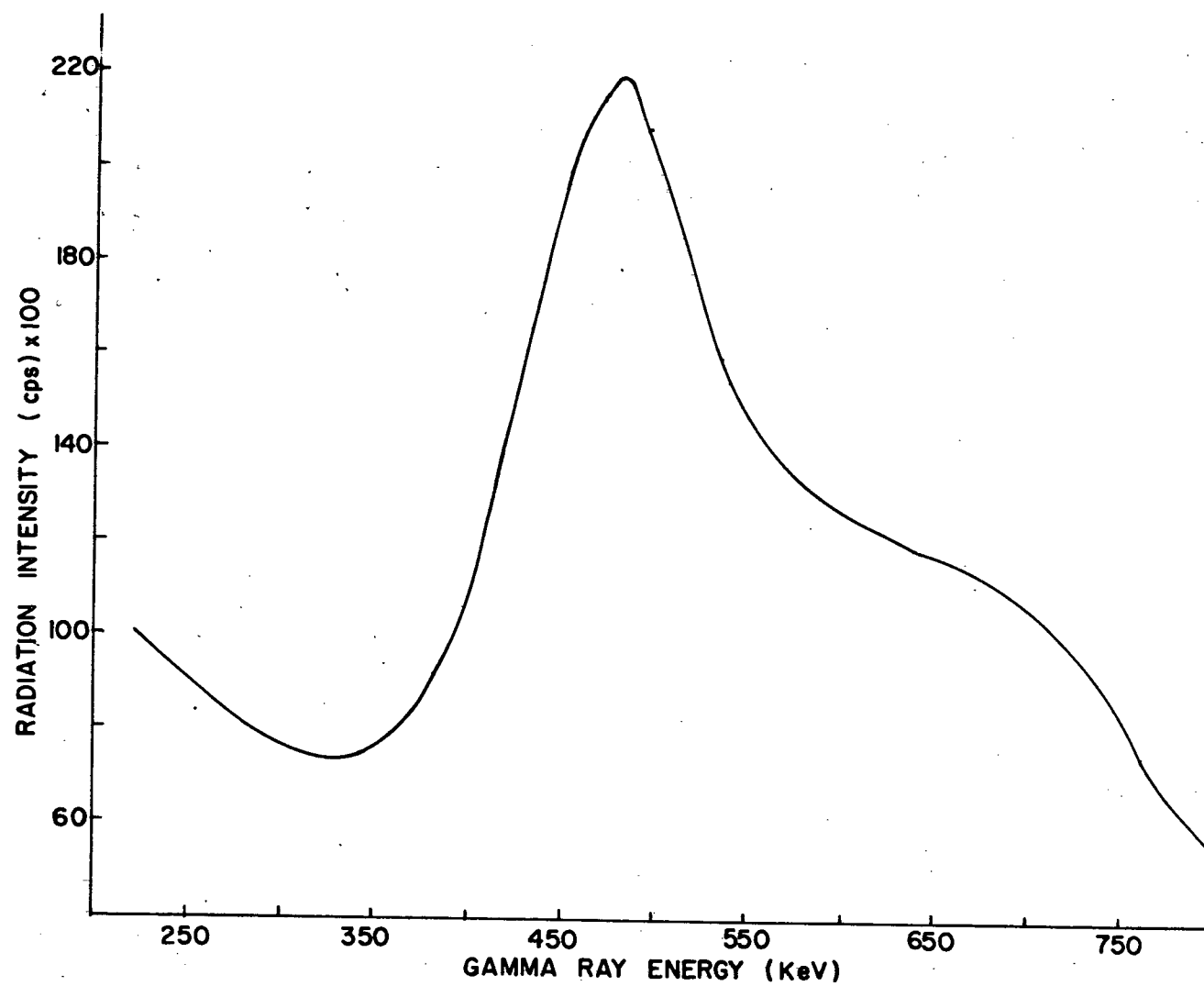
Fig. 16   Gamma ray spectrum for Cu^{64} obtained on the Picker Nuclear scintillation counter.

for the decay of each specimen, the activities were normalized for the weight of the sample, these in turn were normalized by dividing by the melt composition determined from the activity of the cast buttons and the results were obtained both in printed form, as well as in plotted form, as a function of the distance from the chill. The plots were produced on the Calcomp Plotter at the U.B.C. Computing Centre.

To check on the performance of the Scintillation Counting equipment, a large number of observations (350) were made on a long lived isotope (Tin^{113}), and the data put through a Goodness of Fit Test. No significant difference was detected between the expected and the observed distributions of the data, i.e., the data corresponded to the "normal" distribution.

2.5.2   Chemical Analysis

To establish that the variations in composition detected by activity measurements do correspond to variations in the solute concentrations, chemical analyses were carried out on some of the samples used for the activity measurements.

The method employed was the electrodeposition of copper from a solution of the alloy sample onto a platinum cathode. This was done by first dissolving the cuttings in a mixture of H_2SO_4, HNO_3 and water (in the proportion 2:1:2), heating to dryness, adding an excess of 1:1 H_2SO_4, and then redissolving the paste in boiling water. The platinum cathode was placed in the solution so obtained and a current

of approximately 1 amp. was passed through the solution for about 1.5
hours, by which time effectively all the copper was removed from
solution. The amount of copper so deposited on the cathode was then
determined from the increase of weight of the cathode, and the alloy
composition then determined from this weight and the initial weight
of the alloy cuttings used in making up the solution.

2.6 Microprobe Analysis

In an attempt to measure directly the variations in the solute
concentrations as a function of the distance from the chill face, scans
of ingot sections were made on a JEOL Model JXA-3A Electron Probe
Microanalyzer. It was found that the short range variations in the
composition due to microsegregation completely masked any macro-
segregation present. Continuous scans were also made with a large spot
size of 50 microns to follow the variations qualitatively, but this did
not yield acceptable results either.

2.7 Temperature measurements

Five thermocouples were positioned along the ingot length at dist-
ances of 0., 1.2, 2.5, 5 and 11.5 cm., respectively, from the chill
face. The chromel-alumel thermocouples were made of 20 gauge wire,
sheathed in glass wool. The sheathed thermocouples were coated with
a layer of Sairset alumina cement, and then thoroughly dried, in order
to prevent electrical contact between the thermocouples and the cast
ingot during solidification. The thermocouples were connected through

an ice-water reference cold junction to a Hewlett Packard Digital

Voltmeter (Model 5055 A), and the emf. generated by each thermocouple

recorded on the printout machine connected to the voltmeter. A

reading was recorded for each thermocouple every 1.25 seconds. Other

measurements were made with a single pen chart recorder, switching

from one thermocouple to another with a multipoint switch, at varying

time intervals. However, this procedure was not found to be satis-

factory primarily due to the large time intervals between successive

readings on any one thermocouple.

The measured values of the emf., taken at known intervals of

time from the start of pouring, enabled temperature profiles to be

established as a function of time, at five positions along the ingot

axis, corresponding to the five thermocouple positions.

2.8 Modification of Casting procedures

2.8.1 Degassing

Degassing was carried out in some of the ingots by adding Foseco

190 Degaser to the melt prior to casting. Following the instructions

enclosed with the degaser, the degaser was introduced into a bell-

shaped perforated graphite plunger, which in turn was introduced into

the melt and agitated. The degassing was carried out when the melt

was cooling to the desired pouring temperature. However, the degaser

had an unpredictable effect on the structure of the cast ingot, yield-

ing both equiaxed and columnar structures at different times.

Efforts were also made to reduce gas dissolution in the cast alloys by melting and casting in a Vacuum Induction furnace. This procedure was found to be unsatisfactory because the casting process tended to be cumbersome, and because the rate of heat removal from the bottom of the mold was too slow. In addition, the ingots produced contained large interior cracks.

2.8.2 Grain Refining

Fine grained equiaxed structures were obtained by adding about 0.5 grams of 5% TiB_2 in aluminium Master alloy to 300 gram melts just prior to casting.

2.8.3 Exudations

To examine the effect of a change in thermal contact between the casting and the chill during solidification, some castings were moved away from the chill to a distance of about 5 mm., 15 seconds after pouring. This caused a reheating of the solid portion of the casting, and consequently, formation of exudations on the ingot surface initially adjacent to the chill.

2.8.4 Thermal conductivity of the chills

Two types of chills were used, one copper (thermal conductivity .9 cal./sec. sq.cm. ^{o}C at $100^{o}C$) and one of stainless steel (thermal conductivity .04 cal./sec. sq.cm. ^{o}C at $100^{o}C$). In both cases, the polished top surfaces were coated with a thin layer of colloidal graphite, which did not affect the thermal characteristics of the chill. A large

flow of tap water was passed through the chill, the temperature
and volume of water being considered as effectively constant through-
out all the tests.

3. OBSERVATIONS

3.1 Tabulation of Experiments

An appreciable number of ingots were cast under a variety
of casting conditions. Five different alloy compositions were
investigated, and a series of factors associated with the casting
conditions were considered. This included superheat, thermal con-
ductivity of the chill, cooling rate, cast structure, gas content,
separation of the cast metal from the chill during solidification,
and others.

The castings to which Cu^{64} was added to the melt, are listed
in Tables I,II,III, along with the casting conditions. Individual
castings will be referred to by the heat number listed. Most of
the castings were of the Al-10% Cu alloy, since this alloy should
exhibit the maximum inverse segregation at the chill face, as re-
ported in previous investigations[8]. The values of the superheat
listed in the Tables were determined from the difference between
the pouring temperature and the equilibrium liquidus temperature
for that particular alloy.

3.2 Homogeneity of the melt

In order to determine whether the castings containing the
radioactive tracer were macroscopically homogeneous, i.e., whether
the tracer was thoroughly mixed in the melt, autoradiographs were

TABLE I

DATA AND RESULTS FOR Al-Cu INGOTS

COMPOSITION	CASTING NUMBER	CHILL	MOLD	SUPERHEAT °C	MELT ACTIVITY SAMPLING	SPECIAL TREATMENT	INGOT STRUCTURE	NORMALIZED INGOT COMPOSITION Co	EXTRAPOLATED CHILL FACE COMPOSITION % Cu	CHILL ZONE L_c(x500) μ	FIGURE #	COMMENTS C= COLUMNAR E= EQUIAXED C+E= MOSTLY COLUMNAR
Al-5% Cu	130	Copper	Furnace	10°C	Chill	–	E	1.15	5.26	18		
	93	Copper	Fibrefrax	39°C	Chill	–	C+E	1.00	5.28	9		
	94	Copper	Fibrefrax	54°C	Chill	Exudations	C+E	1.28	15.6		22	
	80	Stainless	Fibrefrax	107°C	Chill	–	C	1.03	–	–	32	
Al-20% Cu	71	Stainless	Furnace	180°C	–	–						Excessive scatter due to small sample sizes
	72	Stainless	Furnace	180°C	–	–	C					
	82	Stainless	Fibrefrax	103°C	Chill	–	C	.99	–	–	34	
	126	Copper	Fibrefrax	30°C	Chill	–	C+E	1.19	20.32	12		
Al-25% Cu	83	Stainless	Fibrefrax	103°C	Chill	–	C	1.01	–	–	35	
	127	Copper	Fibrefrax	30°C	Chill	–	C+E	1.22	–	–		

TABLE II

DATA AND RESULTS FOR Al-Cu INGOTS

Al-10% Cu

CASTING NUMBER	CHILL	MOLD	SUPERHEAT °C	MELT ACTIVITY SAMPLING	SPECIAL TREATMENT	INGOT STRUCTURE	NORMALIZED INGOT COMPOSITION C_0	EXTRAPOLATED CHILL FACE COMPOSITION % Cu	CHILL ZONE L_c (×500)	FIGURE #	COMMENTS C= COLUMNAR E= EQUAXED C+E= MOSTLY COLUMNAR
123	Copper	Furnace	10°C	Chill	–	E	1.04	10.2	5	38,39, 40	
96	Copper	Furnace	70°C	Chill	–	C	1.04	10.42	8		
75	Stainless	Furnace	160°C	–	–	C+E	–	–	–		Scatter too high due to small sample sizes.
76	Stainless	Furnace	160°C	–	–	C+E	–	–	–		
98	Copper	Fibrefrax	94°C	Chill	slow water flow	C	.87	10.41	19		
85	Copper	Fibrefrax	91°C	Chill	exudations	C+E	1.24	25.8	–	23	
44	Copper	Fibrefrax	93°C	Tube	–	C+E	0.99	–	–	28	
97	Copper	Fibrefrax	84°C	Chill	structure changed	C+E	1.00	–	–	36	
45	Copper	Fibrefrax	65°C	Tube	–	C+E	1.14	10.05	15	29	
179	Copper	Fibrefrax	50°C	Chill	–	C+E	1.12	10.16	15		
95	Copper	Fibrefrax	41°C	Chill	degassed	C+E	1.00	10.5	9	21	
125	Copper	Fibrefrax	20°C	Chill	–	C+E	1.21	10.15	19		
46	Stainless	Fibrefrax	91°C	Tube	–	C	1.04	10.2	8	30	
84	Stainless	Fibrefrax	91°C	Chill	TiB_2	E	1.01	10.27	6	37	
47	Stainless	Fibrefrax	67°C	Tube	–	C+E	1.06	10.37	18	31	

TABLE III

DATA AND RESULTS FOR Al-Cu INGOTS

Al-15% Cu

CASTING NUMBER	CHILL	MOLD	SUPERHEAT °C	MELT ACTIVITY SAMPLING	SPECIAL TREATMENT	INGOT STRUCTURE	NORMALIZED INGOT COMPOSITION C_0	EXTRAPOLATED CHILL FACE COMPOSITION % Cu	CHILL ZONE L_c (×500)	FIGURE #	COMMENTS C= COLUMNAR E= EQUIAXED C+E= MOSTLY COLUMNAR
21	Copper	Furnace	160°C	Tube	–	C	0.74	15.05	6	27	
20	Copper	Furnace	115°C	Tube	small ingot	C	1.31	–	–	26	
18	Copper	Furnace	80°C	Tube	–	C+E	.96	15.42	12	25	
19	Copper	Furnace	40°C	Tube	–	C+E	.96	15.42	7	24	
124	Copper	Furnace	10°C	Chill	–	E	1.28	15.41	20		
73	Stainless	Furnace	150°C	–	–	C+E	–	–			Excessive scatter due to small sample sizes.
74	Stainless	Furnace	150°C	–	–	C+E	–	–			
128	Copper	Fibrefrax	20°C	Chill	TiB_2	E	1.23	15.37	10		
81	Copper	Fibrefrax	100°C	Chill	–	C	1.00	15.52	10	33	
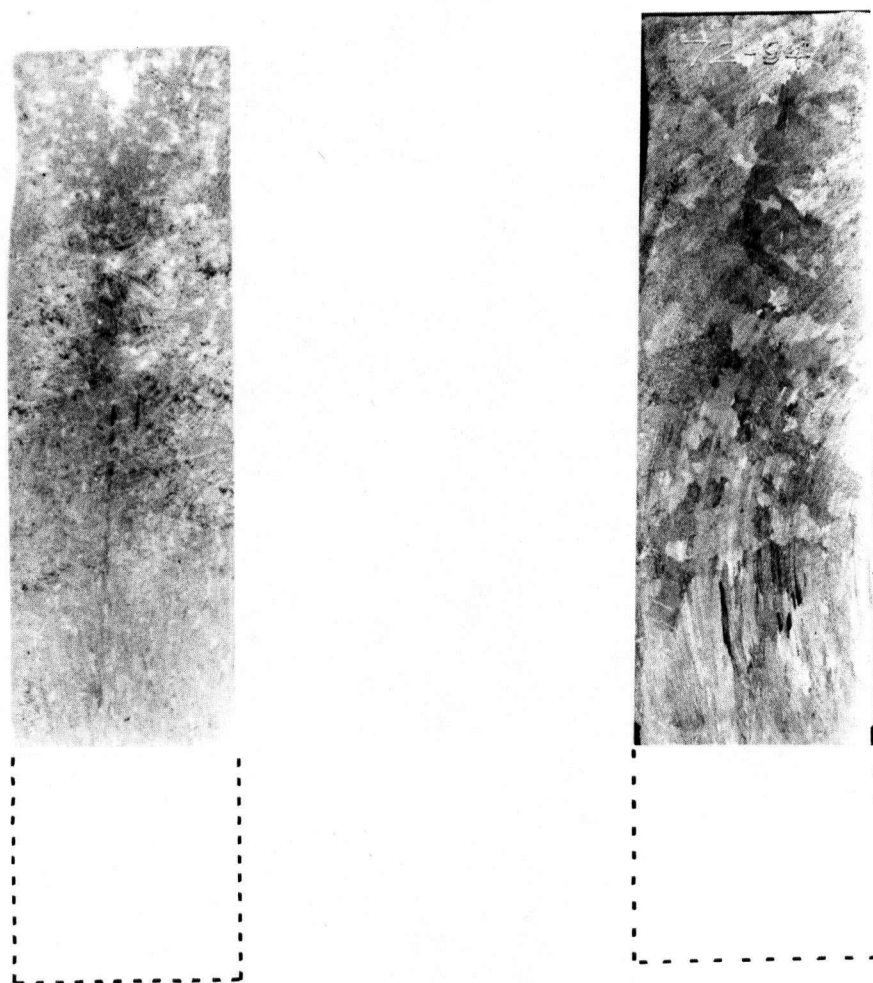
Fig. 17   Autoradiograph and corresponding etched surface of an Al-Cu ingot
           (ingot 94).
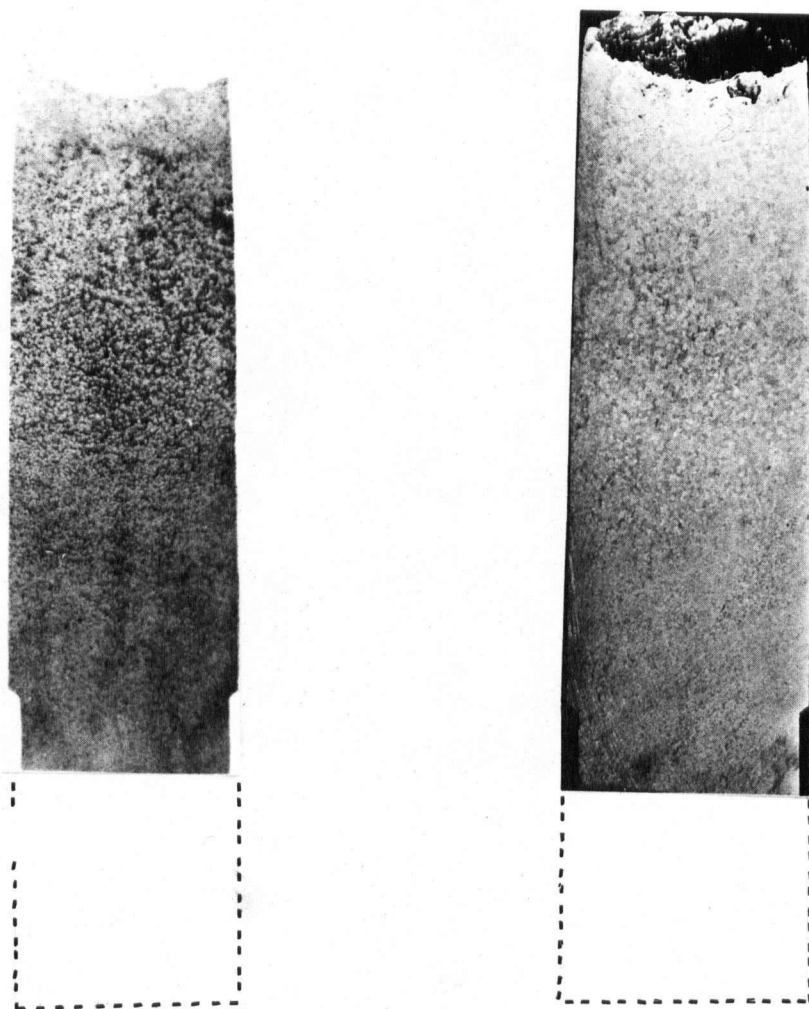
Fig. 18   Autoradiograph and corresponding etched surface of an Al-Cu ingot
(ingot 84).

made of the parts of the ingot remaining after the cuttings re-
quired to measure the composition variation were removed from the
ingot. The autoradiographs established that the liquid was mixed
sufficiently to uniformly disperse the tracer addition, and also
gave an indication of the structure of the casting.

Examples of two such autoradiographs and the corresponding
etched surface of columnar and equiaxed ingots are shown in Figures
17 and 18. The Figures show that there is no significant macro-
segregation of the tracer in the ingot, and, that the cast struct-
ure on the etched surface is delineated in the autoradiograph.
Since the lower part of the casting, adjacent to the chill was not
autoradiographed, inhomogeneities may be considered to be present
in this region. However, in view of the uniform distributions
shown in the autoradiographs, the probability of such an occurrence
is considered to be small. The relative position of the auto-
radiographs with respect to the whole ingot is outlined in the
Figures.

3.3 Cast structure

Most of the castings that were used for the determination of
macrosegregation were columnar, for at least half of the overall
ingot length, starting at the chill face. In view of the fact
that only the first 2 cms. of the ingot was significant for the
present analysis, no attempt was made to make the whole of the
ingot columnar. It was noticed that the use of higher superheats

yielded ingots with longer columnar zones.

The castings in which the grain refiners were added, had a fine-grained equiaxed crystal structure uniformly throughout the casting. The grain size of one such casting, of Al-10% Cu alloy was about 1 mm. diameter.

It was generally observed that exudations or sweat beads were not present on the chill face in nearly all of the ingots examined. It will be shown later that exudations are present on the chill face of the ingot, as deduced from composition analysis, but that the thickness of the exuded layer must be very small. In general, the chill face of the ingots was smooth and flat.

Microporosity was observed to be present in most of the ingots examined, as detected optically. The microporosity is believed to be due to the presence of hydrogen in the molten aluminium. The hydrogen was introduced into the melt during the relatively short period of time that the melt was exposed to air during casting.

In general, ingots cast in the preheated furnace using technique (a), (Section 2.3), showed a longer columnar zone than the ones cast in the fibrefrax tubing, employing procedure (b). The columnar grains had a smaller diameter when the ingots were cast in the fibrefrax tube. Macrostructures of three ingots, one cast using casting technique (a), one using (b), and the third cast in the vacuum induction furnace are shown in Figure 19.
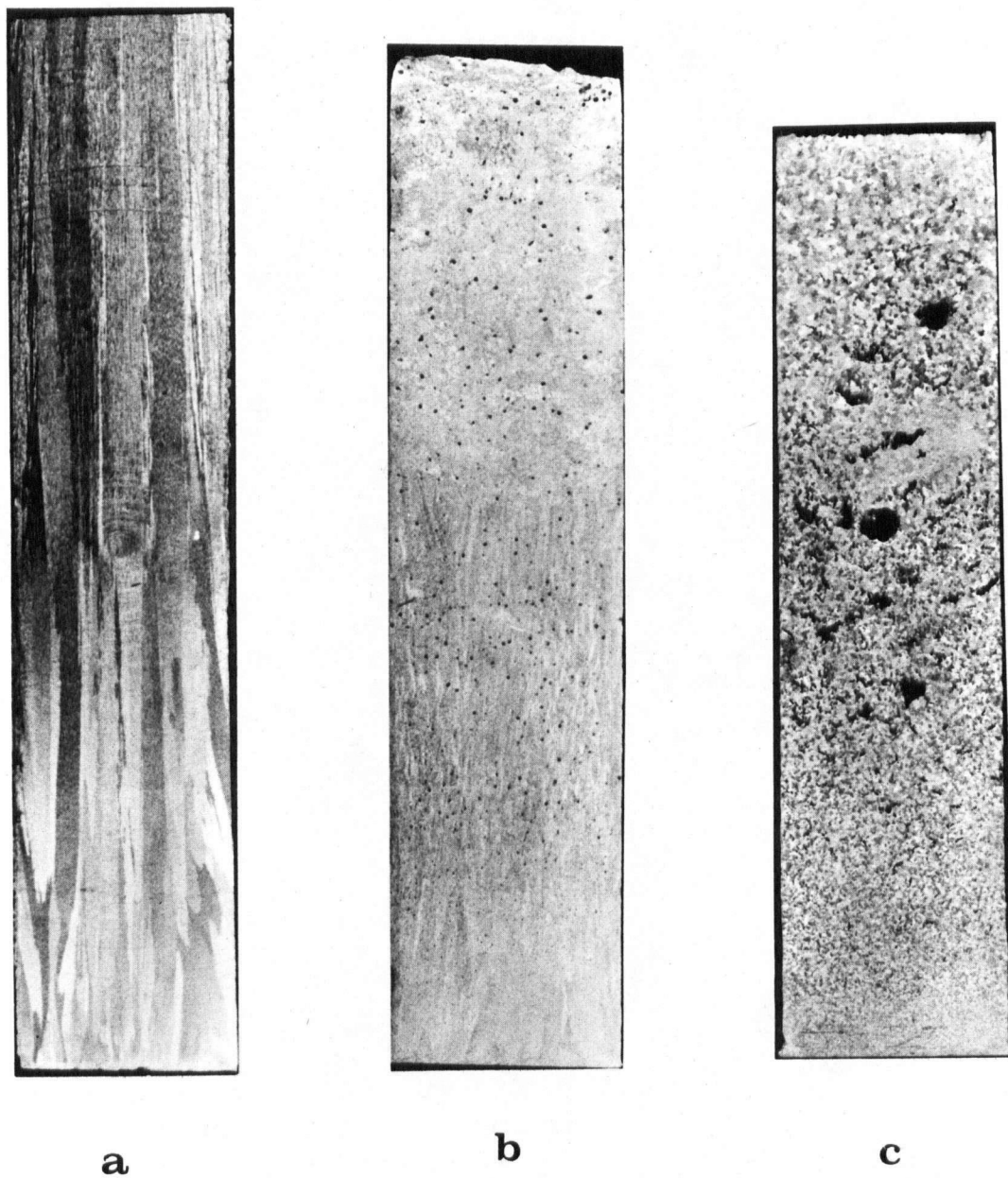
Fig. 19   Macrostructure perpendicular to the chill face of Al-Cu ingots cast
           (a) in the furnace arrangement
           (b) in fibrefrax molds
           (c) in the vacuum induction furnace.

3. 4 Measurement of the initial melt composition

Tests were carried out to determine the change of the mean
composition of the melt with time, due to the loss of either the
aluminium, or copper from the liquid alloy into the oxide layer
covering the melt. Cu^{64} tracer was added to the melt and was
vigorously stirred in. Samples were taken at 5 minute intervals
from the melt, over a duration of 20 minutes, and cast into copper
molds. For the duration of the test, the temperature of the molten
metal in the crucible was kept at $700^{o}C$, by adjusting the power
to the induction coil. The chill cast samples were then machined
into small cuttings, which were packed into vials, and the activ-
ity of these samples determined on the scintillation counter. It
was found that there was a small loss of Al from the melt with
time, but that this loss was too small to make any significant
difference to the measurement of the melt composition. The rate
of increase of the copper composition in the melt is shown in
Figure 20. The activities have been normalized with respect to
the average activity of 10 samples obtained from the ingot cast
from the remaining melt. Since the normal time between the re-
moval of the sample from the melt, and casting was usually less
than 2 minutes, it was considered that this loss was insignificant
in the present investigation.

For each ingot, direct measurements of the activity and there-
fore Cu^{64} concentrations in the melt were made prior to casting.
The sampling procedure used in each test (tube or chill casting)
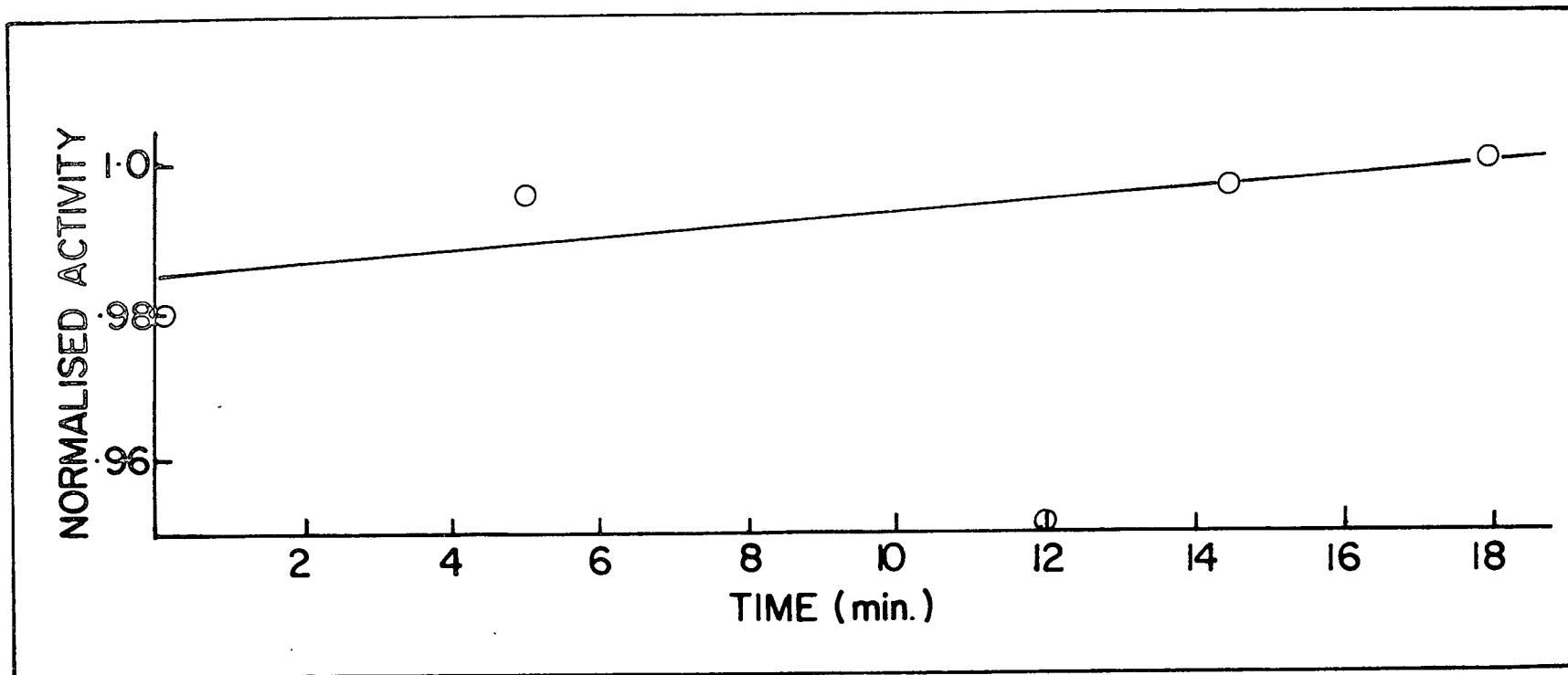
Fig. 20   Normalized activity of samples taken at different times from the same melt.

is listed in Tables I, II, and III. The melt activity measured was used to normalize the activity measurements of cuttings taken to establish the segregation in the casting. If segregation is confined to the chill zone of the casting, then the normalized concentration of Cu^{64} away from the segregated zone should be unity. These values (normalized ingot composition C_o) are listed in Tables I, II, and III. An examination of the values obtained from the chill casting technique shows that 90% of the samples tested had a value of C_o obtained by normalizing, to within 5% of unity. This does not include samples 123 to 130 which had high activities giving slightly erroneous results due to saturation effects during counting. For the melt sampling using a quartz tube, approximately 25% of the values of C_o were within 5% of unity, 50% within a range of 5 to 15% of unity, and the rest greater than 15% from unity.

These results indicate that the tube sampling technique is not as satisfactory as the chill casting technique to determine the melt activity. The accuracy and reproducibility of C_o indicates reproducible measurements of concentration in the cuttings taken from ingots away from the chill zone. In the case of ingot 129, samples for the mean composition of the ingot were obtained using the method of Kirkaldy and Youdelis.

The ingot was split longitudinally, and samples were machined from one half of the ingot for the determination of the segregation of copper with increasing distance from the chill face. The other half of the ingot was clamped on a vise and the cut surface milled over the

entire length of the ingot, the cuttings were thoroughly mixed, and their activity measured to determine the average ingot composition. It was found that the activities measured from standard samples taken from the cuttings did not give consistent results. This method for obtaining C_o was therefore not considered satisfactory in the present tests.

3.5 Distribution of Cu^{64} along the ingot length

3.5.1 Observation of macrosegregation near the chill

Figure 21 illustrates the main features found in the solute distribution near the chill face of the ingots.

(a) The first point, adjacent to the chill, has an abnormally high composition in comparison to the adjacent points and the remainder of the curve.

(b) There is a gradual decrease in composition with distance from the chill face.

(c) After the gradual decrease, the composition remains constant over the rest of the ingot examined. This composition is taken as the mean composition of the ingot.

(d) In some cases, a small solute depleted zone, just before the increase in composition (b) was observed.

The concentration indicated by the first point (feature (a)) in Figure 21, is 10.7% Cu, which is much lower than the eutectic

Fig. 21   Normalized activity vs. distance from the chill face for the composition and casting conditions indicated.

composition of 33% Cu for Al-Cu alloys. In other ingots of Al-10% Cu, the initial composition measured varied in the range 10.0 to 11.5% Cu. Such a high concentration could only result from the formation of a thin layer of eutectic exudation on the chill face. The thickness of the eutectic to produce a composition of 11.5% Cu in the first point was calculated to be 3 5 microns which would not normally be observed visually. As a result of the presence of the eutectic layer, the first point was neglected in the analysis of the composition distribution.

The chill face concentrations reported here were obtained by extrapolating the composition distribution curves back to the chill face, provided that at least three points were present in the decreasing concentration region (feature (b)).

The composition given by the horizontal portion of the normalized activity distributions (normalized with respect to the melt sample activity), was taken as the mean composition of the ingot in all cases. All the measured compositions were then normalized so as to set the horizontal portion to the value 1.

In many of the following activity distributions, multiple points have been represented for the activity of the same sample. These indicate repeat measurements taken on the same sample at different times. The activities reported in Figures not bearing such multiple points are averages of such repeat measurements. All activities reported are corrected for decay.
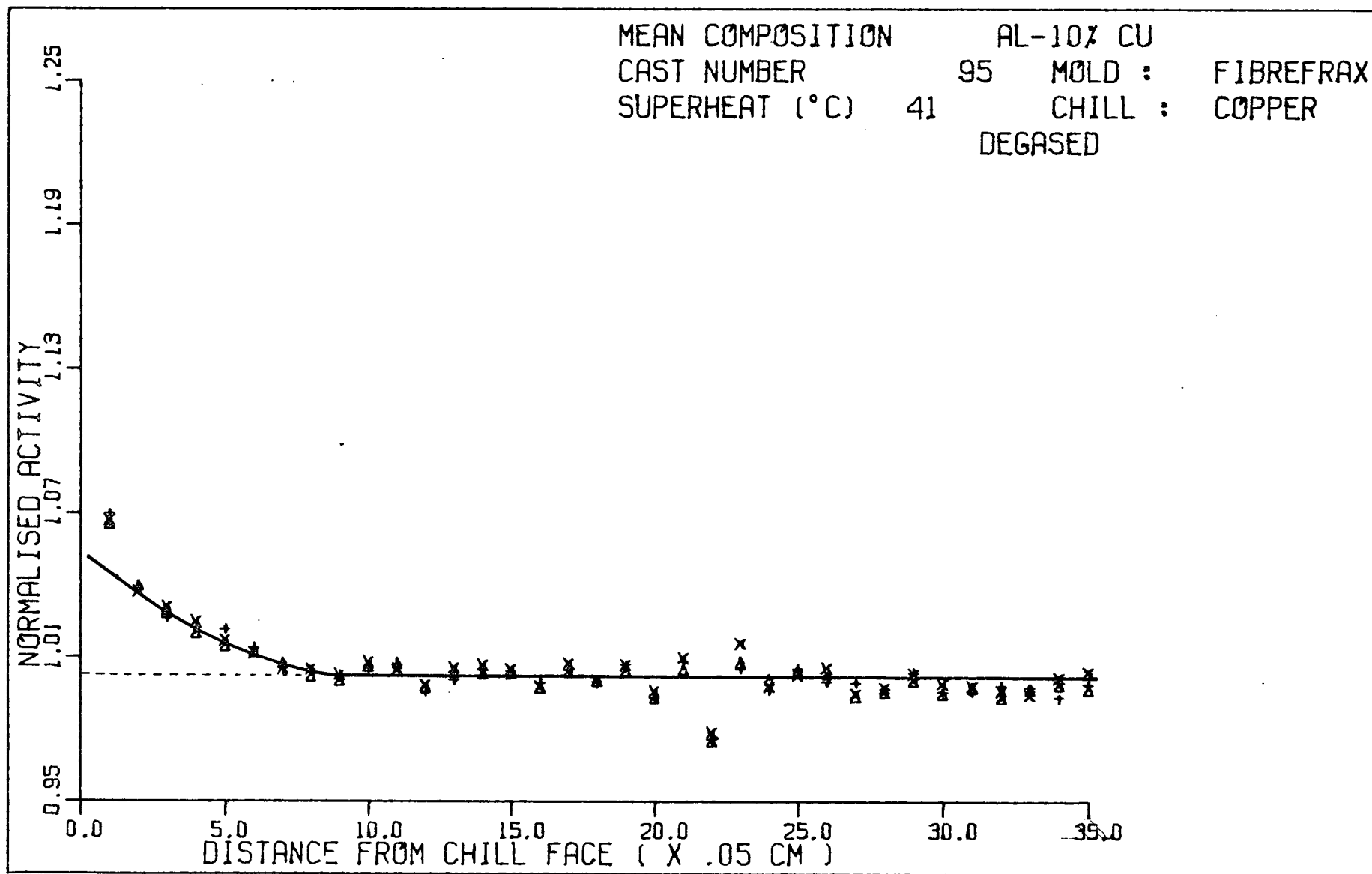
Fig. 22   Normalized activity vs. distance from the chill face for the composition and casting conditions indicated.

Fig. 23   Normalized activity vs. distance from the chill face for the composition and casting conditions indicated.

3.5.2 Exudations

The distribution of Cu^{64} near the chill resulting from the removal of the ingot from the chill face 15 seconds after casting is shown in Figures 22 and 23. A marked increase in the concentration of Cu^{64} at the chill face is observed in both curves, as compared with Figure 21, with the concentration adjacent to the chill approaching the eutectic composition in Figure 23. The effect of removing the ingot from the chill has clearly caused local remelting to occur and the liquid near the eutectic composition to be exuded past the initial cast surface through the remelted interdendritic liquid pipes. Since the amount of eutectic liquid present in the Al-5% Cu alloy due to non-equilibrium solidification is small as compared to the Al-10% Cu alloy, the composition of the exuded material adjacent to the chill does not reach the eutectic composition.

Comparing Figures 22 and 23, the distance through which there is a rise in composition differs, the distance in Figure 23 being appreciably larger. This is attributed to either a larger separation between the chill and the ingot, or more local remelting and subsequent flow of liquid to form exudations in Figure 23. The value of the horizontal portion of the curve in both cases is high (1.25). This is probably due to the flow of the enriched interdendritic fluid towards the chill face of the casting during the formation of the exudations.

3.5.3 Effect of superheat

The composition distributions obtained for ingots of Al-15%
Cu, cast against a copper chill in the preheated furnace chamber
(procedure (a)), is shown in Figures 24 to 27. Here, the variable
being changed is the melt superheat, which varies from 40°C for
Figure 24 to 160°C for Figure 27.

All four Figures show an initial high concentration at the
chill face, with the concentration decreasing away from the chill,
tending towards a constant value. There is a wide scatter in
the points, particularly in Figures 24 and 25, making an extra-
polation of the concentration values near the chill, back to the
chill face, ambiguous.

Comparing the compositions adjacent to the chill, the results
show a decrease in the concentrations with increasing superheat.
They also show the region adjacent to the chill exhibiting higher
solute concentrations is larger for low superheats. A quantitative
comparison of maximum chill face composition and superheat can be
made using the first point adjacent to the chill, or by extra-
polating the points in the region adjacent to the chill, back to
the chill face. Both procedures should give the same results.
However, using the first point gives much higher values for con-
centration at the chill face than the values obtained from the
extrapolating procedures. The large values are attributed to the
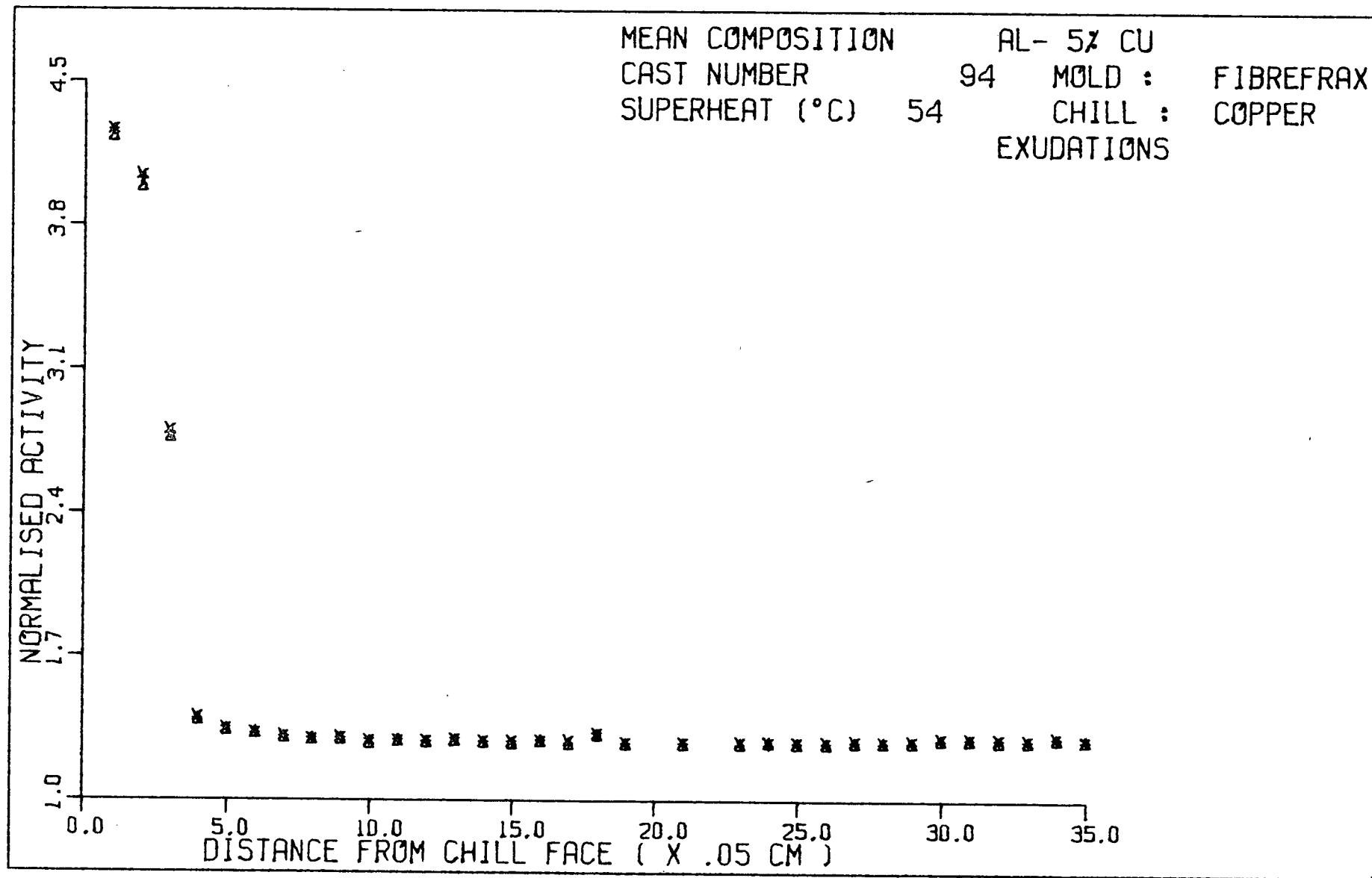exudation of eutectic material at the chill face, separated slightly

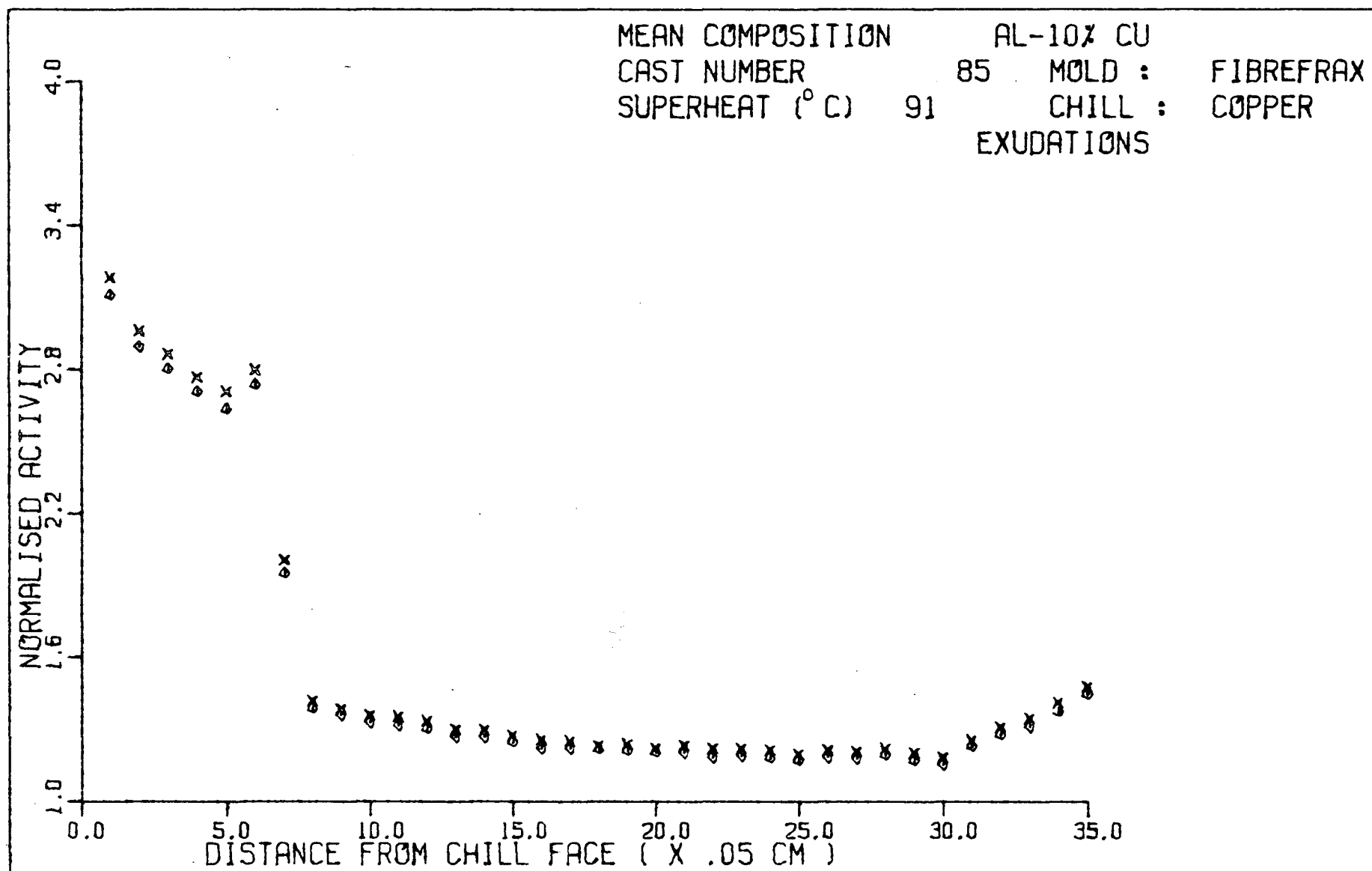Fig. 24   Normalized activity v̇.s. distance from the chill face for the composition and casting conditions indicated.

Fig. 25   Normalized activity vs. distance from the chill face for the composition and casting conditions indicated.

MEAN COMPOSITION   AL-15% CU

CAST NUMBER   20   MOLD :   FURNACE

SUPERHEAT (°C) 115   CHILL :   COPPER
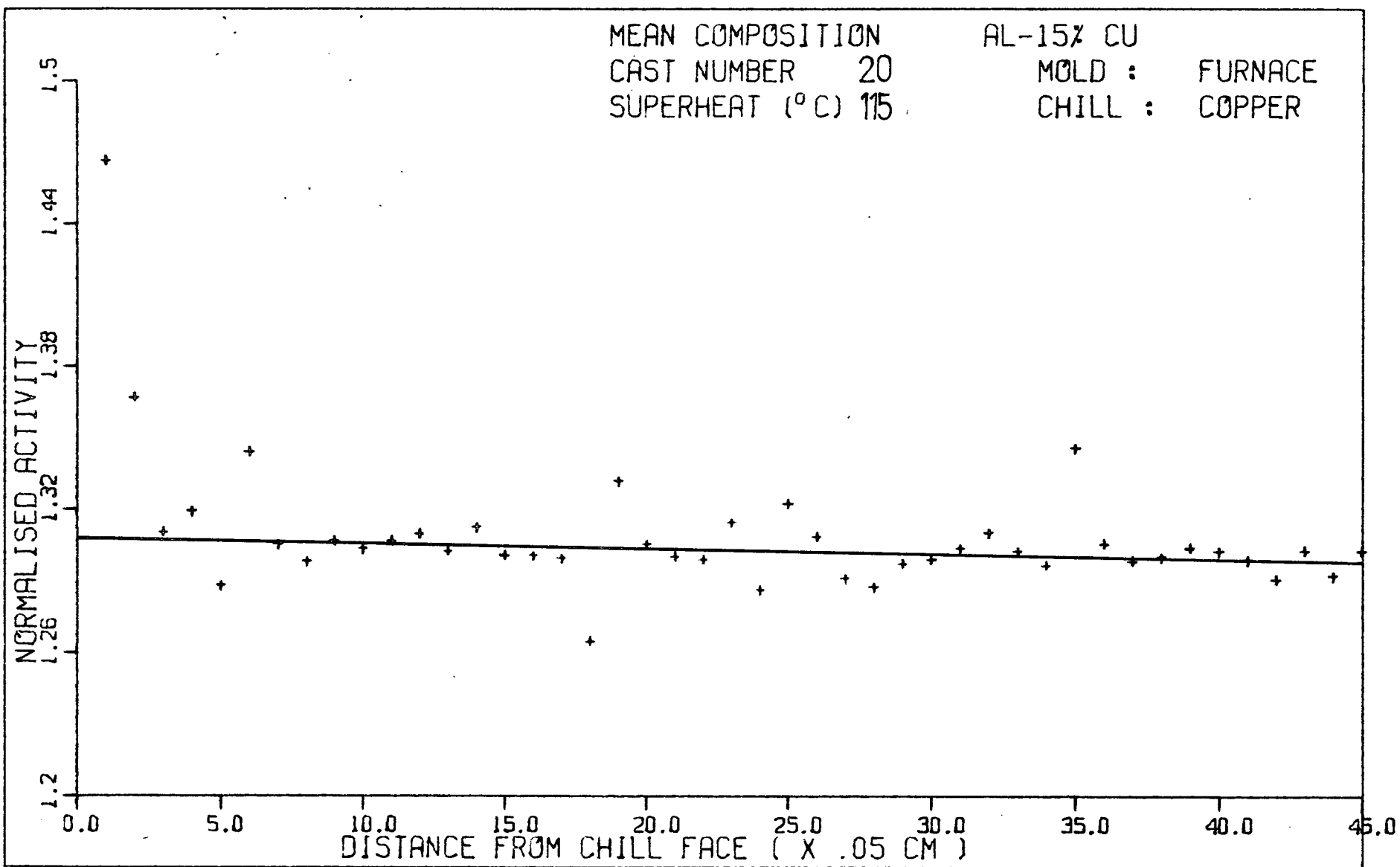
Fig. 26   Normalized activity vs. distance from the chill face for the composition and casting conditions indicated.
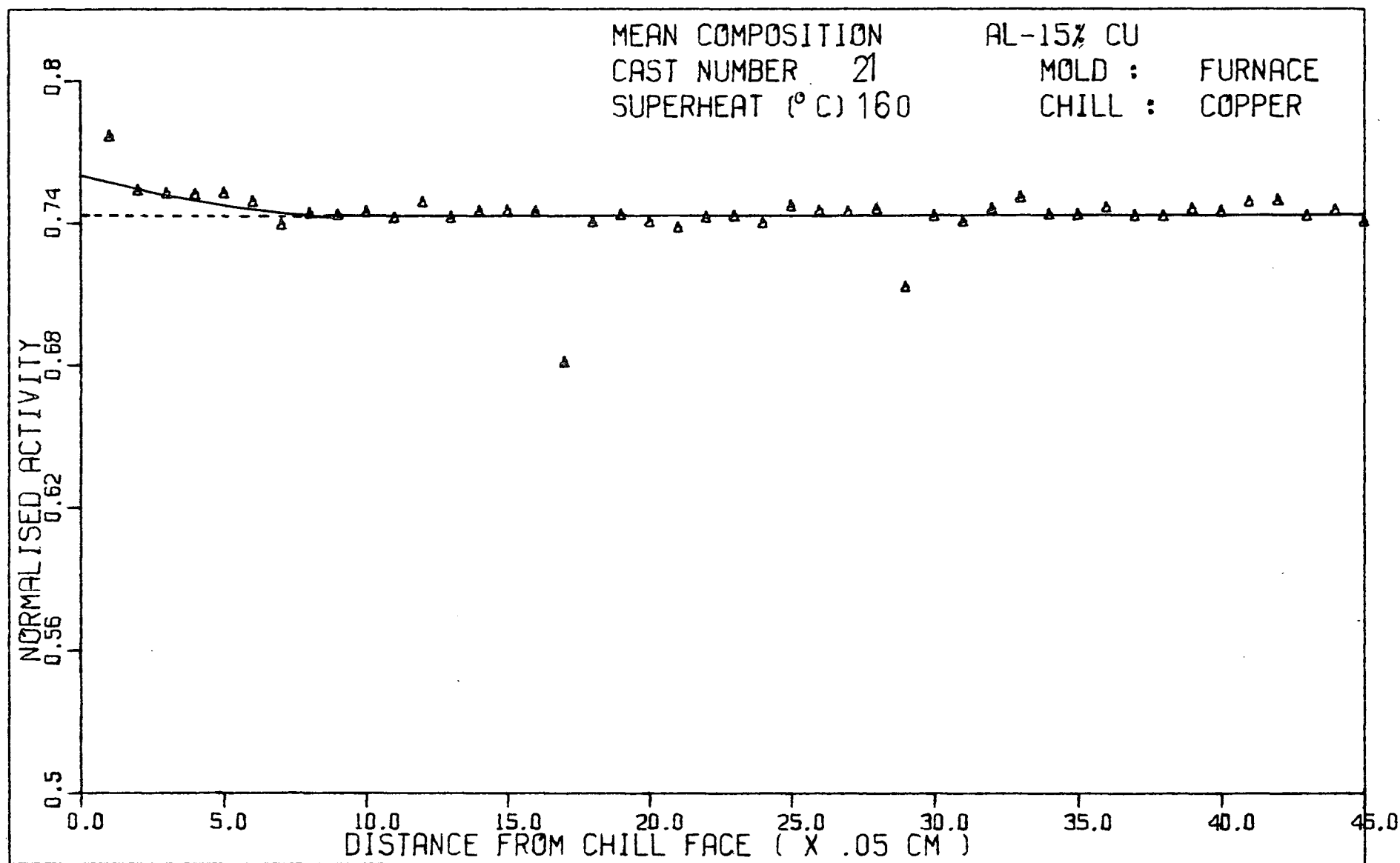
Fig. 27   Normalized activity vs. distance from the chill face for the composition and casting conditions indicated.

from the chill due to volume shrinkage on cooling. Accordingly, it is considered that the first point (and possibly the second) cannot be directly related to the chill face concentrations due to inverse segregation. Extrapolation of the decreasing concentration region is only approximate due to the scatter of the points, the relatively few points in this region, and the non-linearity of the region being extrapolated.

A similar decrease in the chill face concentration with superheat was observed in Al-10% Cu alloys.

Ingot 20 (Figure 26) was a short ingot (Table I), cast to examine the effect of ingot length on segregation in the chill region. No significant difference was observed using the short ingot. However, the comparison was made at a high superheat where the segregation at the chill is small. No comparisons were made at low superheats.

3.5.4 Effect of changing the rate of heat removal

The rate of heat removal was changed by using either stainless steel or copper chills, the former giving a lower rate of heat removal from the ingot during casting. Typical results for Al-10% Cu alloys cast in Fibrefrax molds, using the two chills, are shown in Figures 28 to 31. Figures 28 and 30 are curves of normalized concentration versus distance from the chill for ingots cast on copper and stainless steel chills respectively, at the

Fig. 28   Normalized activity vs. distance from the chill face for the composition and casting conditions indicated.

MEAN COMPOSITION   AL-10% CU
CAST NUMBER   45   MOLD :   FIBREFRAX
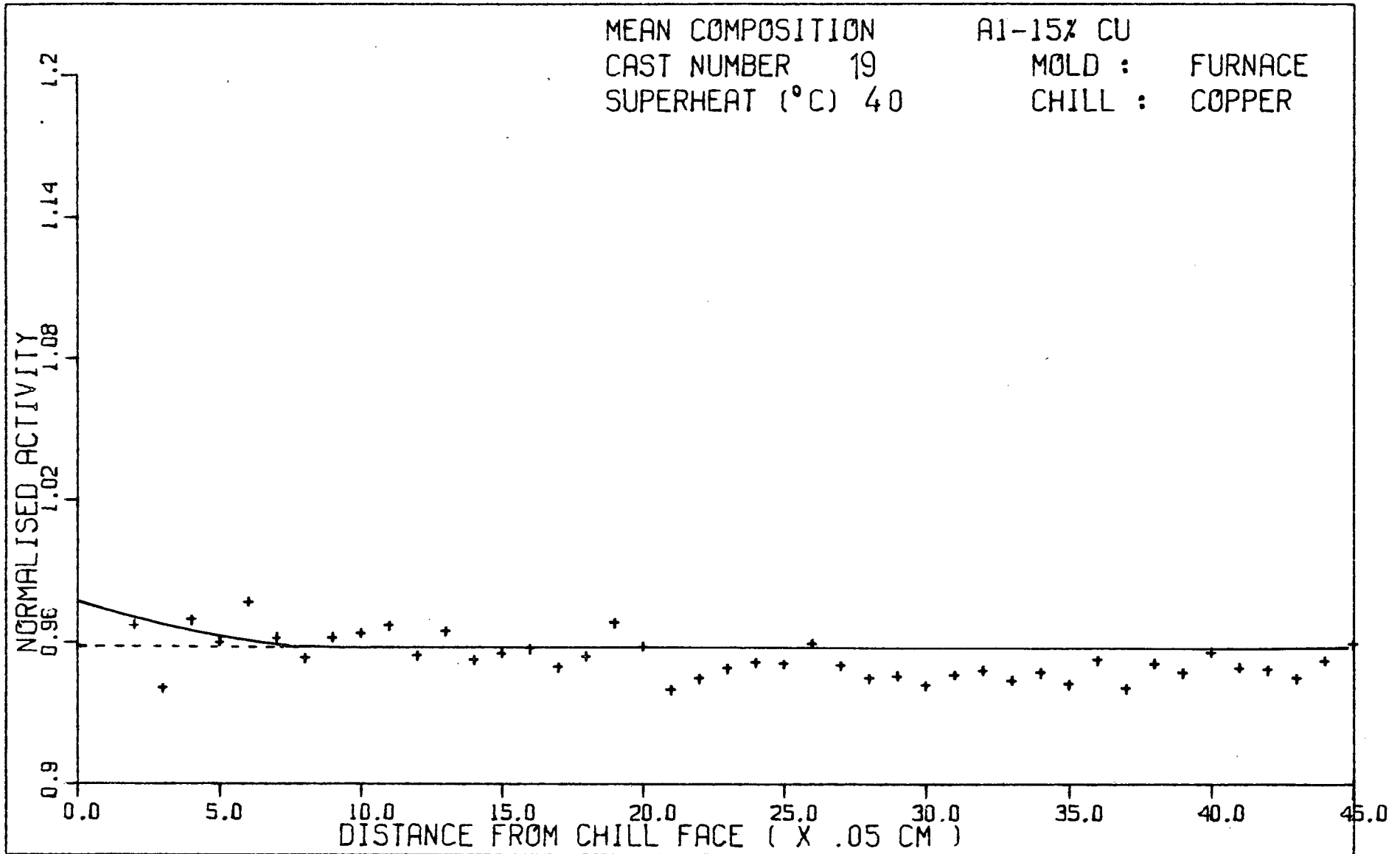SUPERHEAT (°C)   65   CHILL :   COPPER

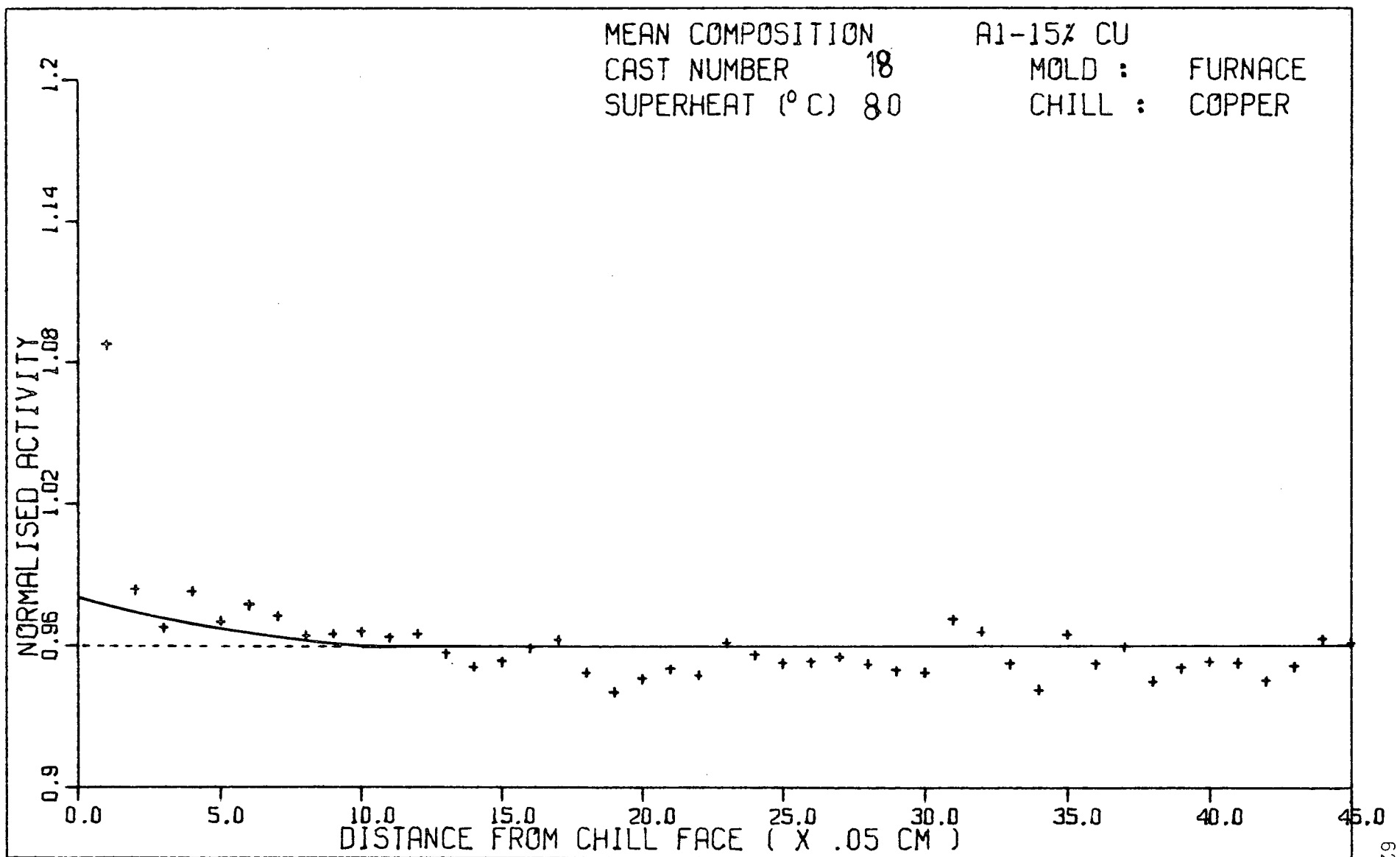Fig. 29   Normalized activity vs. distance from the chill face for the composition and casting conditions indicated.

Fig. 30   Normalized activity vs distance from the chill face for the composition and casting conditions indicated.

Fig. 31 Normalized activity vs. distance from the chill face for the composition and casting conditions indicated.

same superheat (92°C). Ignoring the first point adjacent to the chill, the extrapolated concentration at the chill face is higher for the stainless steel chill (Figure 30), and the distance of the higher concentration adjacent to the chill is larger. (The fourth point on Figure 30 is abnormally low for unknown reasons and is neglected).

The concentration change at the chill zone at a lower super-heat (66°C) for the copper and stainless steel chills is shown in Figures 29 and 31. Lowering the superheat with a copper chill increases the amount and extent of the segregation at the chill zone, (as was expected from the observations in the previous section), as seen by comparing Figures 28 and 29. When the chill is changed to stainless steel, there is a further corresponding increase (Figures 29 and 31). Accordingly, reducing the thermal conductivity of the chill increases the amount and extent of segregation in the chill region for the same alloy cast at the same superheat.

3.5.5 Effect of changing composition

The variations of the normalized activity distributions obtained for ingots of Al-5% Cu, Al-15% Cu, Al-20% Cu and Al-25% Cu respectively, cast on stainless steel chills in fibrefrax molds, at effectively constant superheat of 100°C, are illustrated in Figures 32 to 35. For the case of Al-10% Cu alloy, Figure 30 will be used for comparison, although this alloy was cast at a

slightly lower superheat than the others.

Considering the curves shown in the Figures mentioned above, only Figures 30 and 32 show high concentrations in the first layer adjacent to the chill. These points are associated with exudations, and will be neglected. At low (5%, Figure 32) and high (25% , Figure 35) copper concentrations, no significant segregation is observed in the chill region. For the Al-20% Cu alloy (Figure 34), the first point indicates the possibility of segregation immediately adjacent to the chill, but this may partly result from exudation on the surface. Both the Al-10% Cu alloy (Figure 30) and the Al-15% Cu alloy (Figure 33) exhibit appreciable segregation at the chill face, which extends into the ingot away from the chill face. A quantitative comparison of the segregation will be presented later when the present results are compared to the published observations and theoretical predictions.

3.5.6 Special treatments

The variations in the solute distributions along the ingot axis for alloys of Al-10% Cu, which have been subjected to special treatments as outlined in Section 2.8, are presented in Figures 21, 36, and 37. The effect of adding TiB_2 to the melt of Al-10% Cu alloy before casting, on the segregation in the chill region is shown in Figure 37. In this case, the ingot had a fine, equiaxed
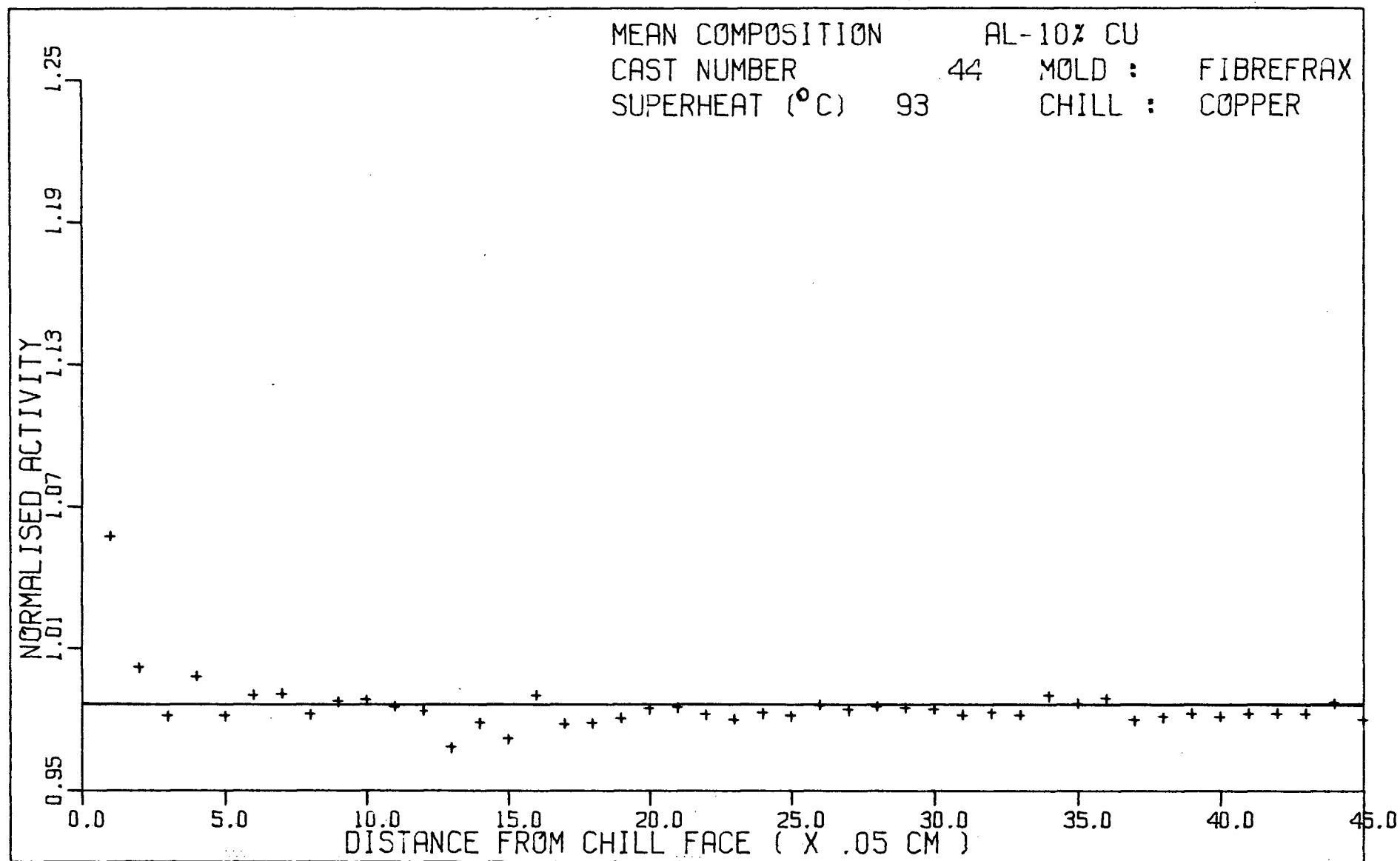
Fig. 32   Normalized activity vs. distance from the chill face for the composition and casting conditions indicated.
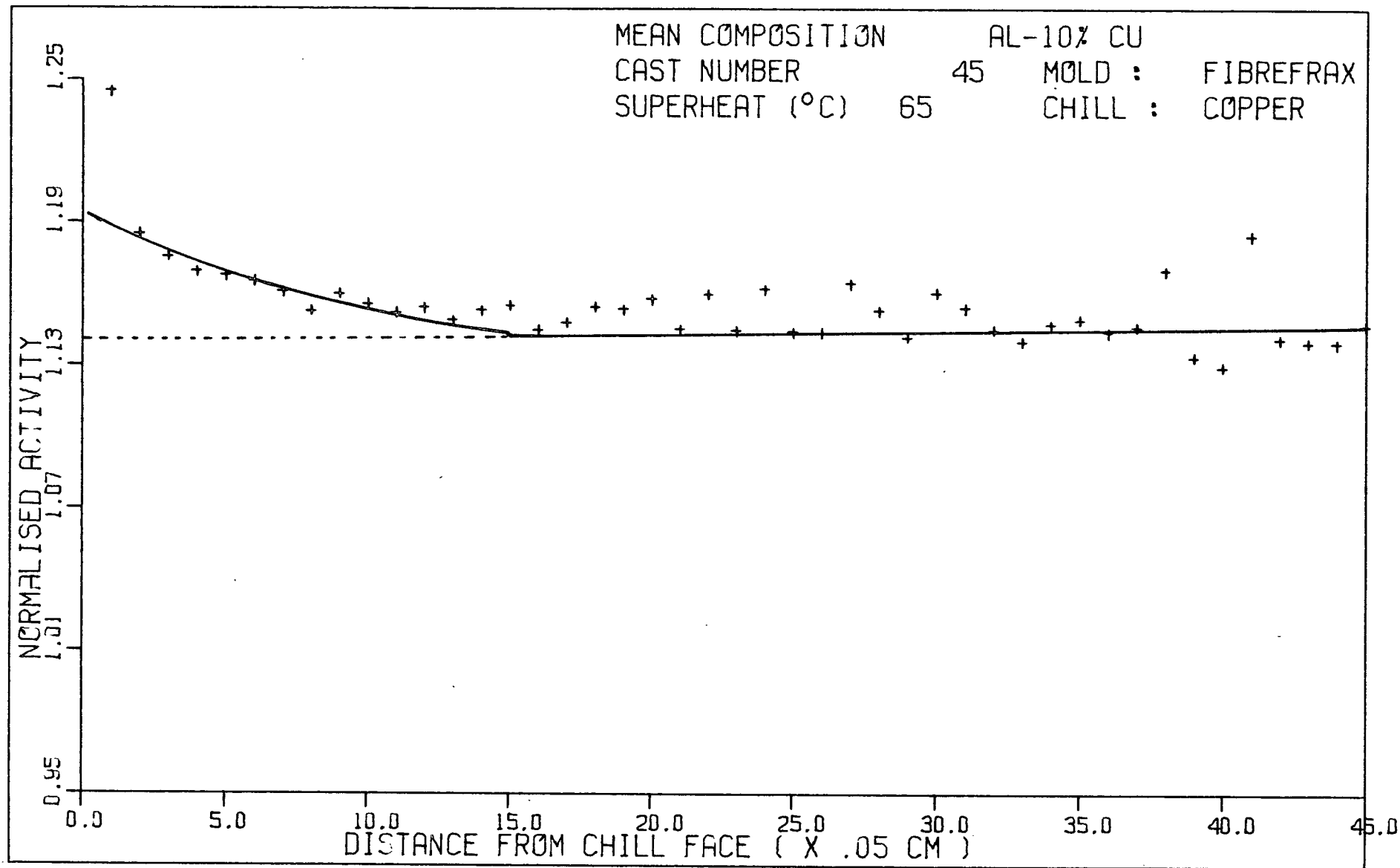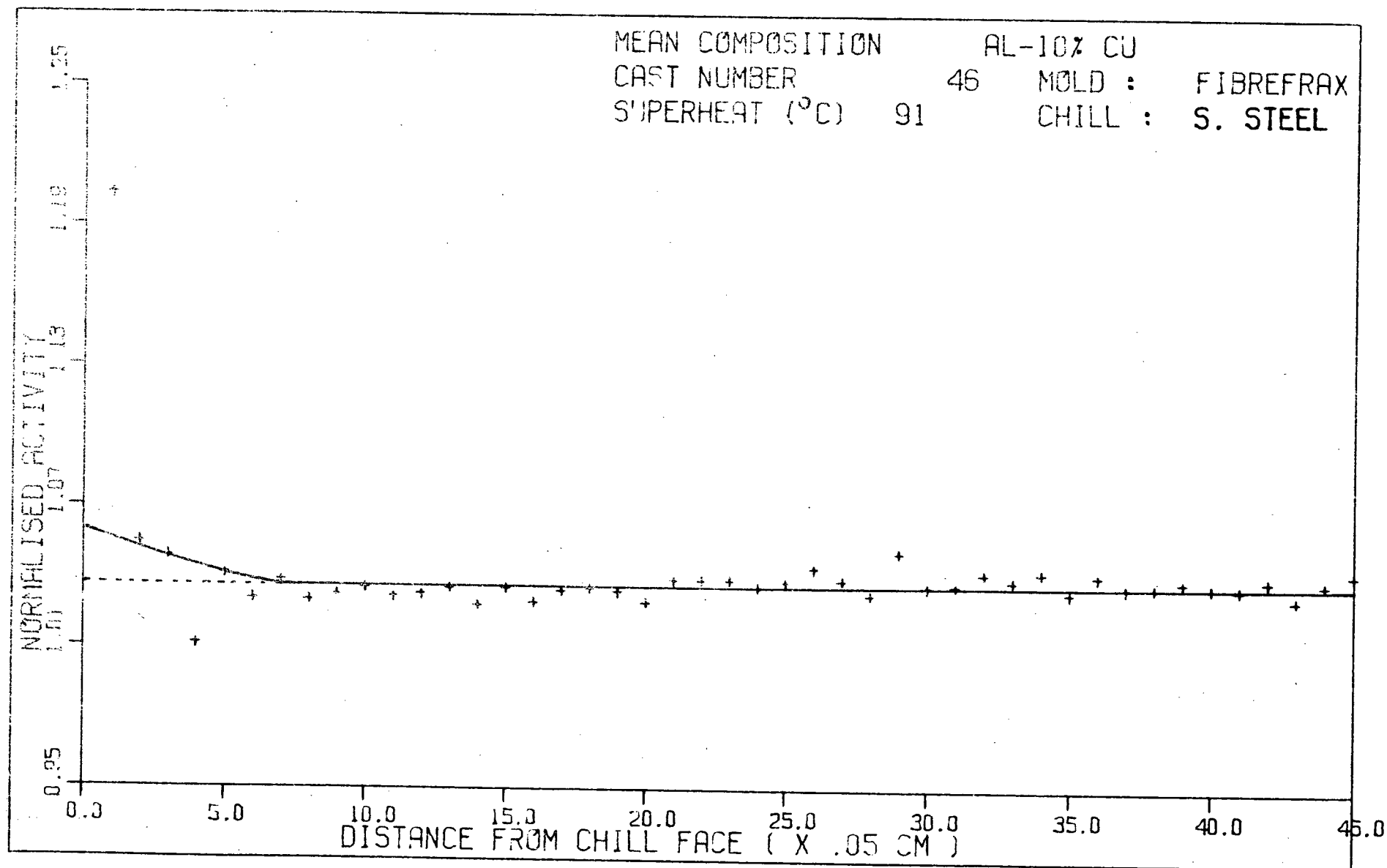
Fig. 33 Normalized activity vs. distance from the chill face for the composition and casting conditions indicated.
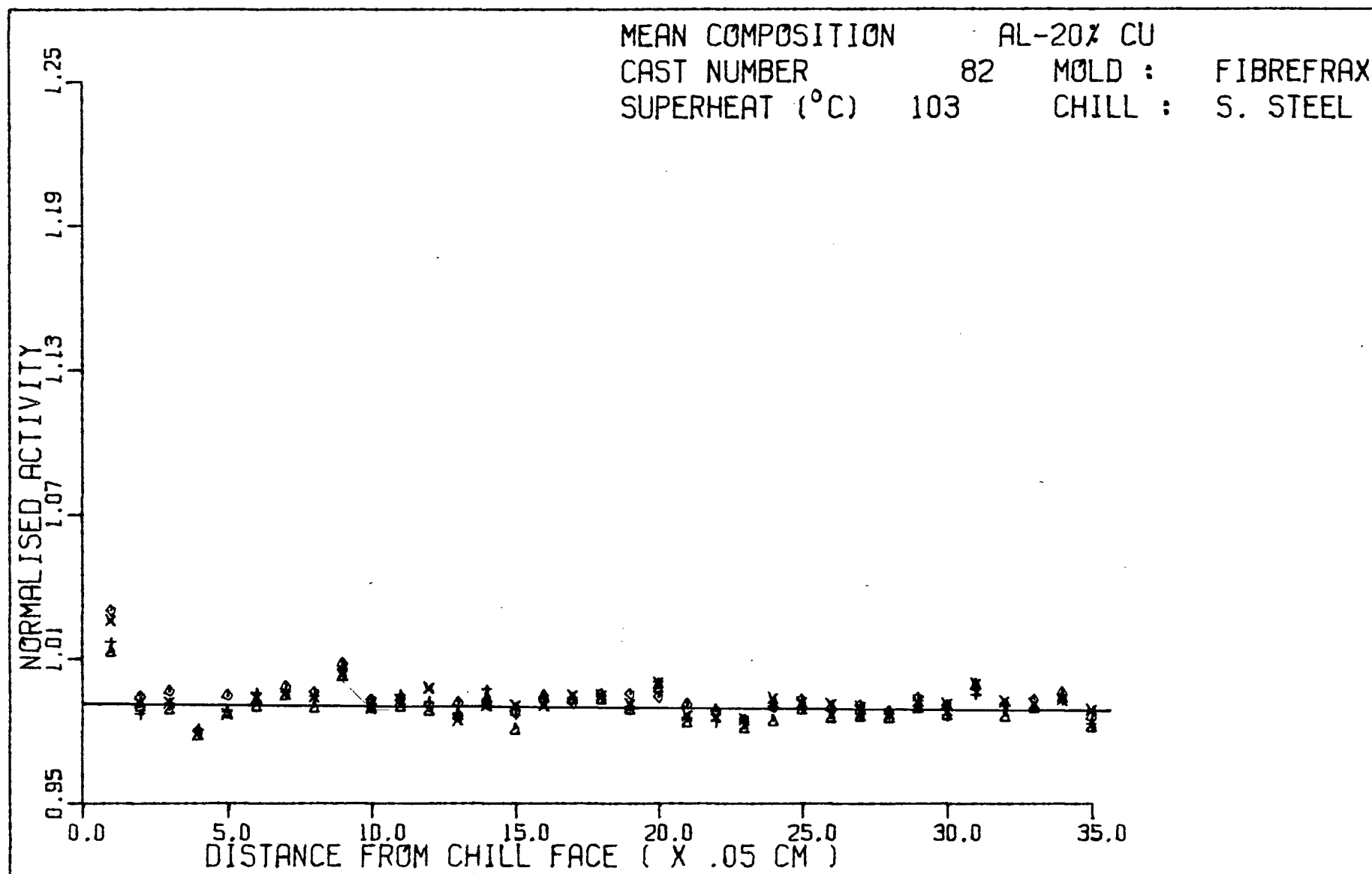
MEAN COMPOSITION ‎ AL-20% CU
CAST NUMBER 82 MOLD : FIBREFRAX
SUPERHEAT (°C) 103 CHILL : S. STEEL

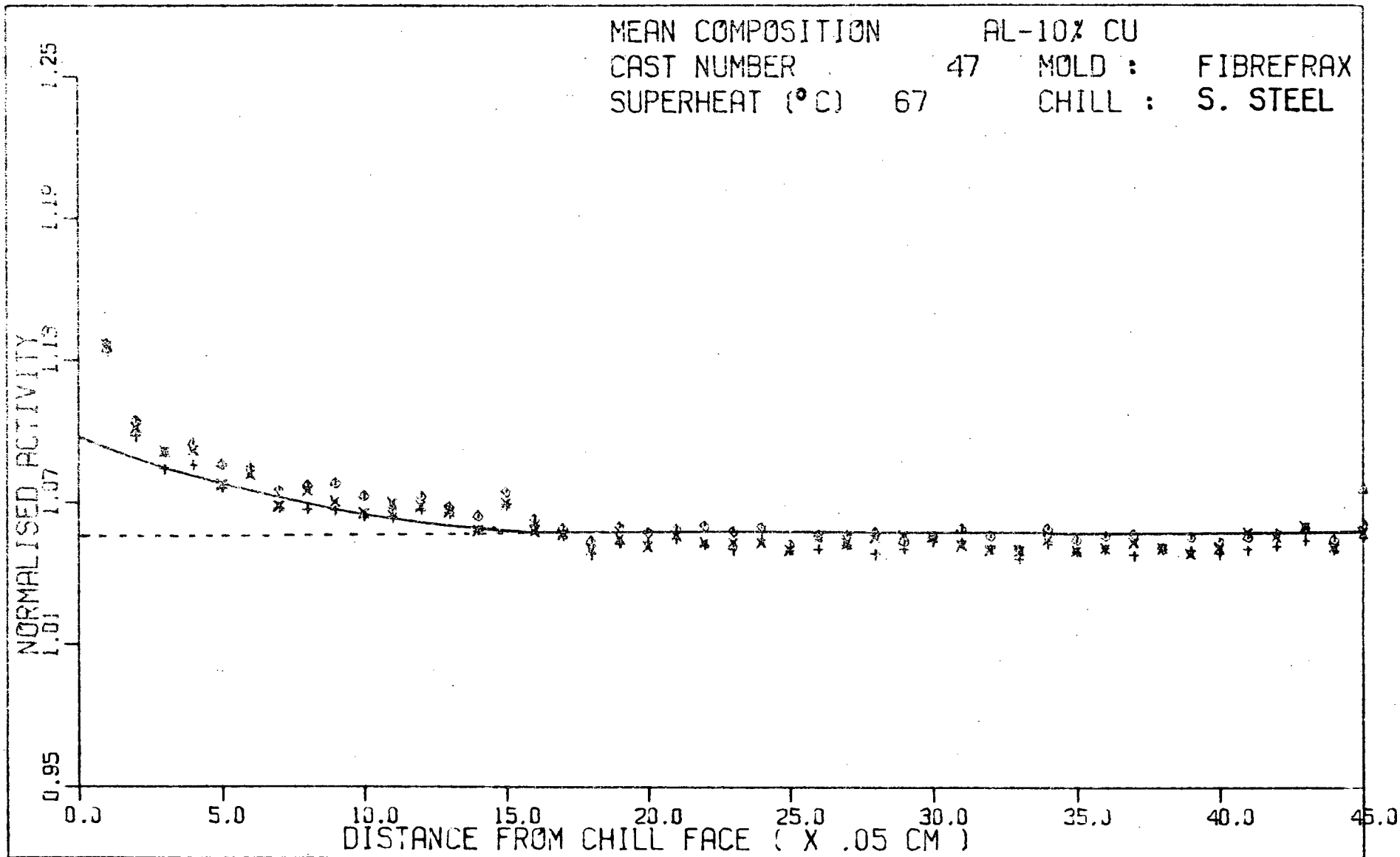Fig. 34   Normalized activity vs distance from the chill face for the composition and casting conditions indicated.

Fig. 35 · Normalized activity vs. distance from the chill face for the composition and casting conditions indicated.

grain size. Comparison of Figure 37 with Figure 30, the equiv-
alent melt without the addition of the grain refiner, shows that
the two curves are essentially equivalent, with the exception of
the point for the section at .25 cm. at the chill in Figure 37,
which is low. This drop in the concentration in this region may be
attributed to the drop in the solute concentration resulting
from the feeding of the interdendritic liquid from this region
towards the chill face during solidification. The addition of the
TiB_2 to the melt, therefore, does not significantly change the
extent of the segregation at the chill.

To determine whether changing the structure during solidif-
ication would affect the segregation, a casting was made in which
the columnar growth was disturbed at a distance of 2.5 cm. from
the chill. The resulting composition distribution curve is shown
in Figure 36. Comparing this curve to the equivalent curve for
a normally cast ingot, shown in Figure 28, it is observed that the
two curves are essentially similar. Accordingly, it is seen that
changing the cast structure near the chill during the solidifica-
tion does not influence the segregation near the chill zone.

The segregation in the chill zone for the Al-10% Cu alloy
which was degassed is shown in Figure 21. Segregation is clearly
evident, and more extensive than in normal casting. This would
suggest that the presence of fine pores in the casting reduces
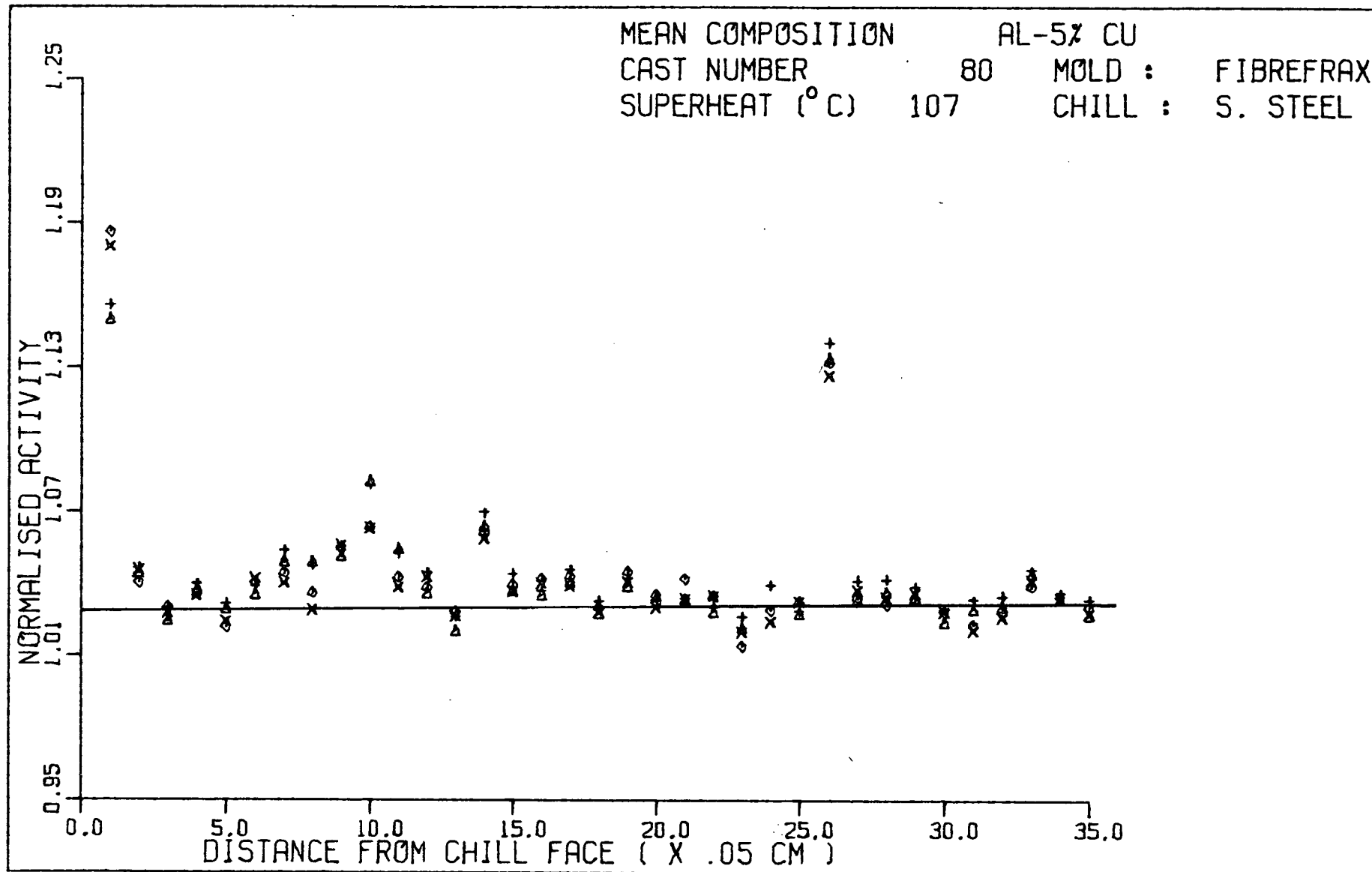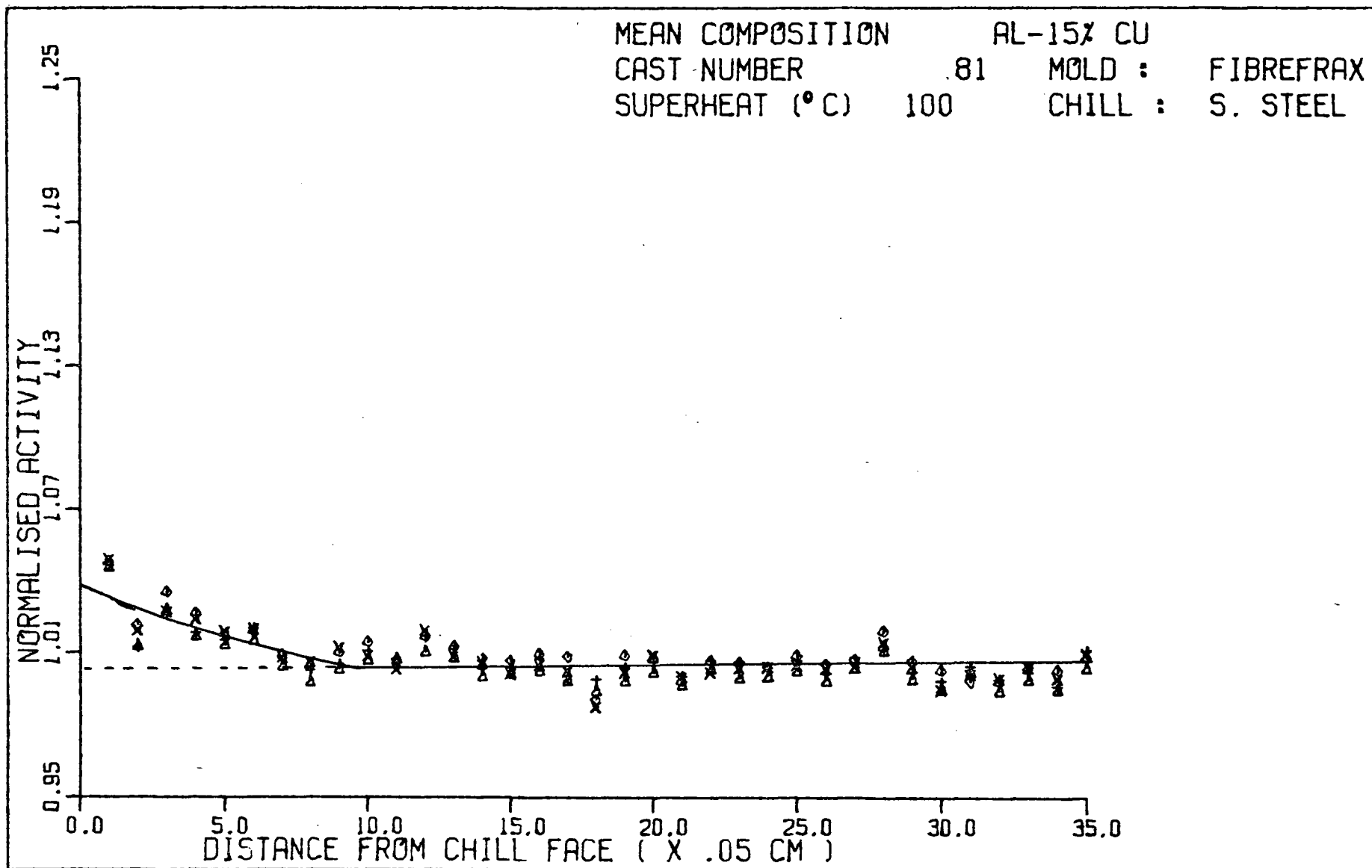the extent of segregation in the chill zone.

Fig. 36   Normalized activity vs.distance from the chill face for the composition and casting conditions indicated.

Fig. 37   Normalized activity vs. distance from the chill face for the composition and casting conditions indicated.

3.6   Saturation effects in the scintillation counter

Saturation effects in the counter, caused by high activity
of the radioactive samples, was investigated by counting samples,
initially possessing a high activity, and then again, later,
when the samples had decayed to lower activity levels. The results
of these tests are shown in Figures 38, 39, and 40, the only var-
iable being the counting time for each sample.

The initial rate of 700,000 counts in 6 seconds gave the
curve for the normalized activity versus distance from the chill
shown in Figure 38. At lower counting rates of 500,000 counts in
12 seconds and 500,000 counts in 60 seconds for the same samples,
the curves shown in Figures 39 and 40 were obtained. The decay
time between Figure 22 and Figure 24 is equivalent to four half
lives of the isotope.

It is noticed from these Figures that the high counting rate
employed in the first case has led to the saturation of the
detectors, thus giving erroneous values for the activities measured
at different times. In the other two cases, employing intermed-
iate and low counting rates, it is seen that the normalized activ-
ity distributions are nearly similar, no significant improvements
in the measurements resulting from the use of the much lower
counting rates employed in the third case. Use of this low count-
ing rate, would, in addition, lead to a greater error in the
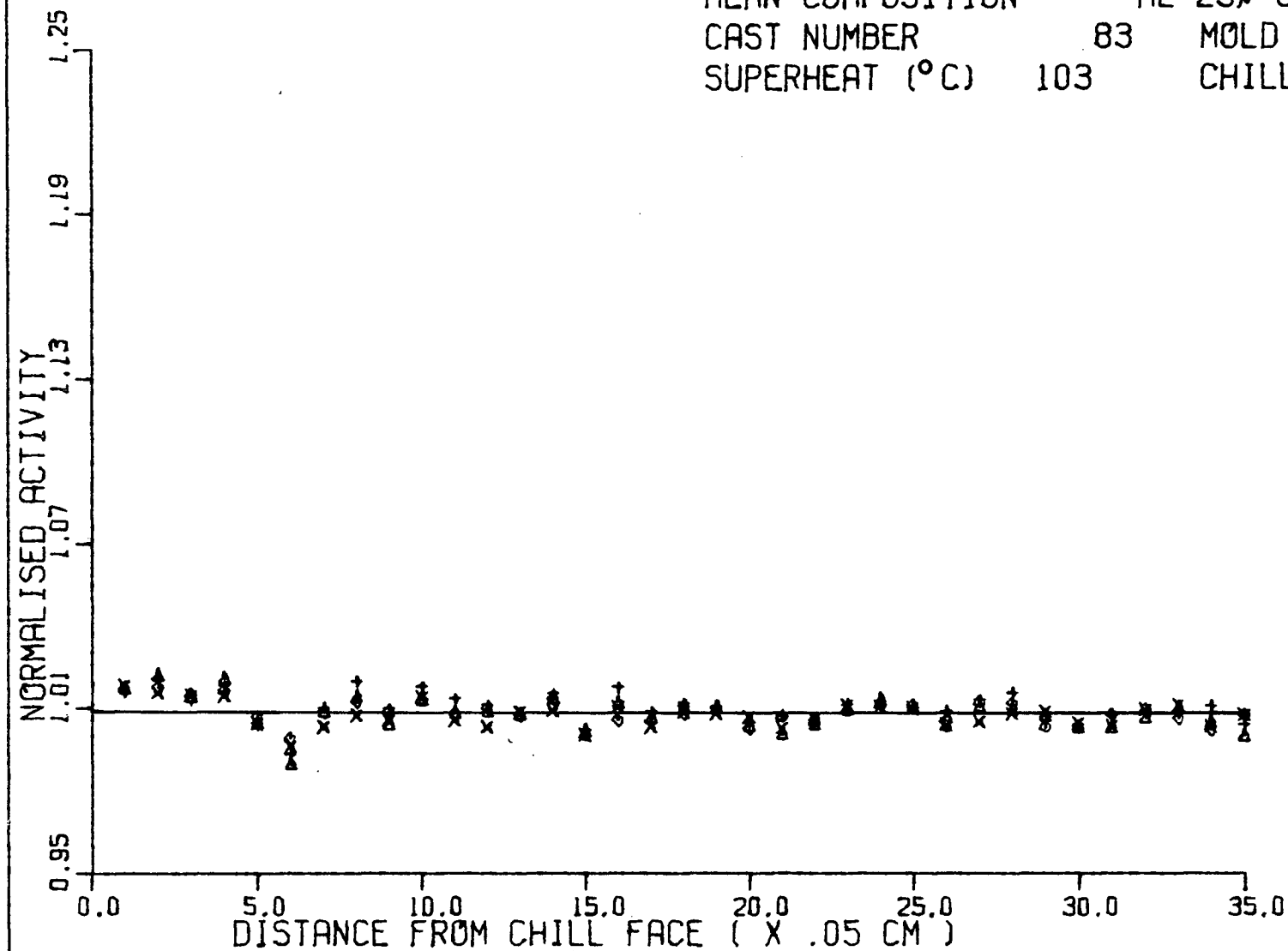activity measurement, since the sample would decay during the
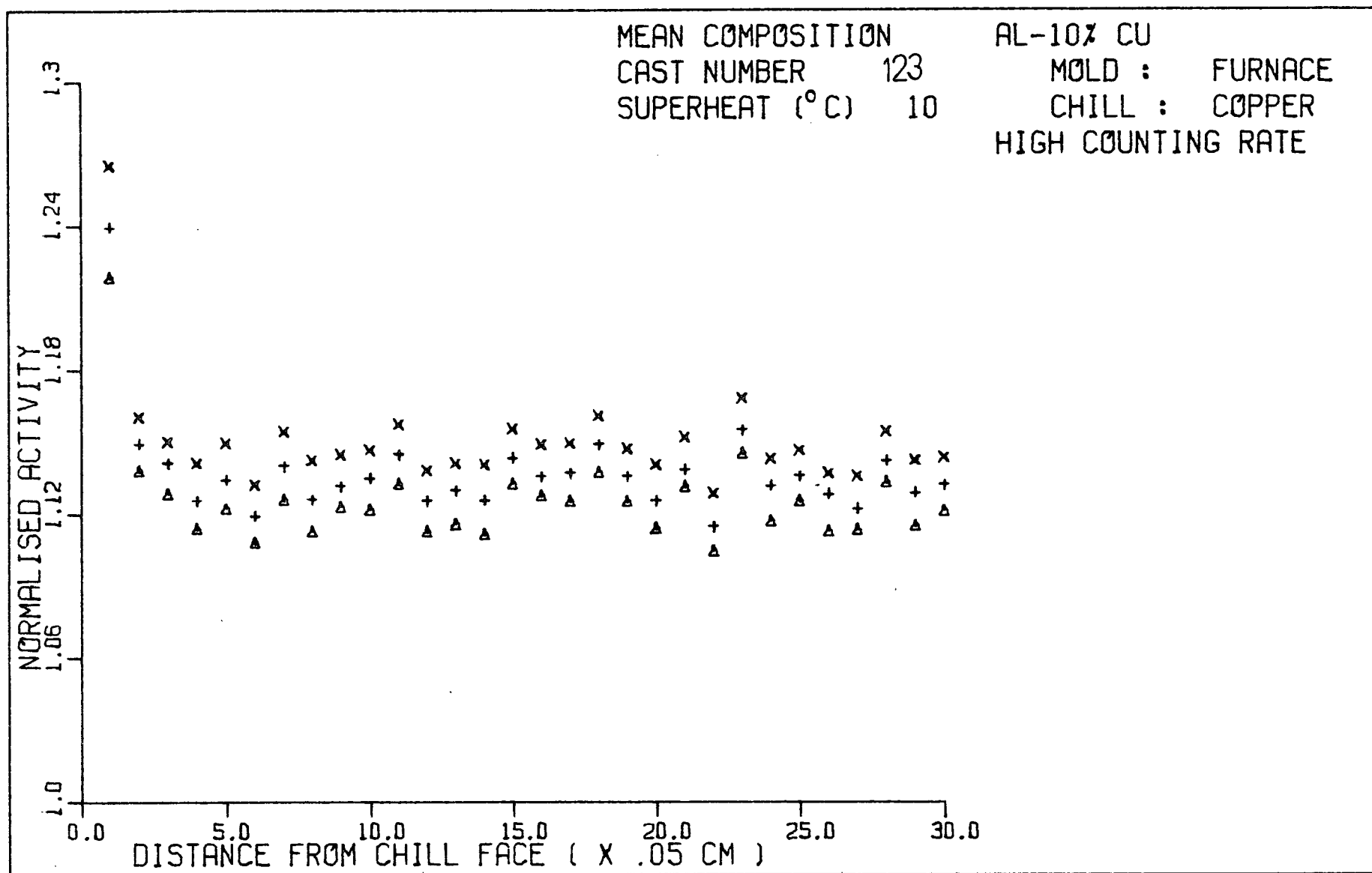
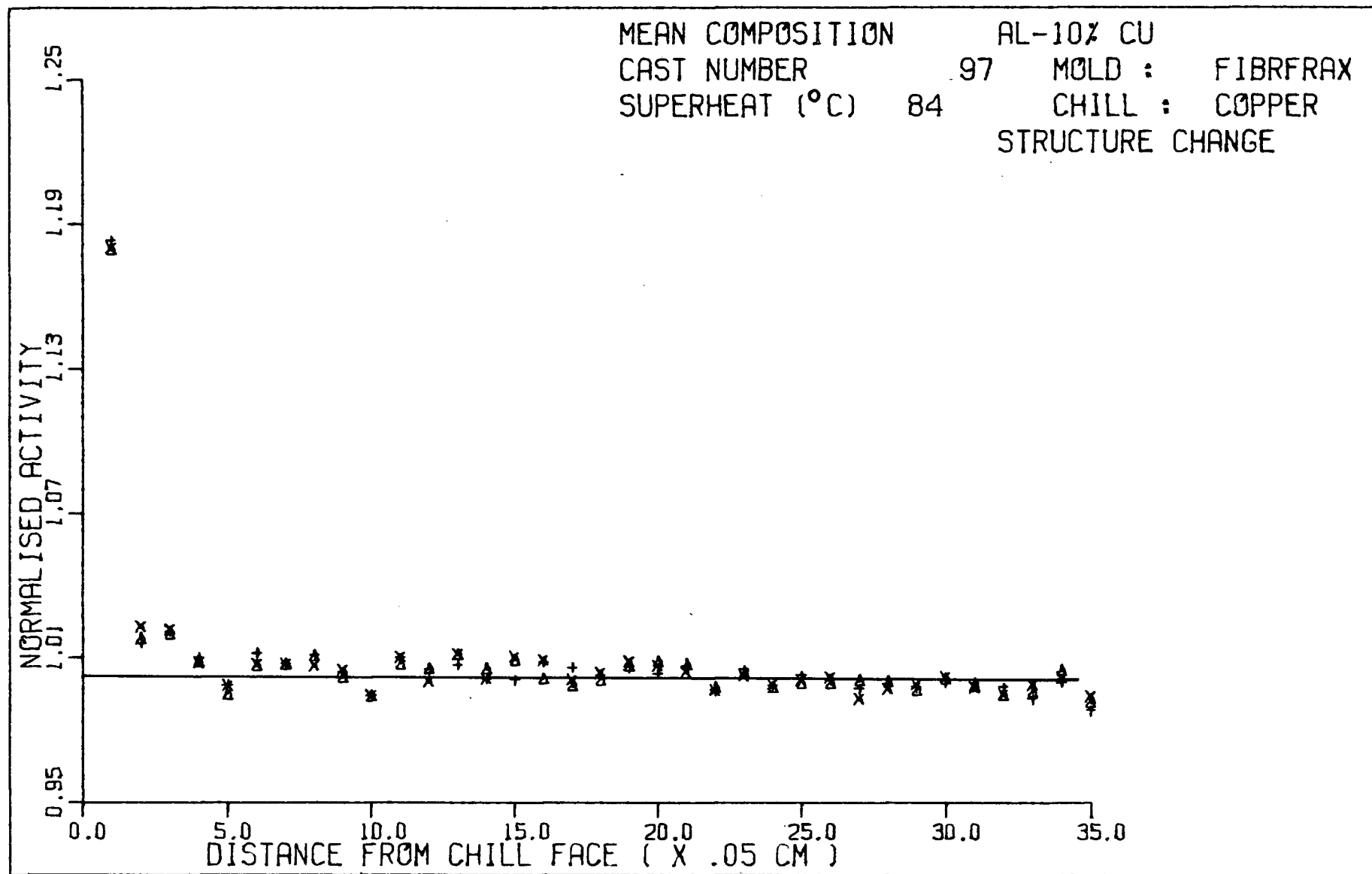Fig. 38   Normalized activity vs. distance from the chill face for the composition and casting conditions indicated.

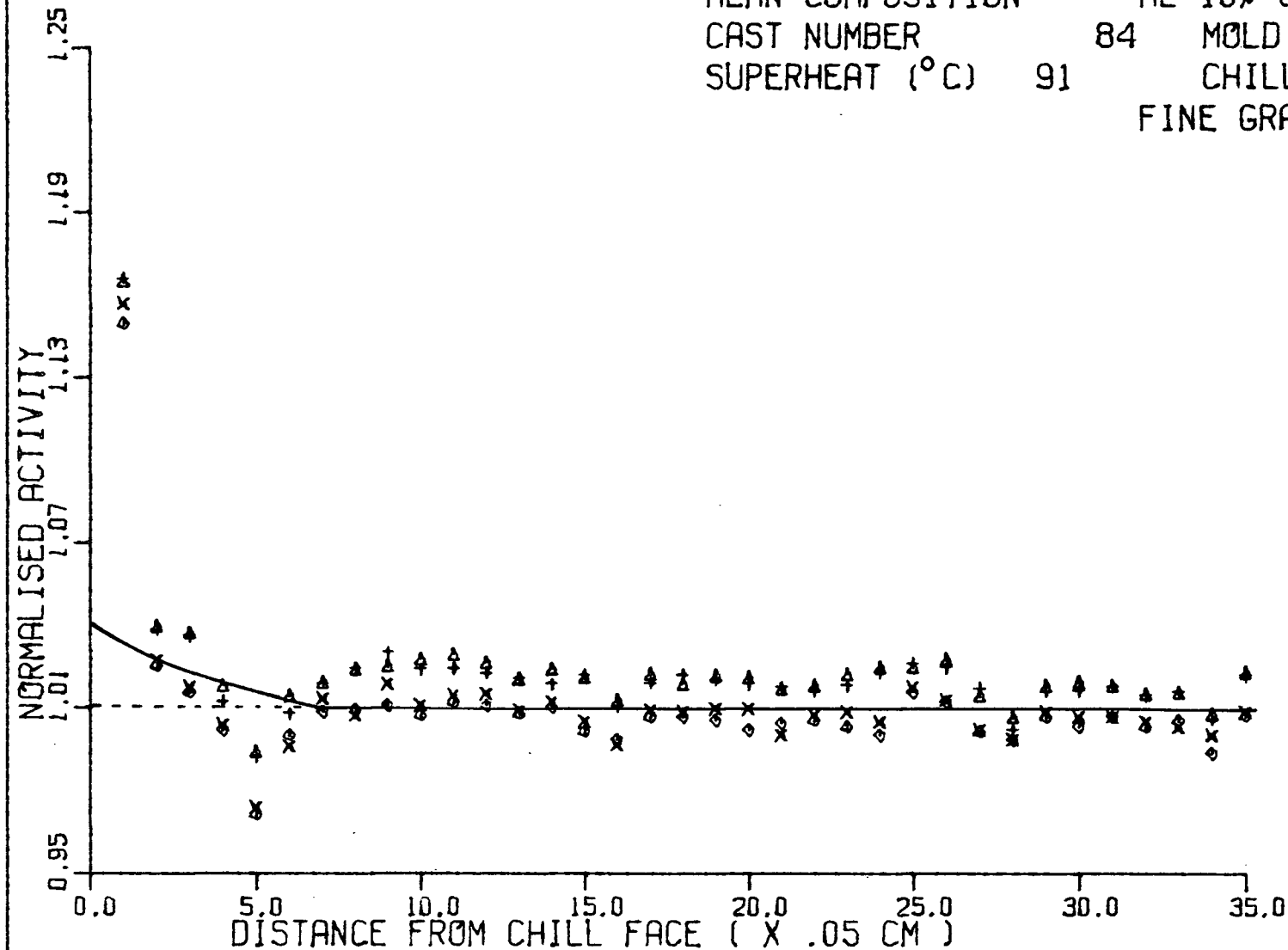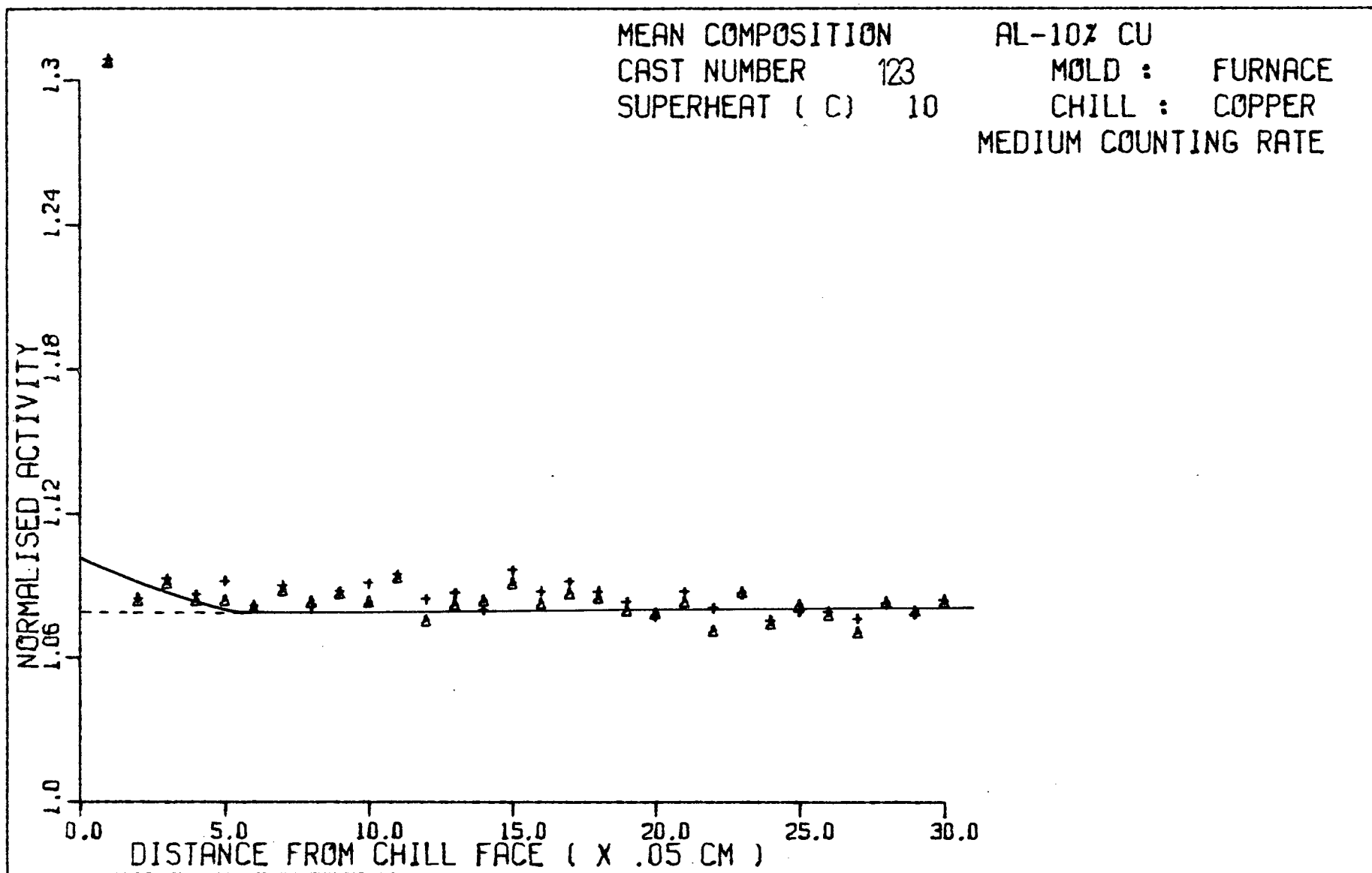Fig. 39   Normalized activity vs. distance from the chill face for the composition and casting conditions indicated.
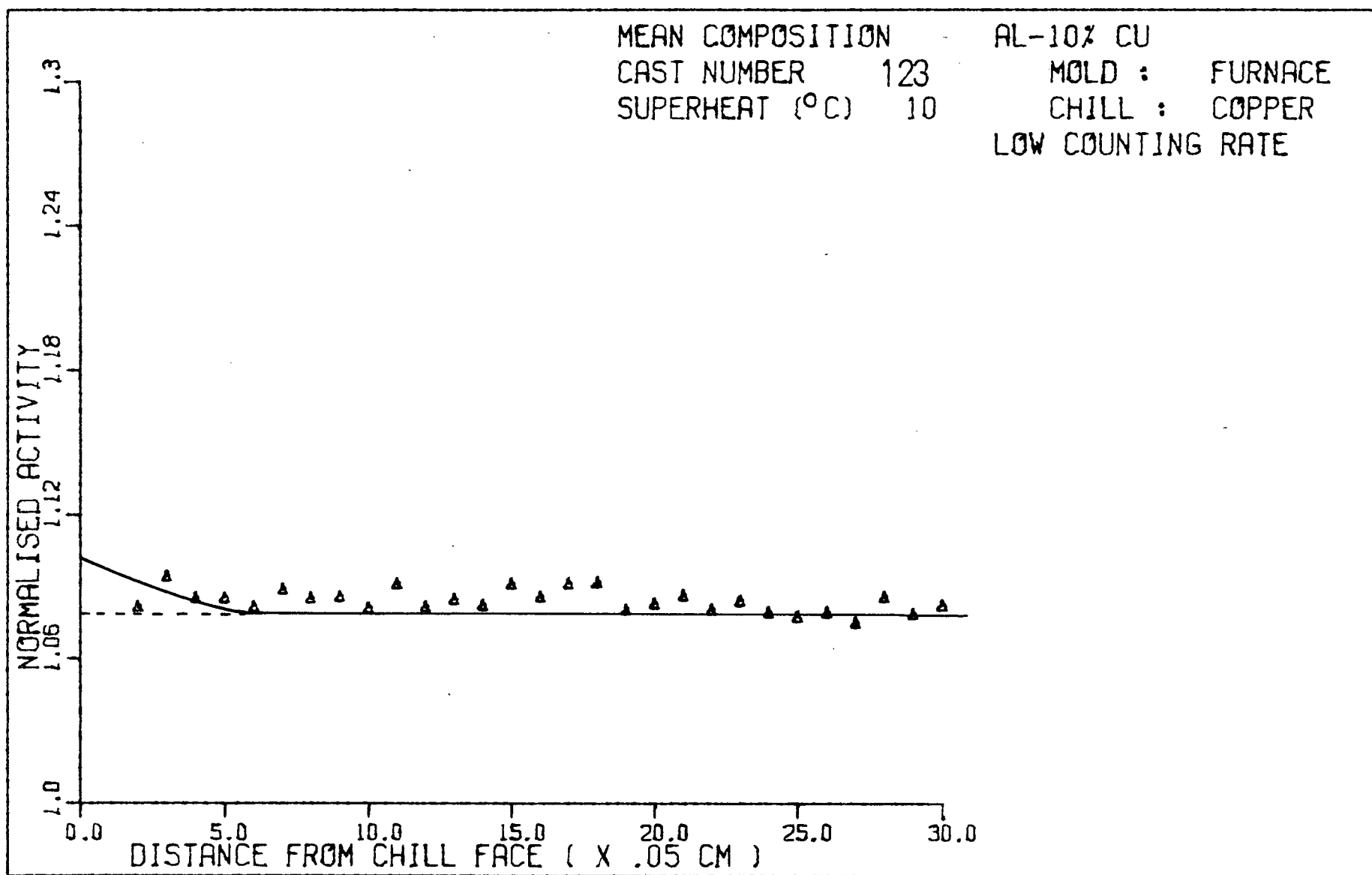
Fig. 40   Normalized activity vs. distance from the chill face for the composition and casting conditions indicated.

counting period, which is a factor that is not corrected for in the calculation of the normalized activities.

3.7 Temperature distributions in the casting during solidification

Temperature measurements were not made on the castings in which Cu^{64} was added in order to relate the freezing conditions directly to the measured segregation. The temperature measurements required the insertion of a series of thermocouples in the casting which would have seriously interfered with the machining of the casting to obtain suitable sample cuttings. As an alternative, castings without Cu^{64} were made under apparently identical conditions with thermocouples, and the results compared to the corresponding castings containing Cu^{64}. An example of the variation of temperature with time at five different positions in the casting are shown in Figure 41 for an Al-10% Cu alloy. The curves rise rapidly initially, indicating fast and uniform response of the thermocouples and the recording equipment to rapid thermal changes. From the curves of Figure 41, the temperature distribution across the casting can be plotted as a function of the distance from the chill at progressively increasing times. The results are shown in Figure 42. At any given time the solid-liquid zone in the casting can be considered to be the portion of the casting between the equilibrium liquidus and eutectic temperatures for this alloy. Accordingly, it is evident in Figure 42
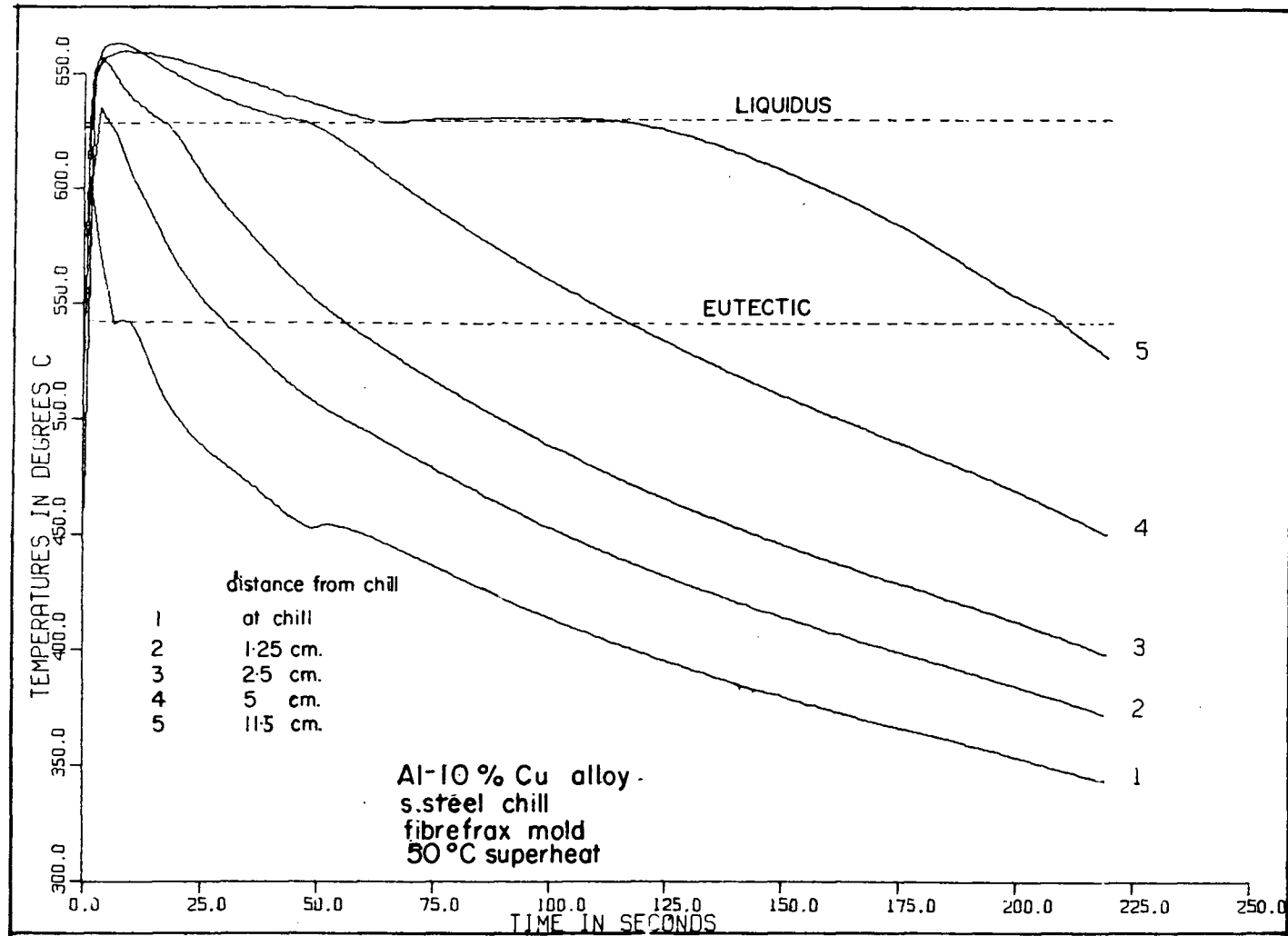
Fig. 41   Cooling curves for an Al-10% Cu ingot under the casting conditions indicated.
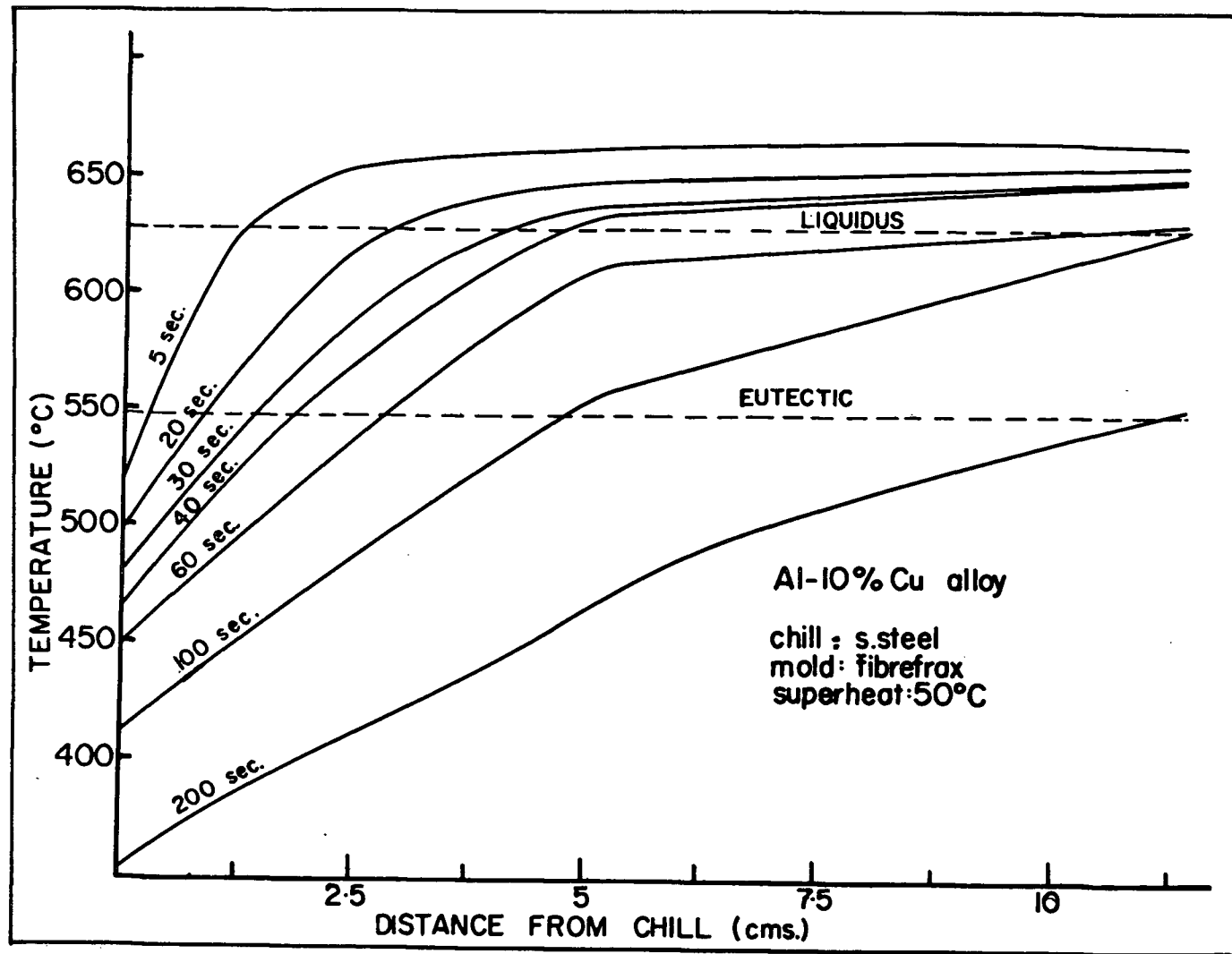
Fig. 42   Temperature distributions in a solidifying Al-10% Cu ingot cast under the conditions indicated.

that the solid-liquid zone increases in length with increasing time after casting, varying from a length of .95 cm. 5 seconds after casting, to 7.5 cm., 60 seconds after casting.
No reheating (which would result from separation of the casting from the chill) of the ingot at the chill face was observed.

The advance of the solid-liquid interface during unidirectional solidification may be assumed to relate to time following the relationship[15],

$$x = A_2(t)^{\frac{1}{2}}$$

where x is the distance from the chill and t is the elapsed time, A_2 being a constant. To determine if this is applicable in the present case, the eutectic temperatures obtained from the cooling curves was plotted as a function of $t^{\frac{1}{2}}$ for four ingots cast on a copper chill, giving the results shown in Figure 43. Corresponding results for ingots cast on a stainless steel chill are given in Figure 44. All the curves are linear in the initial part of the ingot showing that the assumed relationship is applicable in this region and is consistent with the directional solidification of the casting. The liquidus curves do not pass through the origin, because of the superheat of the melt and difficulties in establishing the precise time at which the solidification commenced. The deviation of the curves from linearity in the later stages of solidification is a result of non-directional solidification and
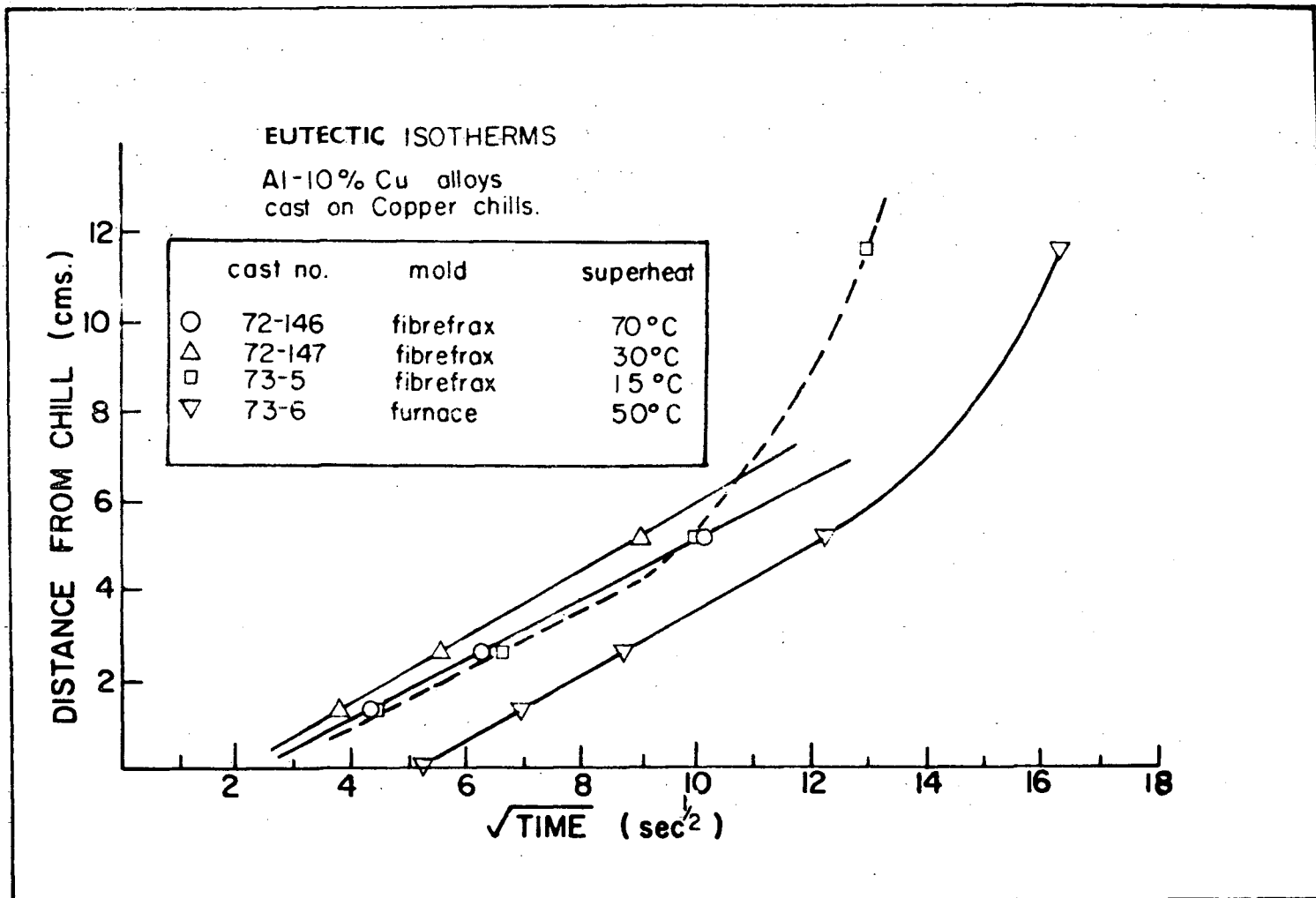
Fig. 43   Movement of eutectic isotherms for Al-10% Cu ingots cast under the conditions indicated.
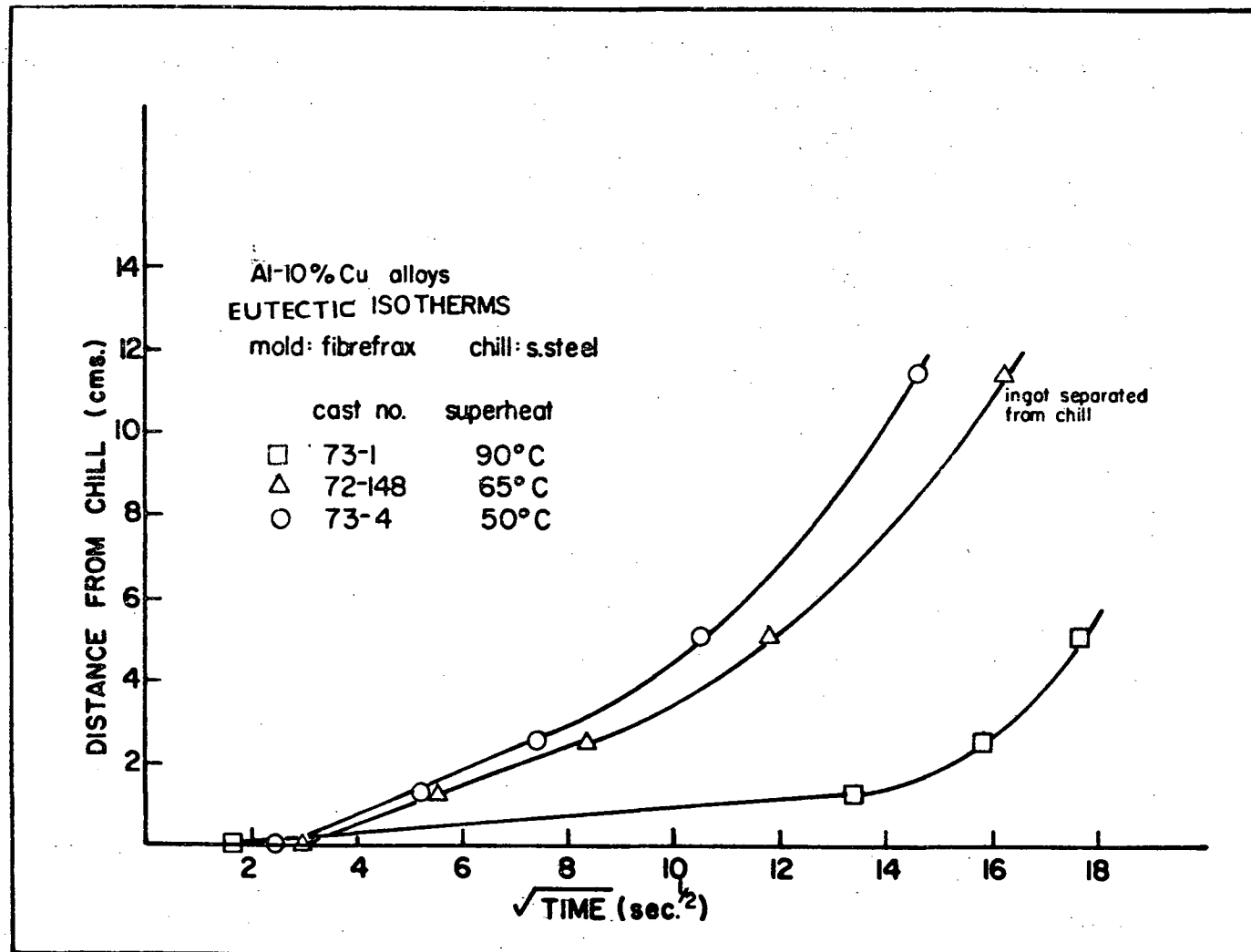
Fig. 44   Movement of eutectic isotherms for Al-10% Cu ingots cast under the conditions indicated.

heat losses from the top surface of the liquid in the mold. Also, the relationship would hold only if the temperature of the chill face is constant, and it is seen from cooling curves that this is not the case for these ingots.

Seven ingots were cast containing thermocouples under a variety of casting conditions, as listed in Table IV. From the temperature measurements the gradient of the temperature in the solid-liquid region G_S was determined (this is when the eutectic temperature is just reached by the chill face), and the length of the solid-liquid zone L_M, as listed in the Table. Using the linear portion of the

$$x = A_1 + A_2(t)^{\frac{1}{2}}$$

curves, where A_1 is the intercept of the curve with the abcissa, the values of A_1 and A_2 were determined as shown in Table IV. The cooling rates and the freezing rates obtained from the temperature data are also listed.

It is seen from Figure 43 that all the curves for the alloys cast in the Fibrefrax molds are quite close, the only significant difference being the displacement of the curves from one another due to the different values of A_1. Due to the difficulties in establishing the exact time of the start of solidification, these values could be slightly in error. However, it would be expected that for the ingots with larger superheats, the values of A_1 would increase. Though this is the case for ingots 146 and 147, the

TABLE IV

TEMPERATURE MEASUREMENTS

Al-10% Cu ALLOYS

CAST NUMBER	CHILL	MOLD	SUPERHEAT °C	G_s °C/cm.	i_M cm.	A_1 (sec.)$^{\frac{1}{2}}$	A_2 (sec.)$^{\frac{1}{2}}$	FREEZING RATE AT 1.25 CM. cm./sec.	AVERAGE DENDRITE ARM SPACING, μ	COOLING RATE - LOCAL SOLIDIFICATION TIME AT 1.25 CM. (sec.)	COMMENTS
72-146	Copper	Fibrefrax	70°C	74	1.08	2.6	.25	.66	26	15	
72-147	Copper	Fibrefrax	30°C	32	2.5	2.1	.25	.84	28.7	14	
73-5	Copper	Fibrefrax	15°C	70	1.77	3.0	.25	.625	30.8	20	
72-148	Stainless	Fibrefrax	65°C	42	1.9	3.0	.36	.417	31.7	25	separated from chill
73-1	Stainless	Fibrefrax	90°C	140	.57	1.7	.41	.069		150	
73-4	Stainless	Fibrefrax	50°C	64	1.25	2.4	.25	.464	28.2	22	
73-6	Copper	Furnace	50°C	20	3.9	5.3	.25	.26	39.4	45	

value of A_1 for ingot 73-5 is much larger than the value obtained

for the abovementioned ingots. The same effect of decreasing A_1

with increasing superheat is found to exist in Figure 44 for the

ingots cast on the stainless steel chills. The ingot 148

separated from the chill on solidification, and therefore shows

a result different than expected.

It has been shown that the solidification rate is related

to the dendrite arm spacing in the casting[16]. To determine how

the dendrite spacing varies with cooling rate in the present case,

transverse sections of the castings used in the temperature

measurements were made at 1.25 cms., from the chill and the

dendrite arm spacing measured on the polished and etched surfaces.

Examples of the dendritic structures of two ingots cast on copper

chills are shown in Figure 45: (b) fibrefrax mold, and (a) furnace

cast. The dendritic structure of (b) is appreciably finer than

that of (a), consistent with the higher freezing rates and steeper

gradients in the first casting. Values of the average dendrite

arm spacings for the seven castings are listed in Table IV.

The dendrite arm spacings are observed to vary appreciably

with casting conditions. The dependence of the spacing on the

superheat is shown in Figure 46, for ingots cast on the copper and

stainless steel chills.

The dendrite arm spacing is observed to progressively decrease

with superheat, with little differences between the copper and the

stainless steel chills. Much larger spacings were observed for the
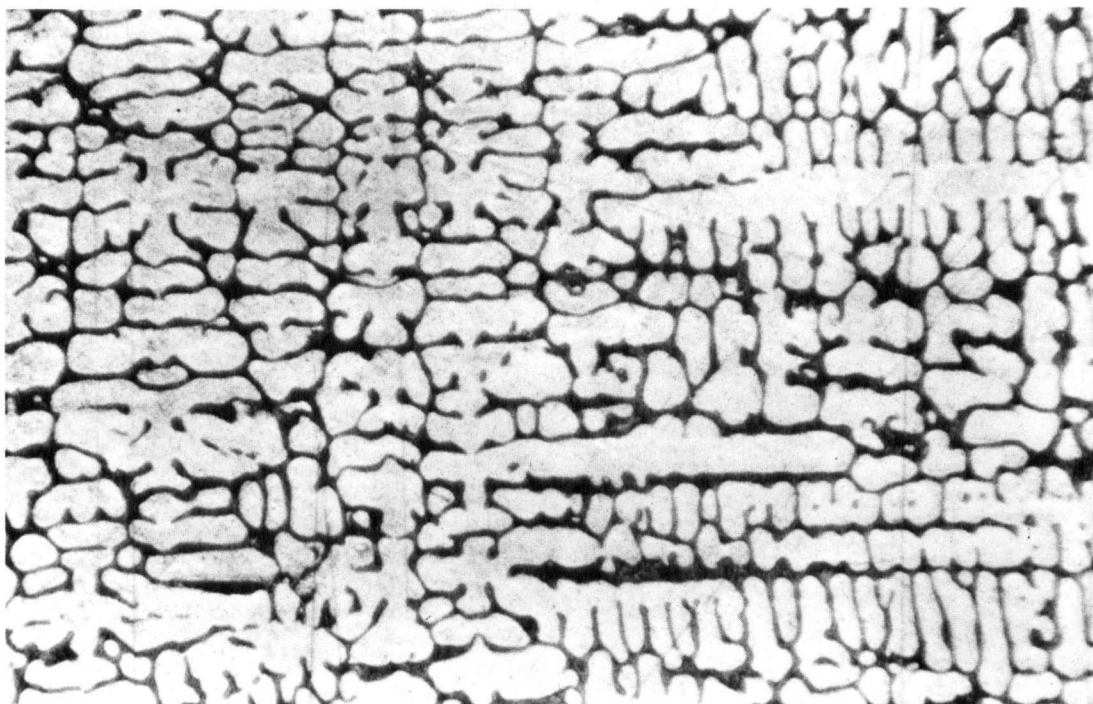
a
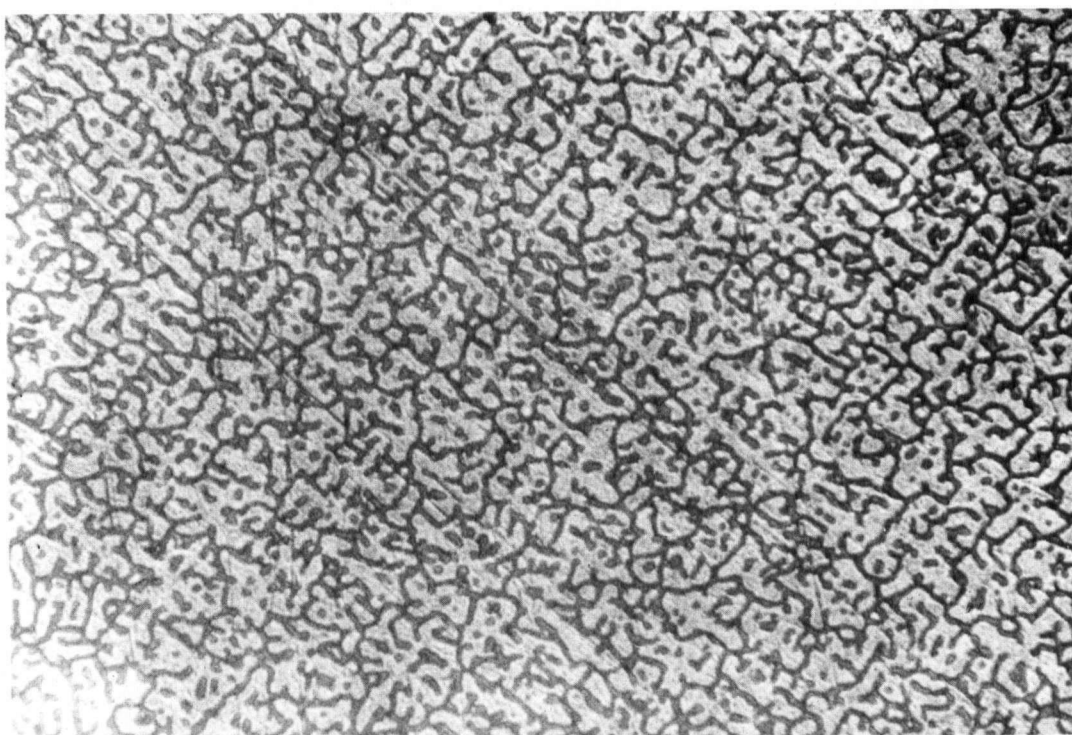
b

Fig. 45   Microstructures of sections parallel to the chill face for Al-10% Cu
          ingots
          (a) cast in the furnace (procedure (a))   100X
          (b) cast in fibrefrax molds   100X
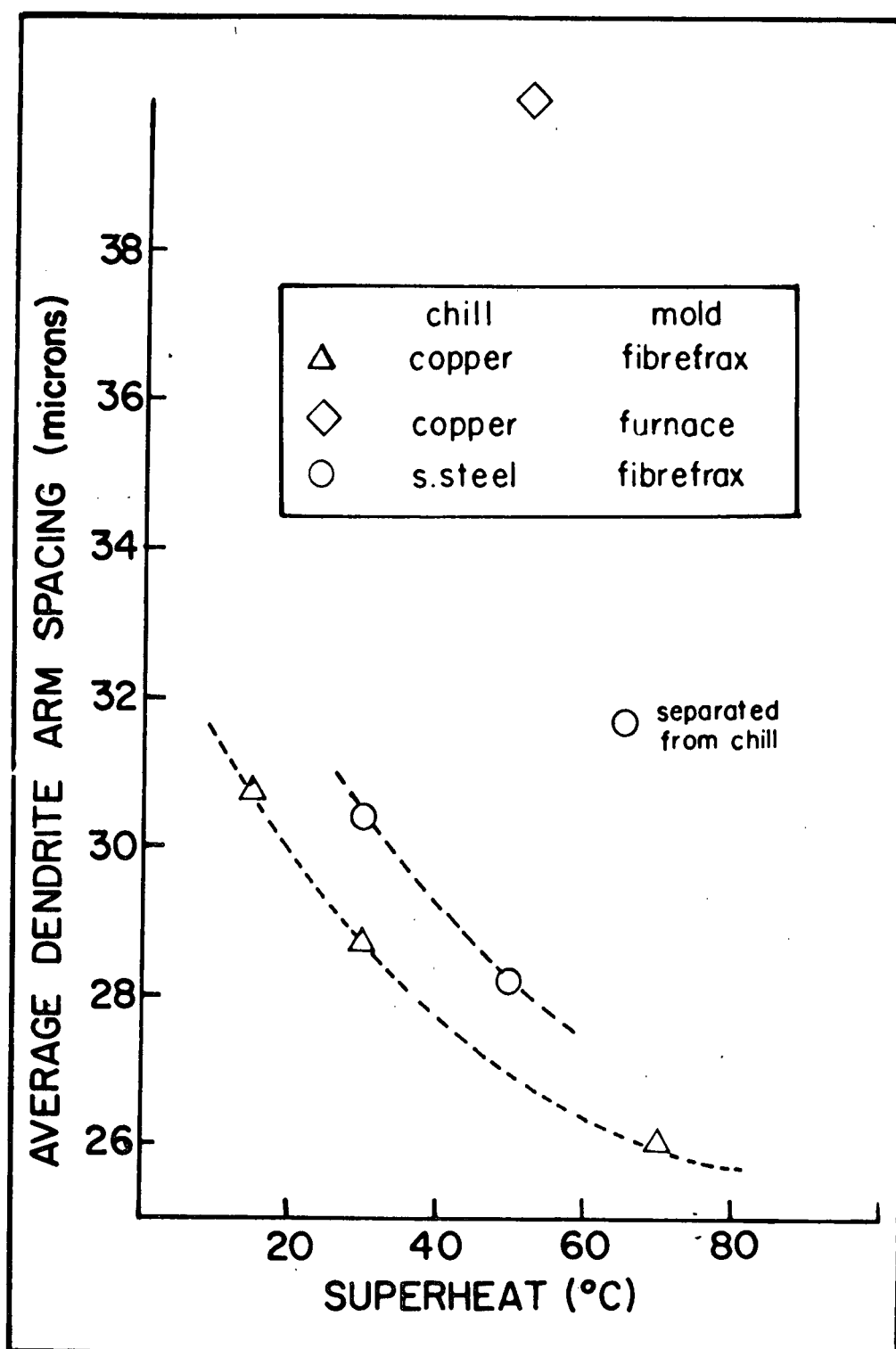
Fig. 46   Dendrite arm spacing vs. superheat for Al-10% Cu ingots cast under the conditions indicated.
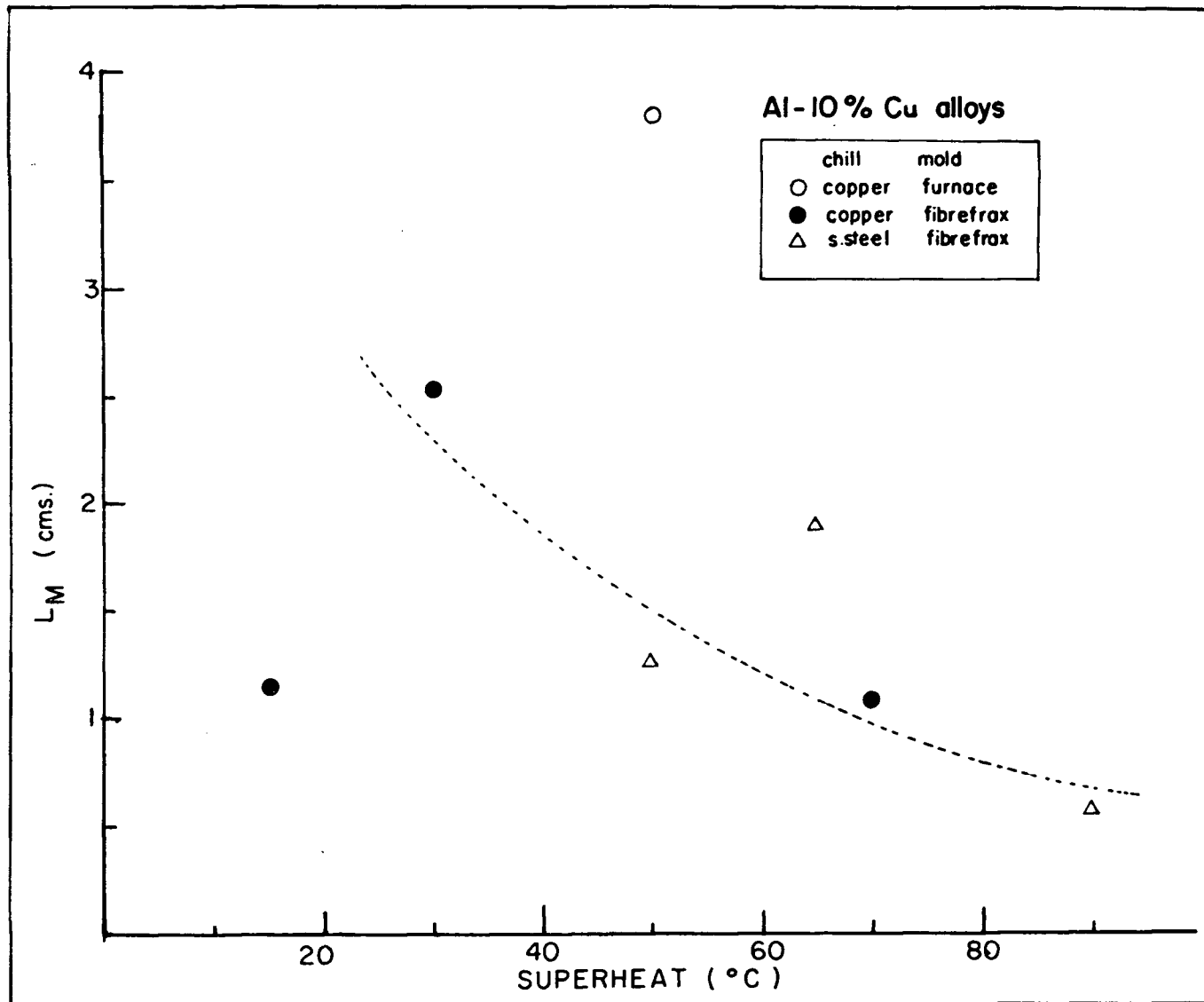
Fig. 47 L_M vs. Superheat for Al-10% Cu ingots cast under the conditions indicated.

furnace cast ingot at about 50° superheat, as compared to casting in fibrefrax molds. An appreciably larger dendrite arm spacing was observed when the ingot separated from the chill during solidification. The variation in the length of the solid-liquid region L_M with superheat is shown in Figure 47. Increasing the superheat progressively reduces the value of L_M for both the copper and stainless steel chills, the values for the two chills being essentially the same. The results for ingot 73-5 may be erroneous due to difficulties encountered during the measurement of the temperature distributions.

3.8 Chemical analysis of ingot samples

The purpose of conducting chemical analysis on a series of samples which had been counted was to establish the correlation between the changes in the measured activity with changes in the copper concentration. It is assumed that the radioactive copper atom is the same as a normal copper atom in this case and the radioactive atoms are uniformly distributed throughout the alloy.

The results of chemical analyses of samples taken from three castings are shown in Figures 48, 49, and 50, superimposed on the normalized activity measurements of the same samples. To plot the chemical analysis results in the same way, the copper concentration values obtained were normalized by copper concentration obtained from the same melt samples used for the activity measurements. Only one analysis was done for any one ingot sample
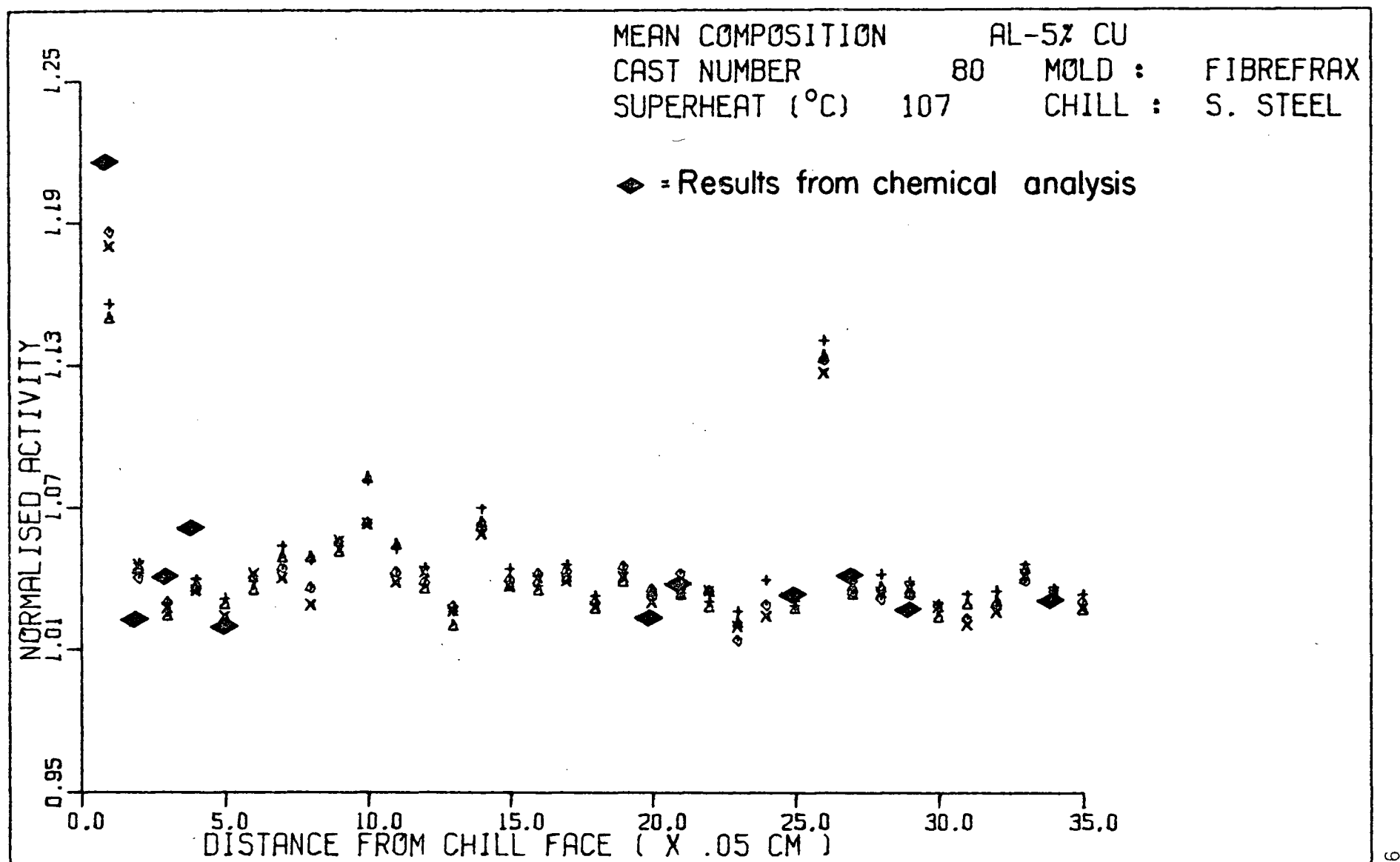
Fig. 48   Normalized concentrations from chemical analysis superimposed on the normalized activity distribution.
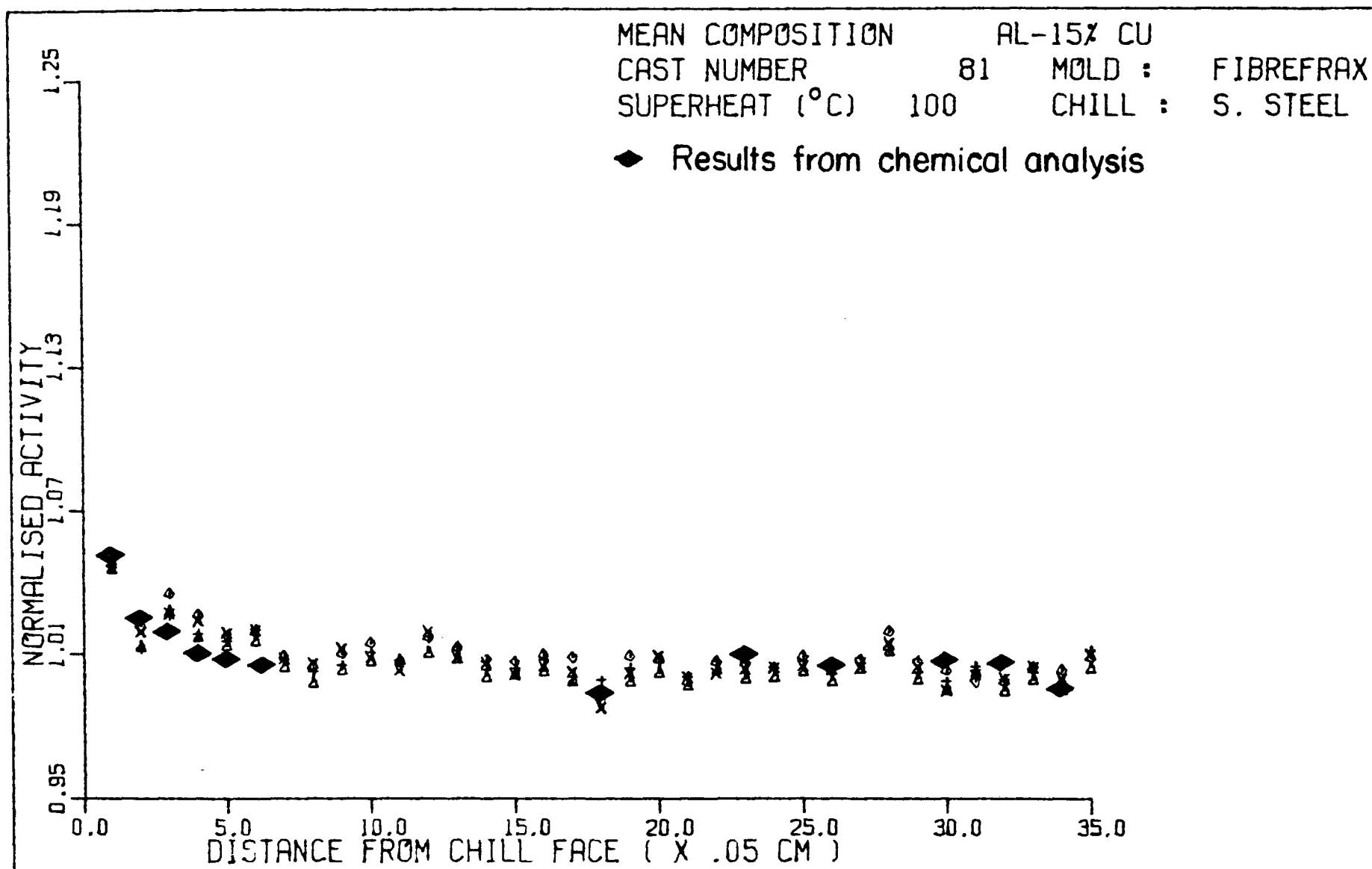
Fig. 49   Normalized concentrations from chemical analysis superimposed on the normalized activity distribution.
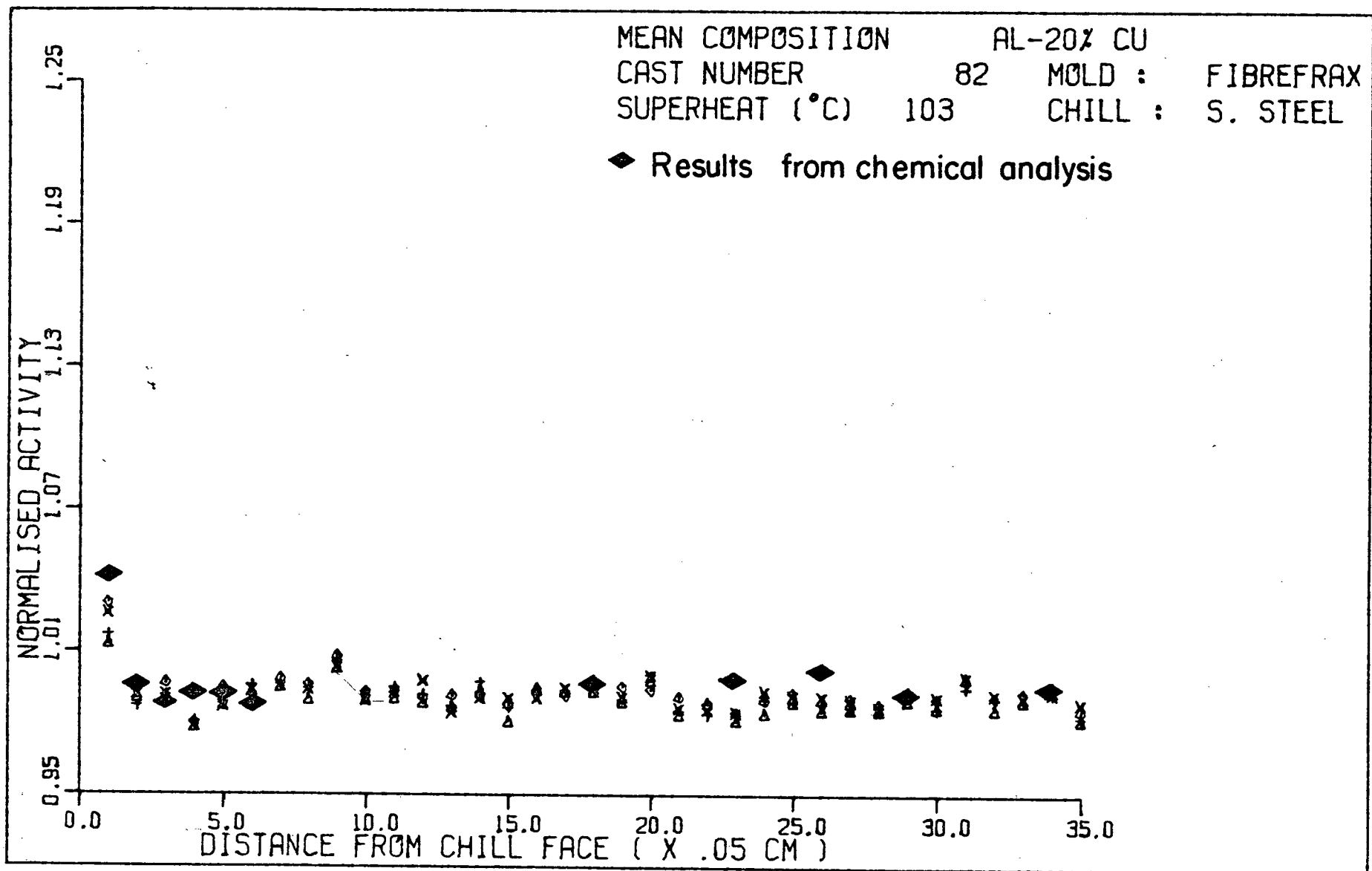
Fig. 50   Normalized concentrations from chemical analysis superimposed on the normalized activity distribution.

since only one gram of material was available per sample. As such, the magnitude of errors in the measurement could not be established.

From Figures 48, 49, and 50, it is apparent that there is no significant difference between the normalized concentrations obtained either from the activity measurements, or by chemical analysis. As such the correspondence of the normalized concentrations was taken to be one-to-one and it was concluded that the activity of the sample containing the radioactive copper is proportional to the concentration of copper in the sample, in all further tests.

3.9 Inverse segregation in Al-Ag alloys

The variation of activity with increasing distance from the chill face for Al-10% Ag and Al-15% Ag ingots cast on copper chills in fibrefrax molds at superheats of 50°C are shown in Figures 51 and 52. In Figure 51, it is seen that there is an initial point with very high activity, which would be caused by the presence of exudation on the chill face of the casting. There is a solute depleted region immediately adjacent to this point, and the composition increases to a steady value towards the interior of the ingot. There is no region clearly showing an increase in composition near the chill face. In view of the criteria used in measuring the chill face segregation for the Al-Cu alloy ingots, it is seen that there is no chill face segregation evident in
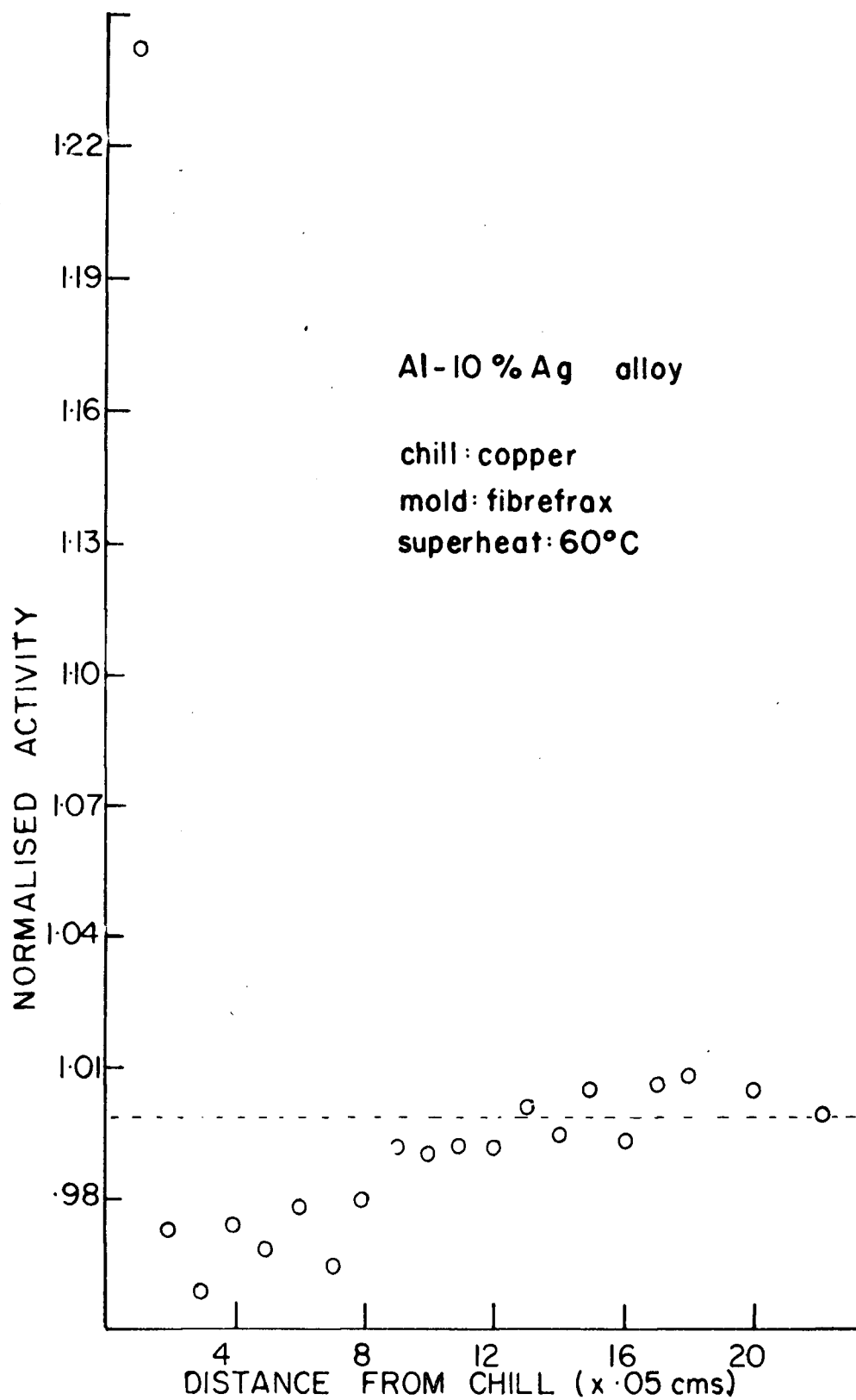
Fig. 51   Normalized activity vs. distance from the chill for an Al-10% Ag ingot.
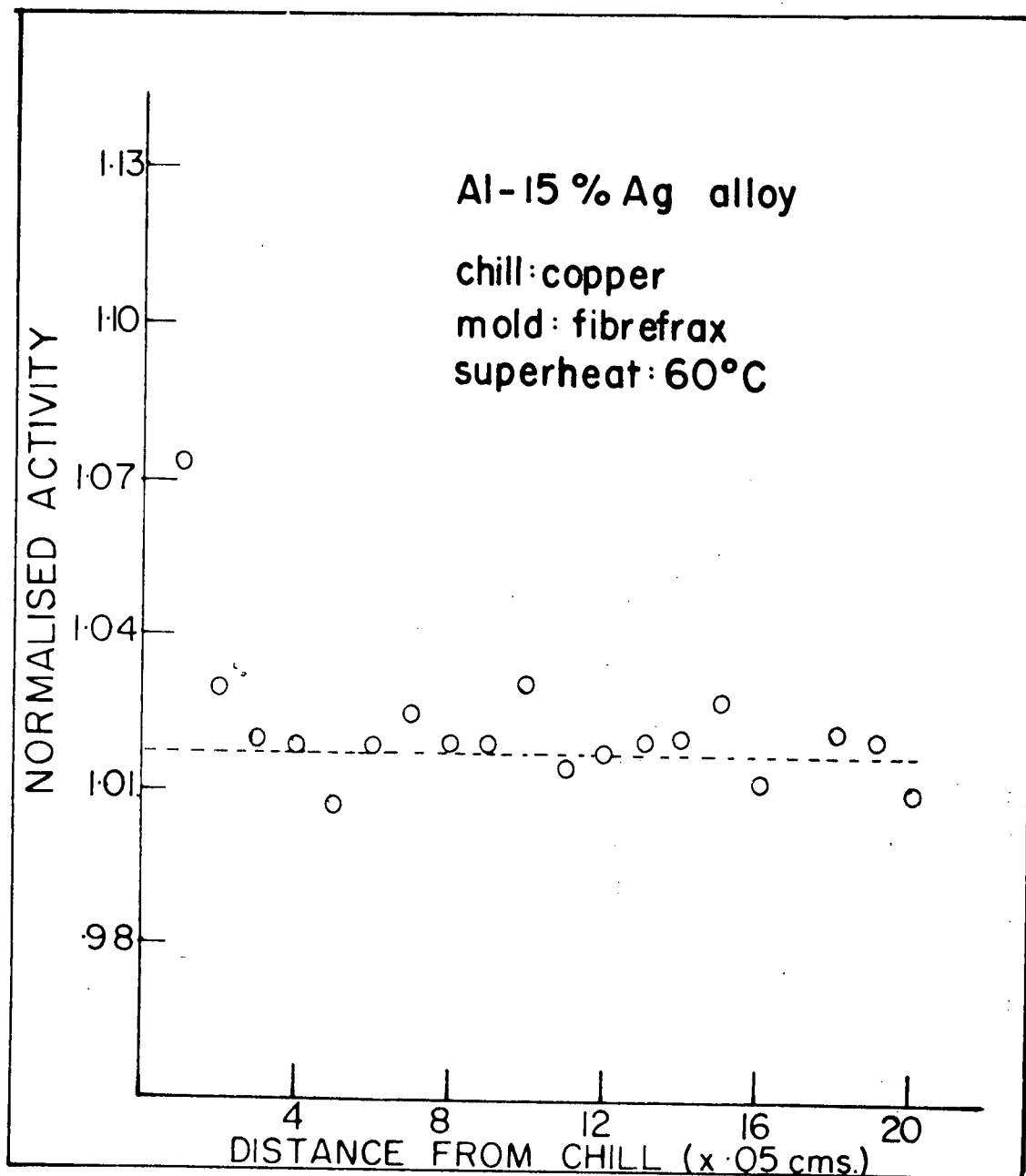
Fig. 52   Normalized activity vs. distance from the chill for an Al-15% Ag ingot.

this ingot.

In Figure 52 for the Al-15% Ag alloy, it is observed that the composition is essentially constant, with a slight increase towards the chill face. This increase cannot be definitely attributed to the presence of chill face segregation in the ingot in view of the scatter of the measurements. As is the case with other castings, the first point adjacent to the chill shows a high activity due to the presence of exudations.

4.   DISCUSSION

In the Al-Cu system, the present results show that:

1. Maximum segregation occurs at the chill face of cast
    alloys.

2. The amount of segregation at the chill face is small.

3. The extent of the segregation away from the chill face
    is small.

4. The chill face composition is markedly dependent on:

    a) alloy composition

    b) melt temperature on pouring (superheat)

    c) temperature gradient in the cast material

The present results will be considered in detail, as they

relate to the observations and theoretical predictions reported

in the literature.

4.1 Scatter of the results

Kirkaldy and Youdelis[8] (Figure 3) report close agreement

between their experimental observations and the theoretical values

for maximum chill face segregation, with little experimental

scatter.

To obtain this fit, extrapolations were made on the basis

of only one or two experimental points and the results complicated

by the presence of exudations having a high alloy concentration at

the chill face. In the results summarized by Pell-Walpole[1],

appreciable scatter of results are reported in inverse segrega-
tion measurements as a function of alloy composition and other
casting variables.

In the present results, variations of the activity and con-
centration measurements for neighbouring specimens remote from
the chill zone were observed. This scatter is directly attribu-
ted to microsegregation in the ingot which is always present.
The sample size for counting (1 gram) was chosen to be sufficiently
large to minimize the effect of microsegregation and still enable
enough samples to be obtained from the casting to measure the
segregation. Scatter is still present in the measurements, the
amount varying for different castings depending on the casting
conditions. In all cases, the full set of samples for a given
casting were counted at least three times, and the results averaged.
In the observations, the multiple sets of data have been plotted
in several figures, to show the scatter between successive count-
ing sequences. This scatter is due to the stability of the count-
ing system and the statistical fluctuations of the activity of a
given sample, the loss of activity due to the decay between the
counting sequences having been corrected for. It can be seen that
there is much less scatter of repeat counts of a given sample,
than scatter between neighbouring samples due to microsegregation,
in most cases.

A horizontal line of best fit is drawn through the average
data of normalized activity as a function of distance from the

chill, and the extrapolation of the curve in the chill zone to the chill face is based on at least three points above the mean composition. It is considered that the present extrapolation is more reliable than that previously reported in the literature, based on more points being used, which fit a reasonably smooth curve, and rejection of the value of concentration of the material adjacent to the chill face.

4.2 Chill face segregation

The chill face segregation measured in the present investigation, based on the extrapolation of the segregation in the chill zone, is plotted in Figures 53 and 54, as well as the theoretical curve derived from the Scheil analysis. The points in Figure 53 are for ingots directionally cast in the preheated furnace as in casting procedure (a). The points in Figure 54 are for ingots directionally cast in the fibrefrax molds (procedure (b)). The type of chill used, the superheats, and the cast numbers are indicated in the curves.

Considering the experimental results plotted in Figures 53 and 54, it is evident that there is a very large scatter in the chill face segregation observed for both casting procedures used. In some of the castings, no inverse segregation was detected. This is particularly anomalous in the light of the excellent agreement between theory and experiment reported by Kirkaldy and Youdelis. This difference may be accounted for in part, by the
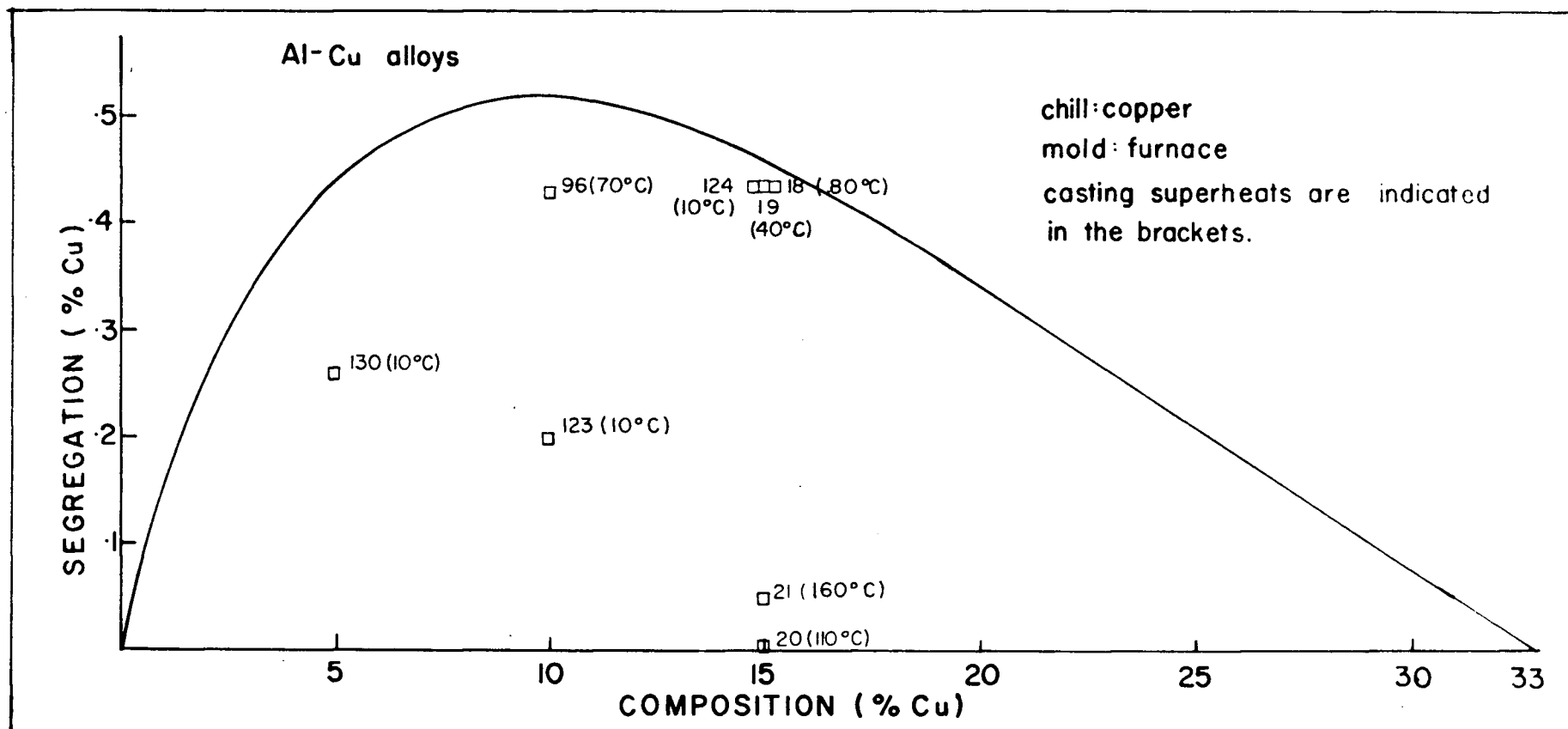
Fig. 53   Theoretical predictions and experimentally obtained chill face segregations.
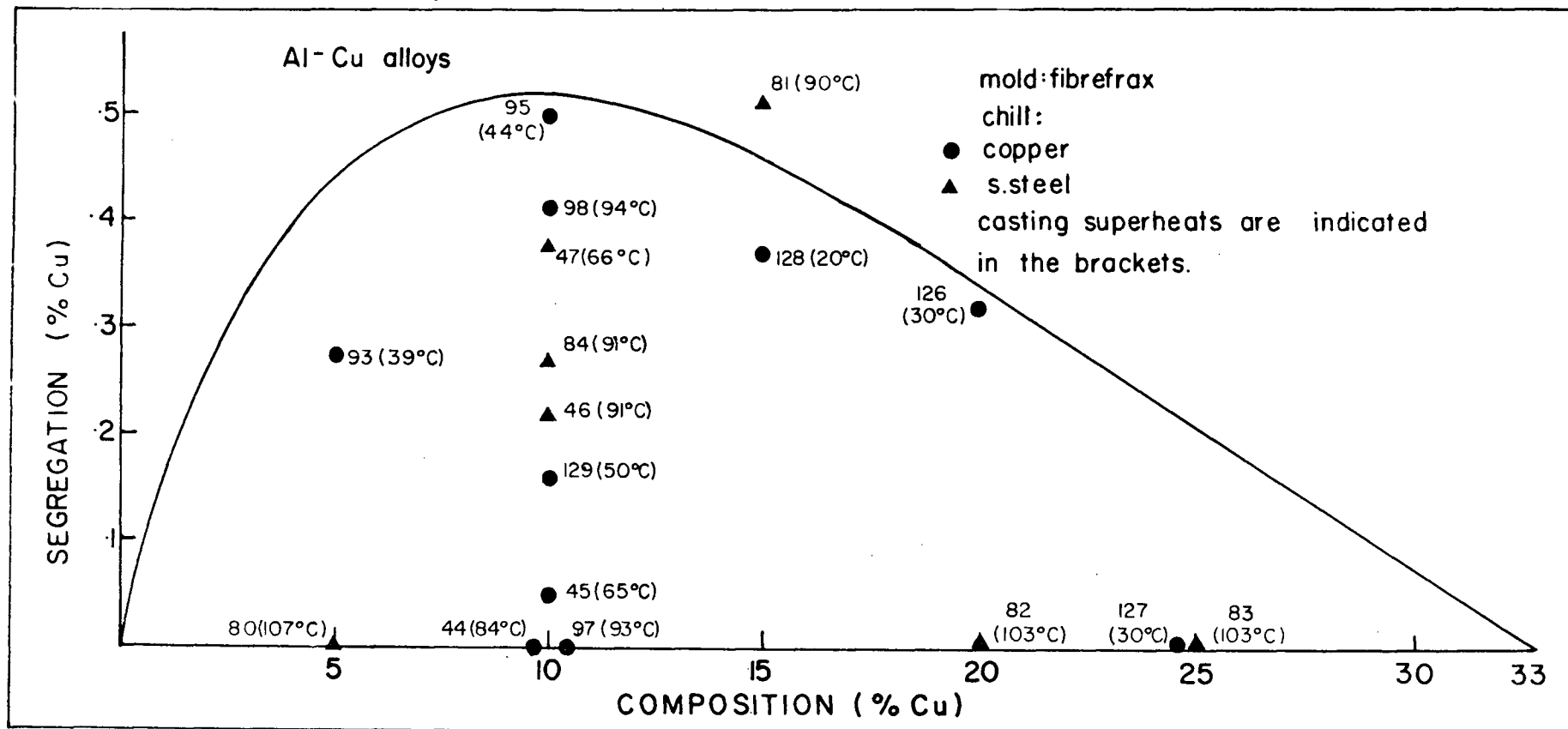
Fig. 54   Theoretical predictions and experimentally obtained chill face segregations.

difference in the casting superheats employed, and the chill used. It can be observed from Figure 54, that the chill face segregation is markedly dependent on both the casting temperature and the chill used. Decreasing the pouring temperature or reducing the thermal conductivity of the chill increases the chill face segregation. These observations are in accord with those described by Pell-Walpole[1], in which the extent of segregation observed in various alloys increases with a decrease in the rate of cooling. However, in discussing the inverse segregation in Al alloys reported by Woronoff, he notes that increasing the mold conductivity increases the amount of inverse segregation observed, which is clearly in conflict with the present results.

The superheat used by Kirkaldy and Youdelis for all their ingots was 40°C, and the chill material was polished steel coated with a thin layer of alundum paste. Accordingly, these conditions give results closest to the stainless steel chill and lower superheats of the present experiments, where the results tend to approach the theoretical predictions.

4.3 Effect of superheat and the thermal conductivity of the chill

To show the dependence of the segregation on the superheat more clearly, the results of Figure 53 and 54 have been replotted. The chill face segregation of three alloys Al-5% Cu, Al-10% Cu, and Al-15% Cu are shown in Figures 55, 56, and 57 respectively, as a function of the superheat. The chill face segregation
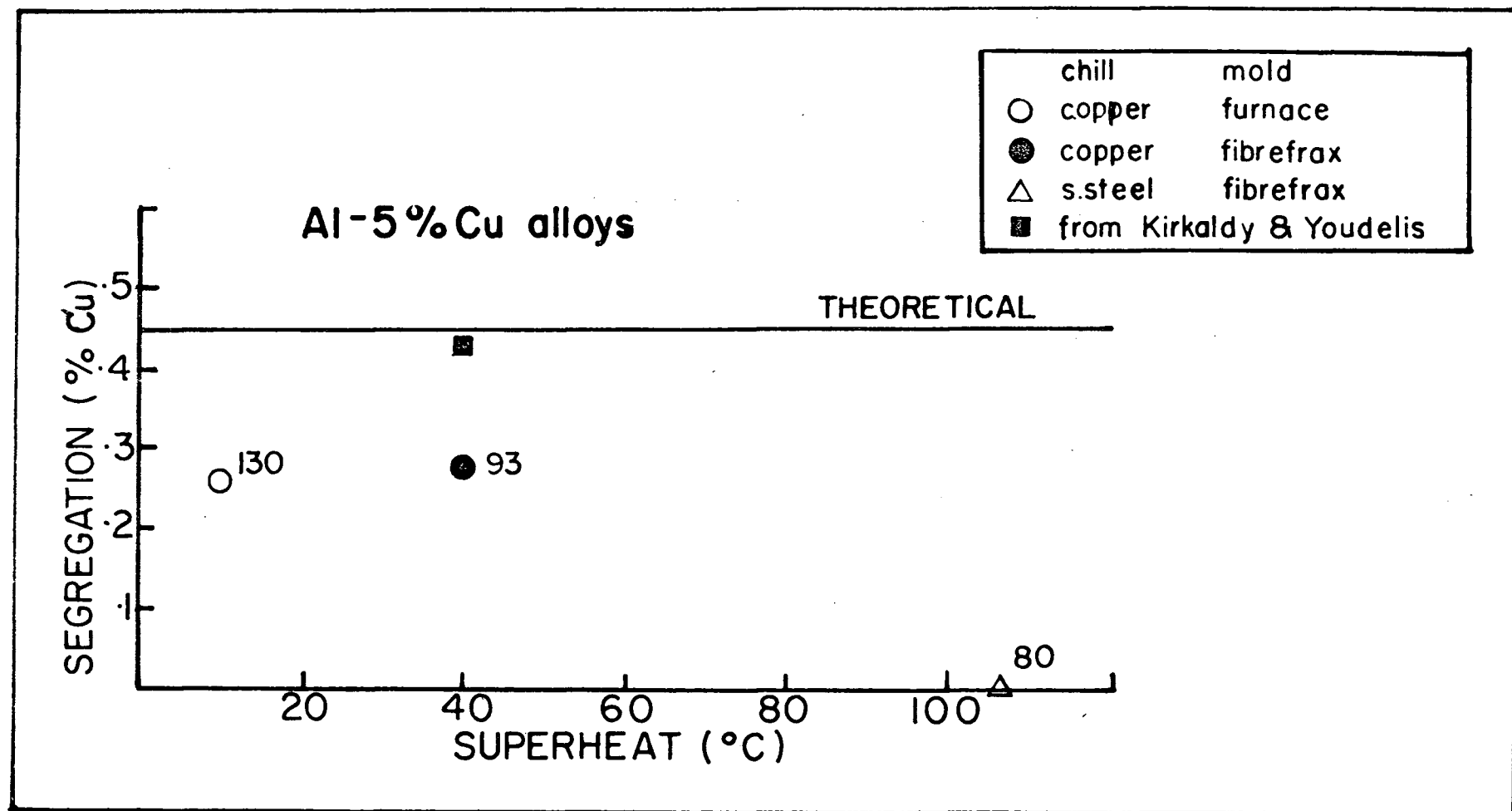
Fig. 55   Chill face segregation vs. superheat for Al-5% Cu ingots cast under the conditions indicated.

measured by Kirkaldy and Youdelis are also indicated in the
Figures, and the values of segregation as calculated from the
Scheil theory are shown as solid horizontal lines.

In Figure 55, only three points are shown corresponding to
the measurements of the present investigation. All of these
points are seen to lie below the expected value of the segrega-
tion, with no segregation being measured in the case of ingot 80.
It can be observed that lowering the melt superheat results in an
increase in the segregation measured.

In Figure 56, all the points lie below the theoretical
value. Consider the data from the ingots cast on the copper chill
in the fibrefrax molds (filled circles), ignoring the values ob-
tained from ingots 98 and 125. The chill face composition is
seen to decrease progressively with increasing superheat, with
the segregation reaching zero past a casting superheat of 80°C.
Ingot 125 shows a smaller segregation, possibly due to non-
directional solidification. In case of ingot 98, the water flow
to the chill block was markedly reduced, significantly changing
the casting conditions. This situation is anologous to reducing
the thermal conductivity of the chill. The chill face segregation
with the stainless steel chill also decreases with increasing
superheat, but is significantly higher than the segregations
obtained for the copper chill, for a given superheat. Ingot 96,
cast on the copper chill in the furnace arrangement, shows a high
chill face segregation, close to the theoretically expected value.
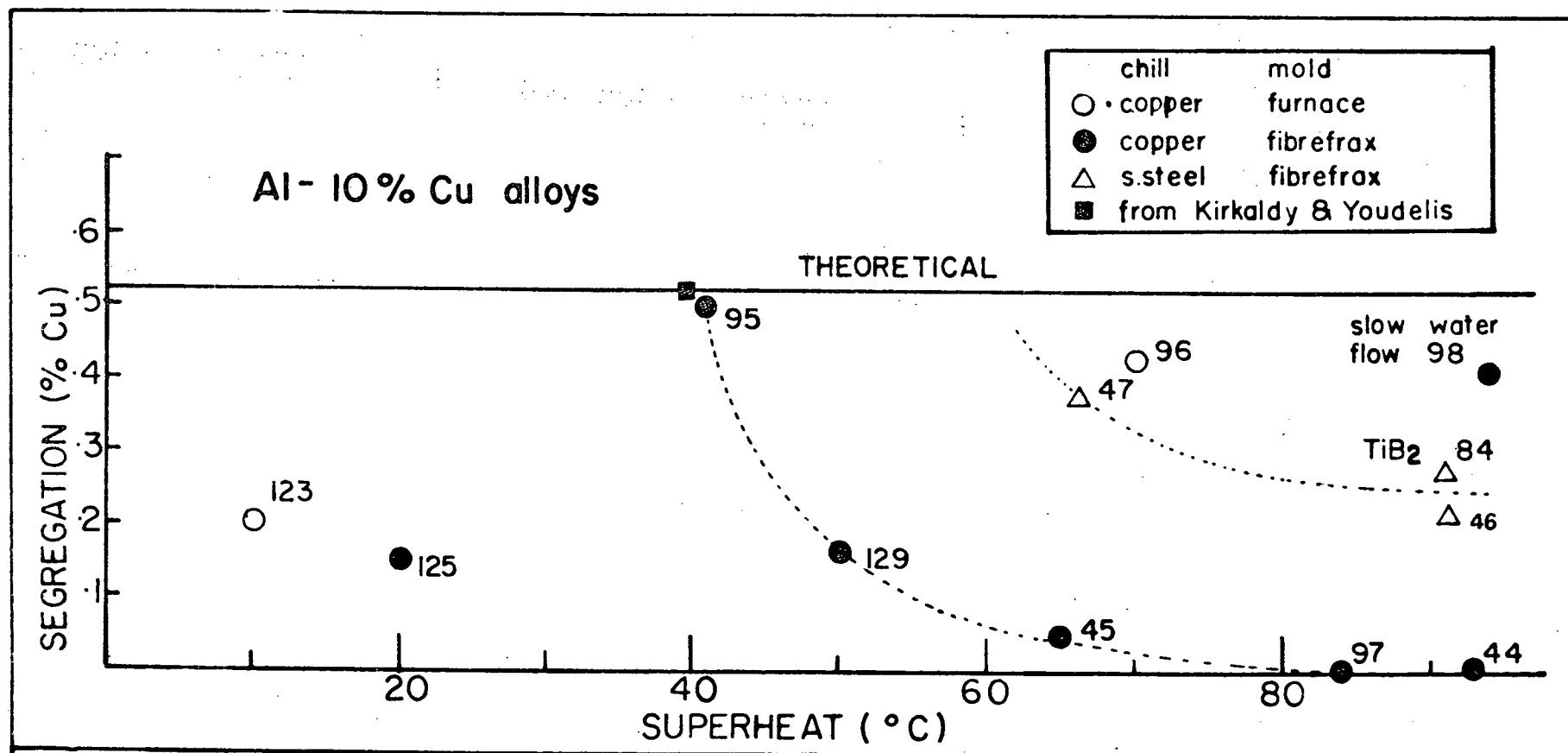
Fig. 56   Chill face segregation vs. superheat for Al-10% Cu ingots cast under the conditions indicated.

However, the ingot 123 cast at low superheat shows a much lower value of chill face segregation, though it would be expected that the slower rate of heat removal would lead to segregation higher than those obtained from casting, either on the copper chill or the stainless steel chill in the fibrefrax molds. This low value may be due to extensive nucleation in the bulk of the liquid resulting from the low casting superheat.

In Figure 57, the emphasis is on Al-15% Cu alloys cast in the furnace arrangement, using a copper chill. Here it is seen that lowering the superheat causes an increase in the amount of the chill face segregation. Changing the size of the ingot cast (using a smaller melt size for ingot 21) does not significantly affect the chill face segregation obtained. This demonstrates that the amount of segregation only depends on the freezing conditions in the first parts of the ingot to solidify. Ingot 81, cast in the fibrefrax mold with a stainless steel chill shows a very large chill face concentration, much larger than the theoretically expected maximum, even though the superheat is high. The reason for this is not known. Ingot 128, which had a fine grained structure due to the addition of a grain refiner, shows a chill face segregation close to the theoretically expected value. The presence of inverse segregation in ingots possessing an equiaxed grain structure is in accord with the findings reported by Adams[11].
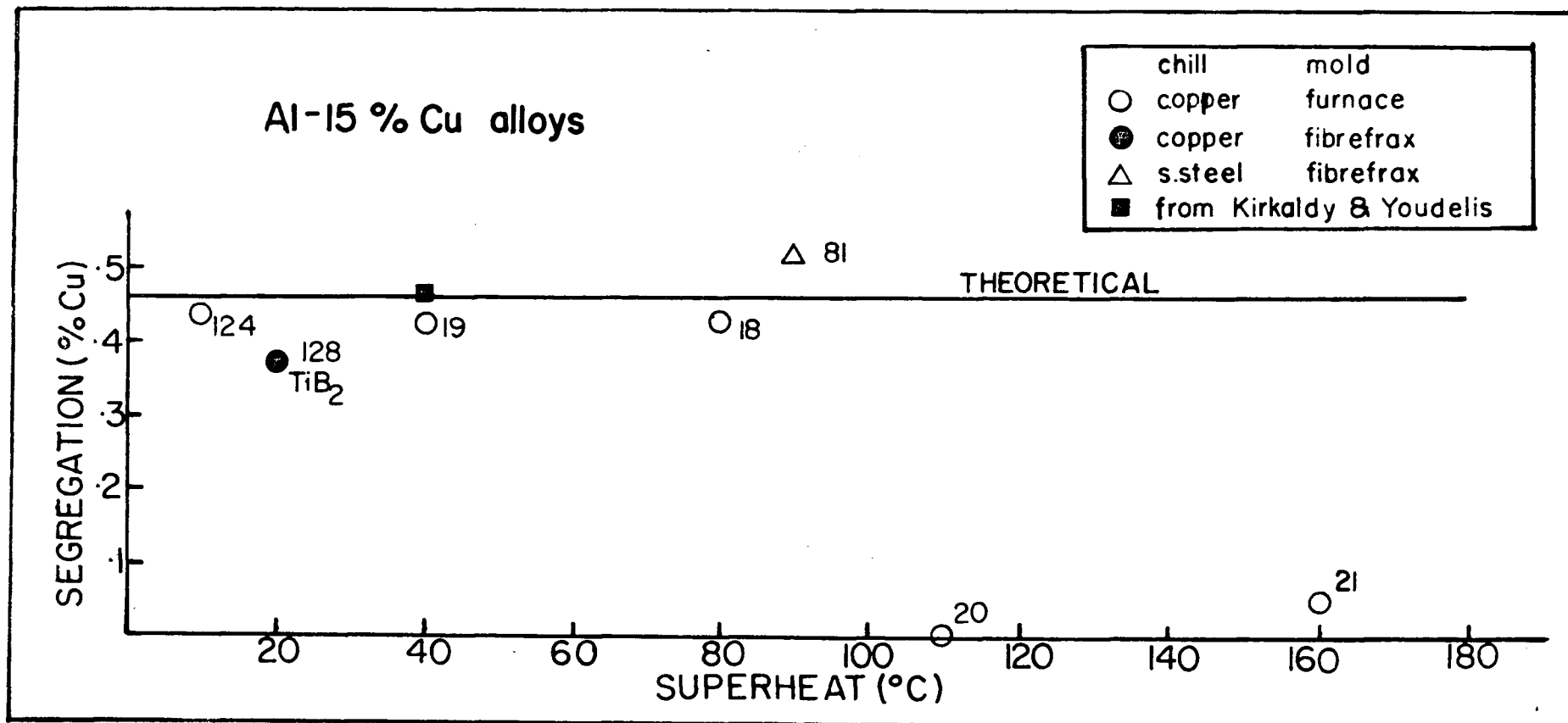
Fig. 57 Chill face segregation vs superheat for Al-15% Cu ingots cast under the conditions indicated.

4.4 Exudations on the chill face

It was generally found that the chill faces of ingots cast in the present work were free of massive exudations or sweat beads, the faces appearing smooth. Kirkaldy and Youdelis reported that exudations were generally observed on chill faces of their ingots. A section of one of their ingots, perpendicular to the chill face, showing exudations, is reproduced in Figure 58. The structure of the chill face of ingot 85 of this investigation, in which exudations were produced by moving the ingot away from the chill face, is shown in Figure 59. The position of the chill face of the ingot in this Figure, before separation of the ingot from the chill, is marked x----x. The thickness of the exudation was large, due to the imposed large separation; only the part immediately below the chill face is shown in the Figure. At the initial chill face, some remelting of the primary dendrites has occurred, and long interdendritic channels can be observed.

For a normal casting, a section through the middle of the ingot, perpendicular to the chill face is shown in Figure 60, the chill face being marked Y----Y. No evidence of remelting or exudations is observed and the interface is flat. In the temperature measurements, no evidence of reheating was detected, indicating no separation between the ingot and the chill face. Since there was no indication of exudations, the corrections applied by Kirkaldy and Youdelis to their data, which are uncertain, were

115.
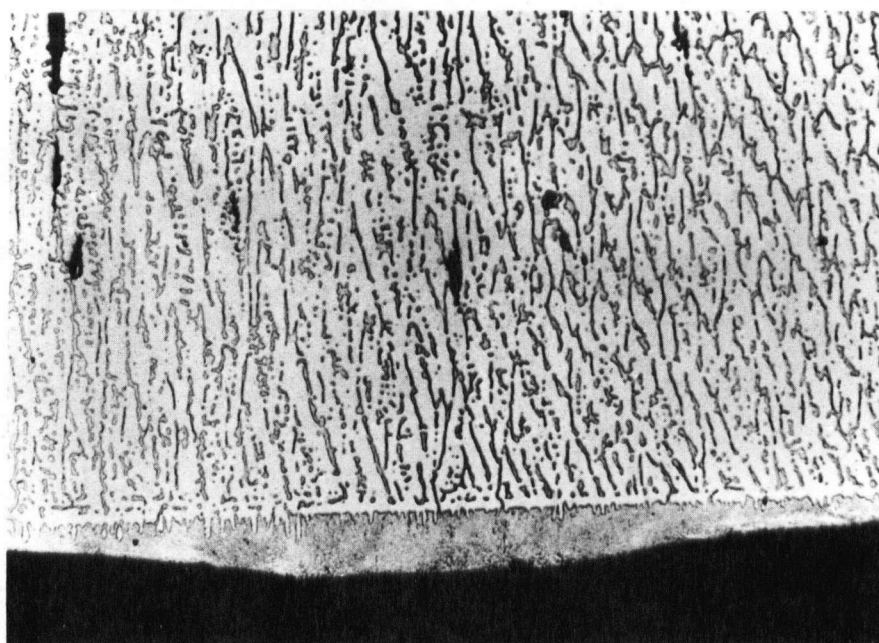
Fig. 58   Microstructure of the base of an Al-10% Cu alloy ingot showing exudations (after Youdelis[6]).
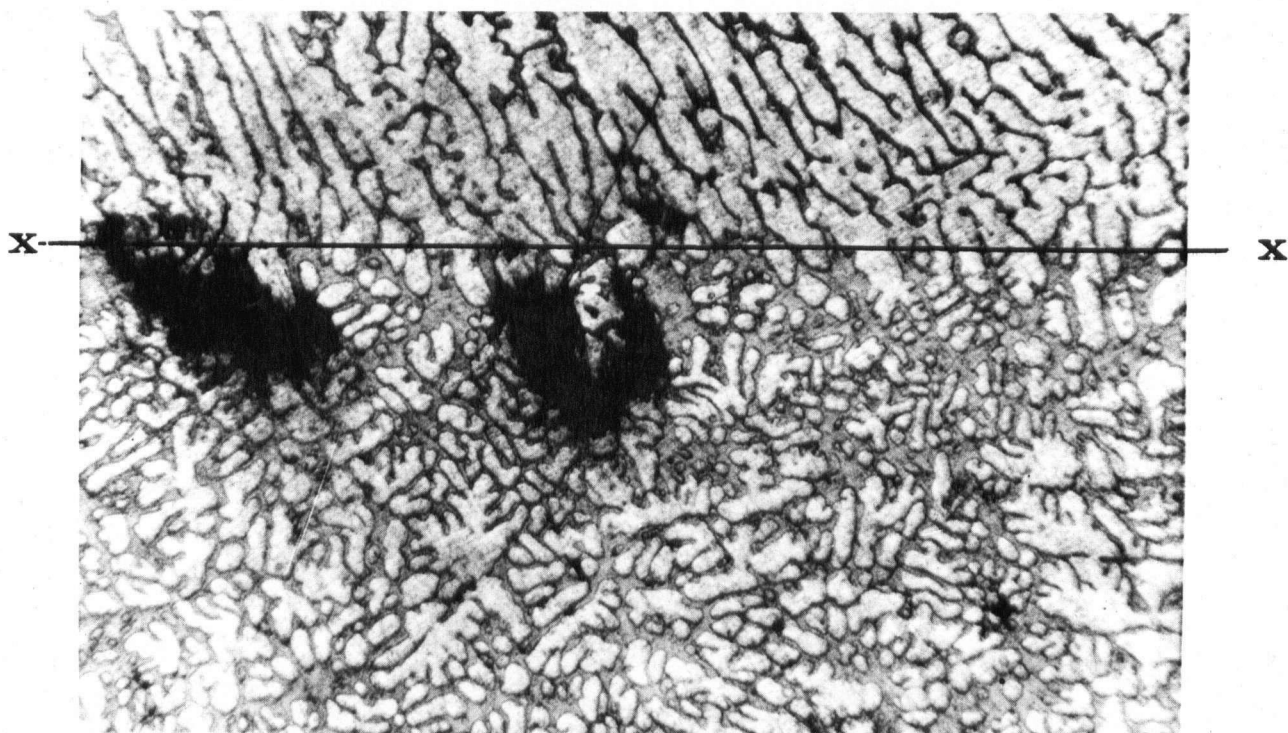
Fig. 59   Microstructure of the base of an Al-10% Cu ingot perpendicular to the chill face from the present investigation, in which exudations were induced.   100X
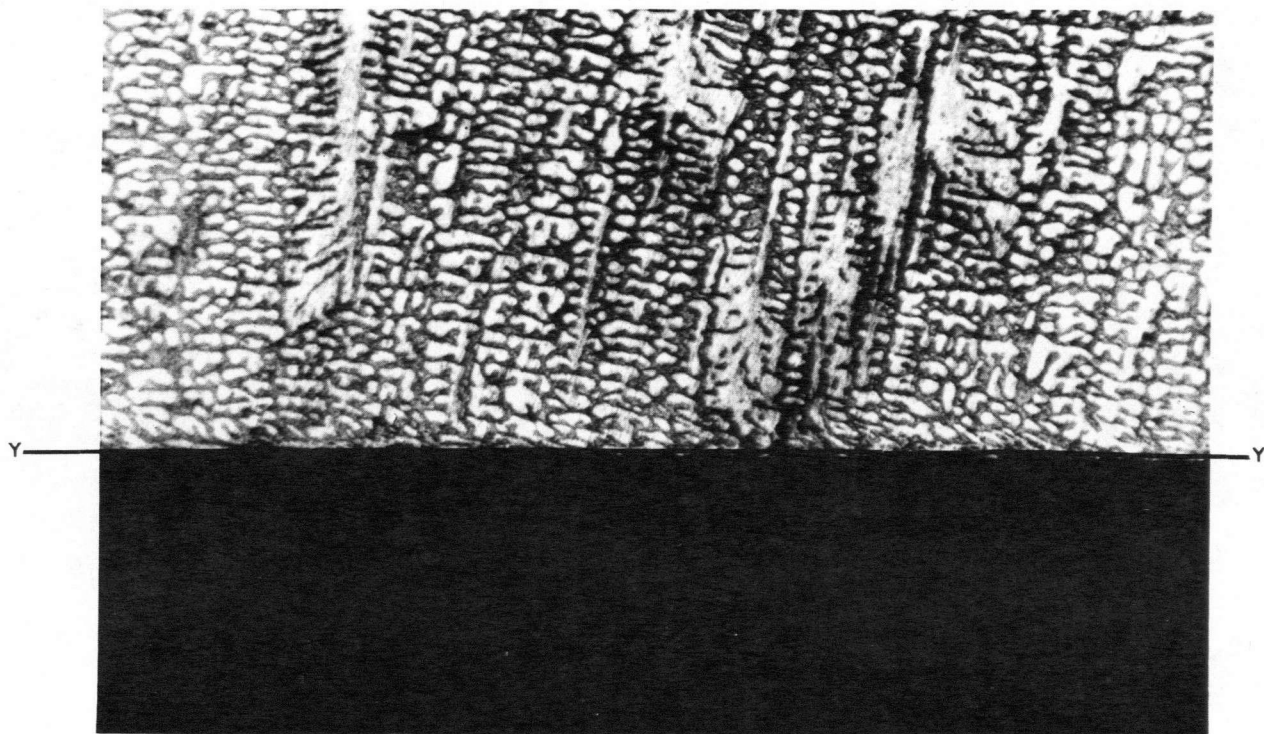
Fig. 60   Microstructure of the base of an Al-10% Cu ingot, perpendicular to the chill face, cast normally, showing absence of exudations.   100X

not applied. No such corrections have been mentioned in the determinations of the chill face compositions carried out by earlier workers (except Adams), who determined the extent of inverse segregation in various alloy systems. In view of the fact that many of them did observe sweat beads on the chill face of the ingots they examined, it is possible that their results are in error. The chill face segregation they measured could be a combination of the actual segregation and the exuded eutectic. The theory of the mechanism of inverse segregation assumes that no exudations are present.

4.5 General mechanism for inverse segregation

As described previously, lowering the melt superheat causes the following effects:

a) increase of the chill face composition

b) increase of the extent of segregation into the ingot away from the chill face (increase of the chill zone L_c)

c) increase of the solid-liquid zone length L_M.

d) increase of the dendrite arm spacing

The effects b), c), and d) are all interrelated and affect the magnitude of a). Since inverse segregation is due to inter-dendritic feeding to compensate for solidification shrinkage and specific volume changes with temperature, the feeding must take place in the solid-liquid zone, and the segregation near the chill face will depend on the length L_M. The length of the chill zone L_c will also be greater with larger L_M.

The results of the present work generally indicate that there is no increase in the solute concentration past L_c, contrary to the theoretical and experimental results reported by Adams, and Kirkaldy and Youdelis. It is possible that in the present investigation, there is an overall small increase in the solute concentration over the bulk of the casting, smaller than the scatter limits of the data. The concentration increase reported by Kirkaldy and Youdelis beyond L_M is very small, and may not be evident in the present results.

Flemings et al. have predicted that for parallel liquidus and eutectic isotherms, moving at a constant rate in a direction perpendicular to the chill face, the composition in the region of the ingot at a distance greater than L_M from the chill, is equal to the mean composition of the ingot. In the Flemings et al. analysis, it was assumed that L_c, the chill zone length, equals L_M, the mushy zone length. In the present results, it was found that L_c does not equal L_M, L_c being smaller for all the cases examined. The values of L_c for the ingots examined are listed in Tables I, II, and III, and plotted in Figure 61 as a function of superheat for the Al-10% Cu alloys. In Figure 61, it is evident that L_c decreases rapidly with increasing superheat, and for a given superheat, L_c is larger for the stainless steel chill than for the copper chill. The dotted lines in the Figure have been included to show the trend of the data and should not be considered as representative of the functional dependence of L_c
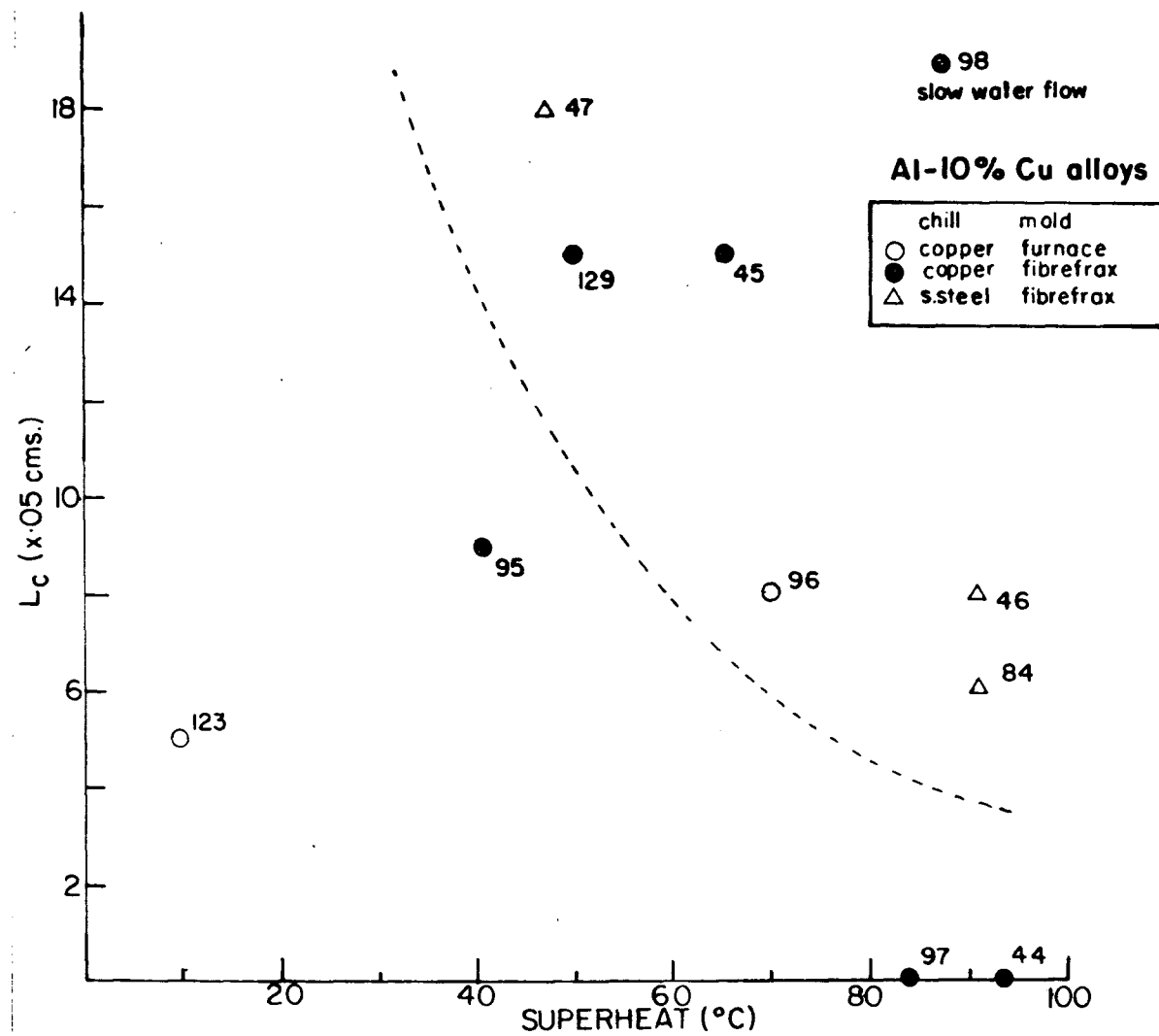
Fig. 61 L_c vs. superheat for Al-10% Cu alloys for the casting conditions indicated.

on superheat. Comparing the values of L_c in Figure 61 with the values of L_M (Figure 47), at a given superheat, it is noted that L_c is smaller than L_M.

The difference between L_c and L_M can be attributed to incomplete back feeding of liquid through the interdendritic channels, characterized by a "Tortuity Factor". If the flow of liquid down the channels is restricted during solidification, small voids should be produced due to inadequate feeding of liquid. Voids, in the form of microporosity were observed interdendritically in the castings examined, as described previously. The presence of voids would not affect the values of the normalized activities obtained after sectioning the ingot. This is because the voids were quite small, and, as compared with the bulk of cuttings taken for the analysis, the total volume of the pores is negligible. The presence of voids is only significant when density measurements are used to determine the variations in composition of the ingot.

The extent of interdendritic flow associated with inverse segregation will be related to the size and distributions of the liquid channels present. This, in turn, is related to the dendrite arm spacing, and therefore, to the superheat on casting. At higher superheats, the dendrite spacing in the chill zone is small, and the liquid channels are therefore small leading to retardation of backflow and low chill face concentrations. Lowering the superheat increases the relative channel size and therefore results in

high chill face concentrations.

Stainless steel chills produce higher solute concentrations at the chill face than copper chills for similar conditions of casting. The present results show a small decrease in L_M for stainless steel, compared to copper, and an increase in both the L_c and the dendrite arm spacing. The increased dendrite arm spacing results in backflow occurring more readily with the stainless steel chill, in agreement with the larger L_c obtained. The increased backflow would result in an increase in the concentration at the chill face, as observed.

In the ingots cast at very low superheats, little chill face segregation was observed, contrary to the general trend of increasing segregation with decreasing superheat. This is attributed to a change in the manner of solidification. Under normal casting conditions, progressive solidification occurs away from the chill face. At very low superheats, it is likely that extensive nucleation occurs well ahead of the general solidification front. Under these conditions, backflow of enriched liquid would be markedly reduced, giving low chill face segregation.

4.6 Effect of the cast structure on segregation

Fricke[18] has reported, on the basis of decanting experiments on Al-Cu alloy castings, that inverse segregation results from a columnar to equiaxed transition during solidification. This

conclusion has been refuted by Edwards and Spittle[19] on the basis of inverse segregation detected in small, fully columnar ingots produced by electroslag melting. The present results show that inverse segregation is obtained in a columnar structure, in agreement with Edwards and Spittle, and previously reported results. It is still possible that inverse segregation may occur when the structure transition occurs. To test this hypothesis, in one test (97), the columnar structure was changed to equiaxed during solidification by adding Foseco degassing compound when the interface was 2.5 cm. from the chill. It was found that changing the structure had no effect on the distribution of copper along the ingot, i.e., the distribution was the same as that observed in a fully columnar casting (44).

Castings with a fine equiaxed grain structure were made using TiB$_2$ grain refiners. The segregation obtained in this case (84) is very similar to casting (46) produced under similar conditions. In the case of the fine grained ingots, inverse segregation occurs by liquid feeding through the channels between partially solidified grains. Solidification of the fine grained material is considered to occur progressively, roughly similar to columnar growth, with nuclei forming just ahead of the advancing interface.

4.7 Effect of the gas content of the melt

One of the ingots (95) was degassed with the use of
Foseco degaser. The chill face composition for this ingot showed
very good agreement with the predicted value from Scheil's
theory. It is possible that the presence of small amounts of
gas at the last stages of solidification would block or hinder
the passage of liquid through the interdendritic channels. This
would cause a lower value of chill face composition than would
be expected if flow were not hindered. This was not the case in
the test on ingot 95.

Pell-Walpole reports instances in which the extent of
segregation has been increased by the presence of large volumes
of gas in the melt, the gas being released in the last regions of
the casting to solidify. However, the presence of gas in the melt
had always led to ingots with exudations, and without correcting
for the exudations in the value of the chill face segregations
determined, these conclusions could be in error.

Roth[17] has cast Al-Cu ingots with large gas content in some
ingots, and found that the amount of segregation at the chill
face and the extent of the chill zone was reduced by the presence
of gas. In view of this, the effect of the presence of gas in
the ingot on the final segregation pattern is unclear.

4.8 Comparison of theories

The theory proposed by Flemings et al. is not equivalent to the Scheil theory as claimed, primarily due to the assumption of constant values for the segregation coefficient and specific volumes of solid and liquid. Their demonstration of equivalence was only for a small region of composition variation, and they selected appropriate constant values for that region to give good fit. To treat the quantities mentioned above as variables, makes solutions of the equations derived by Flemings et al. difficult.

The excellent agreement between theory and experiment reported by Kirkaldy and Youdelis was not obtained in the present results. Their good agreement may be partly due to their low casting superheat which results in high chill face concentrations. However, they apply a correction for the exudations observed in their castings, and this may lead to erroneous results. They also give no indication of the scatter associated with repeat observations or scatter resulting from small changes in the casting variables.

4.9 Turbulence during casting

In the present investigation, the casting of the ingot was a dynamic process, in which the molten metal was poured onto a cold chill as in casting procedure (b). The prediction of the theories, however, hold for the condition that the melt is quiescent

when the freezing of the ingot is initiated. Thus an additional variable is introduced into the process, which cannot be explicitly defined.

Roth[17]has reported that stirring the melt vigorously ahead of the advancing solid-liquid interface causes a reduction in the segregation. In the present investigation, the liquid was poured smoothly and quickly into the mold against the chill in the same manner for all the castings produced, using fibrefrax molds. The turbulence on pouring was likely small and died away quickly. For the furnace cooled castings, the melt was quiescent before solidification was initiated. It is considered that the effect of turbulence in the present investigation on the observed segregation is small and can be neglected.

It is thus seen that, fundamentally, Scheil's theory appears satisfactory for determining the chill face segregation, but only under a relatively narrow range of solidification conditions. Changing the solidification variables affects the magnitude of the segregation detected, and in order to be more general, the theory will have to incorporate the effect of these variables.

5. SUMMARY AND CONCLUSIONS

(1) Inverse segregation results from interdendritic backflow of enriched liquid towards the chill face of the ingot.

(2) The segregation is markedly dependent on casting variables such as casting superheat, gas content in the ingot, temperature gradients in the ingot during solidification, the thermal conductivity of the chill and the cast structure.

(3) The chill face segregation increases with decreasing superheat. At very low values of superheat the segregation process changes to give a reduced segregation at the chill face.

(4) Decreasing the thermal conductivity of the chill in the range of superheat from $100^{\circ}C$ to $30^{\circ}C$ increases the segregation at the chill face.

(5) Reducing the gas content of the ingot enhances the chill face segregation in the ingot.

(6) Inverse segregation is present in completely equiaxed ingots that are cast unidirectionally.

(7) The theory of macrosegregation as put forward by Flemings et al., does not become equal to the Scheil solutions for the

Al-Cu system, except for a narrow range of compositions, eve-
though the authors claim equivalence. This is because of the
simplifying assumptions used to reduce the complex mathematical
expressions to yield analytical solutions.

(8) The magnitude of the chill face segregation has been found
to differ from the values reported in the literature and the
quantitative predictions of the theory of inverse segregation.

(9) No significant inverse segregation was observed in ingots
of Al-Ag cast unidirectionally.

6. SUGGESTIONS FOR FUTURE WORK

Using the same radioisotope techniques, the segregation for unidirectionally cast ingots cast at low superheats can be investigated. The effect of the mold and chill conductivity can be studied in further detail, in order to reduce the amount of the chill face segregation, as well as to provide means of reducing the amount of exudations on the chill face.

The variation of the composition throughout the length of the ingot perpendicular to the chill face can also be studied, and the results compared to the theoretically predicted composition distributions, under different cooling conditions. Numerical integration of the theoretical equations will have to be carried out.

The effect of radial temperature gradients on the segregation can also be investigated.

APPENDIX A

A.1 Statistical consideration of radioactivity measurements

The activity emanated by radioactive materials exhibits random fluctuations in intensity due to the particulate, random nature of the emission. In addition, the intensity decays exponentially, the rate defined by the half life of the isotope. As a result, probability laws are applied in analyzing the counting measurements to assess accidental or "indeterminate" errors. The systematic or "determinate" errors are minimized by applying known correction or calibration procedures to the data, and by careful planning of the experiments.

The basic frequency distribution governing random events such as radioactive decay is the binomial distribution, from which the simpler and more familiar Poisson and Gaussian (or Normal) distributions are derived. Since the Gaussian distribution has been found to be relatively easy to handle mathematically, it is used frequently, and is almost as accurate as the Poisson distribution over a wide range. The Poisson and Normal distributions are represented mathematically as

$$P_n = \frac{\mu^n e^{-\mu}}{n!}$$

and

$$G_n = \frac{1}{\sqrt{2\pi\mu}}\, e^{-(\frac{n-\mu}{2\mu})^2}$$
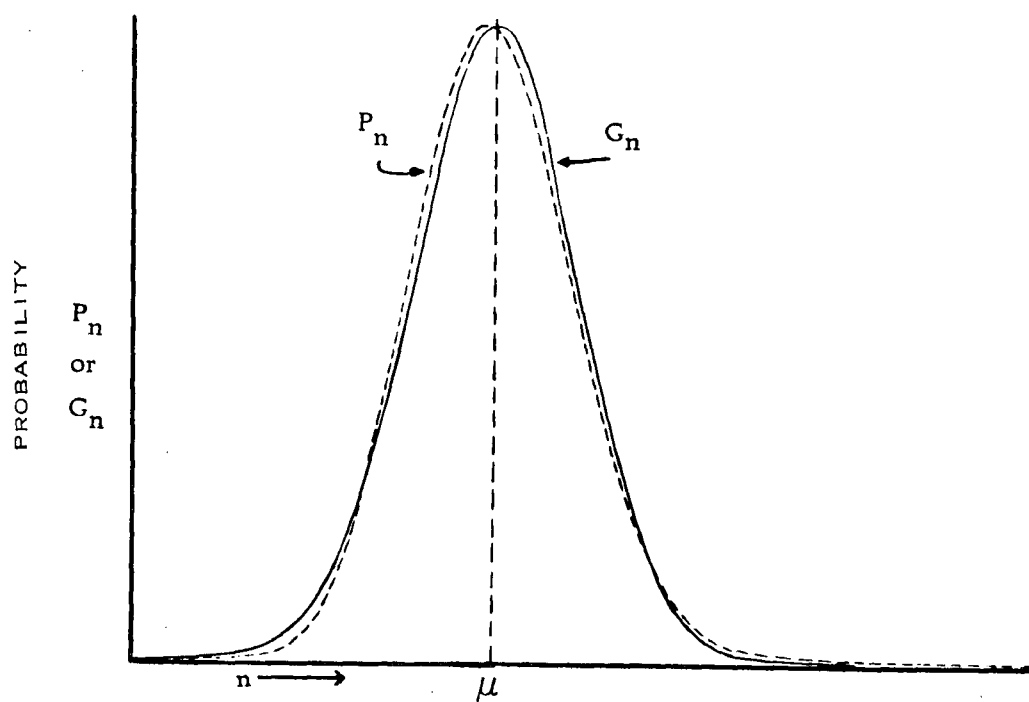
Fig. 62   Comparison of the Poisson and Gaussian distributions.
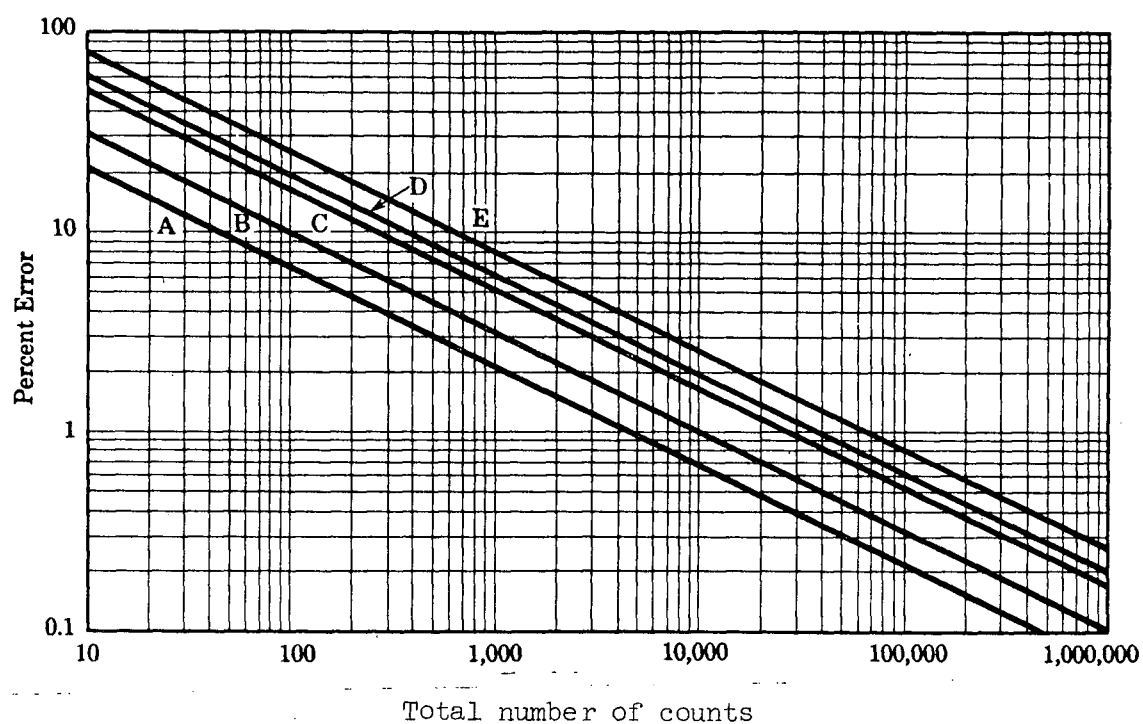

Fig. 63   The error of counting determinations.
        A. Probable error   B. Standard deviation   C. Nine tenths error
        D. Ninety-five hundredths error   E. Ninety-nine hundredths error

respectively, where μ is the actual or true mean of the quantity being measured and where n is the value of any one observation. The difference between the Poisson and the Gaussian distributions is shown in Figure 62.

To test for non-statistical behaviour of the counter, 350 measurements of activity of a sample containing Sn^{113}, (which is a long lived isotope, with a half life of 118 days) were made. The activity of the sample used in this test was comparable to the activities of the samples containing Cu^{64}, so as to provide a test under conditions to those used in the measurements of the variation of the activity along the ingot length for the Al-Cu ingots.

The results of the experiment showed no significant difference from the expected normal distribution. The activity measurements were processed for the "Goodness of Fit" tests with the help of the "Freq" library program at the U.B.C. Computing Centre.

A.1.1 Confidence limits and errors

The confidence of data may be represented in many ways, the most common being those listed below:[20]

(a) The one sigma level is defined by the standard deviation, and there is a 31.73% chance that this level will be exceeded.

(b) The nine tenths error is so named because there are nine chances out of ten that the error in a specific determination will be

less than this value.

(c) The ninety-nine hundredths error signifies a confidence
that errors of 99% of the determinations will be less than
this value. This degree of confidence is highly significant.

Errors used to define confidence levels are listed in
Table V.

A.1.2 Errors in the counting rate determinations

From Figure 63[21], it is seen that in the region where counting
was performed on the ingot samples (about 250,000 counts), the error
in the counting rate is seen to be less than 1% of the total number
of counts. Thus, it was concluded that the activity measurements
made are of high accuracy.

The background counting rate, due to naturally occurring
radioactive materials present in and around the counter, as well
as due to cosmic rays, is an additional source of error encountered.

It has been assumed that there was no loss of the average
activity during the actual counting operation on each sample. To
minimize the error arising from this assumption, the counting times
were chosen to be small.

For a counting time of Δt, and half life $t_{\frac{1}{2}}$, the correction for
such an error would be 0.34% of the total for $\Delta t / t_{\frac{1}{2}}$ = 1%, and 0.69%
for $\Delta t / t_{\frac{1}{2}}$ = 2%.[22]

TABLE V

Errors used to define confidence intervals[20]

p = probability of observing error larger than

$\tau\sqrt{\mu}$ where μ = mean value

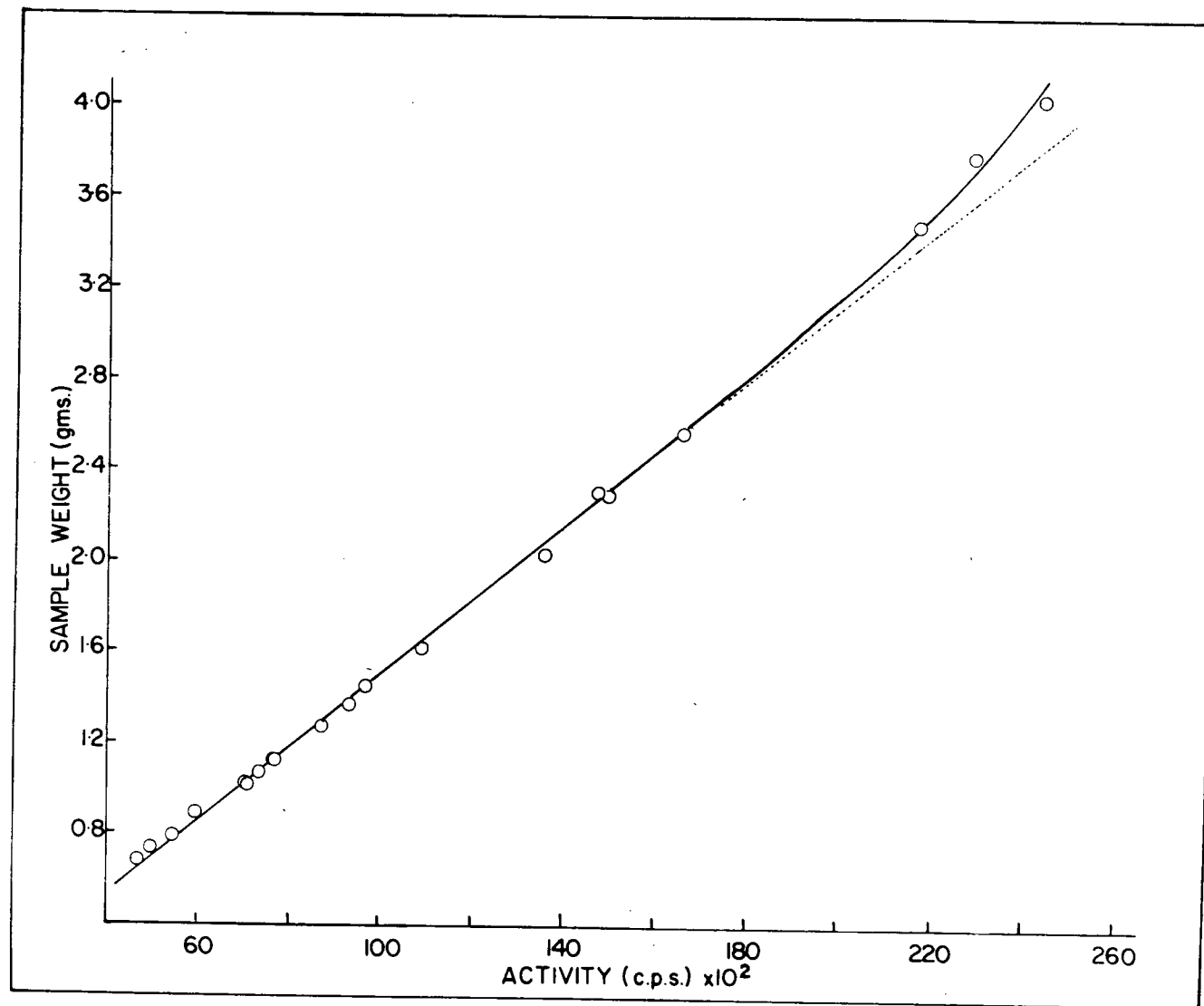| Name of error	τ	p
Probable	0.6745	0.5000
Standard deviation	1.0000	0.3173
Nine tenths	1.6449	0.1000
Ninety-five hundredths	1.9600	0.0500
Two sigma	2.0000	0.0455
Ninety-nine hundredths	2.5758	0.0100
Three sigma	3.0000	0.0027

Fig. 64   Activity vs. weight of the Al-Cu sample containing Cu^{64}.

It was attempted to present samples of similar geometry to the counter, as changes in the geometry of the sample will affect the measurements.

Samples of different weights, cut from chill cast buttons prepared from a well stirred melt with Cu^{64} tracer dissolved in it, were used to check on the combined effect of geometry and absorption of radiation in the specimen. Chill casting small buttons served to reduce segregation effects in the samples. The variation of the activity obtained with respect to weight of the sample is shown in Figure 64.

Aluminium is a weak absorber for gamma rays. It has an absorption coefficient of .08 cm^{-1} for 0.5 MeV gamma rays as compared to 1.127 cm^{-1} for lead. As such, no appreciable loss of activity due to absorption in the aluminium is expected. In case of larger sample sizes, i.e., larger volumes, the absorption effect may play a larger part.

For larger sample weights, it is observed from Figure 64 that the variation of activity with weight changes from the linear relationship found with lower sample sizes. In the region of around 1 gram,(most samples counted were in this region), the variation is linear, and the normalization of the activity with respect to weight in this region is justified.

REFERENCES

1. Pell-Walpole, W.T., and Hanson, D., Chill Cast Tin Bronzes, Edward Arnold and Co., London, 1951, p. 211.

2. Vosskuhler, von H., Z. Metallkunde, 1965, 56, 719.

3. Flemings, M.C., and Nereo, G.E., Trans. Met. Soc. AIME, 1967, 239, 1449.

4. Flemings, M.C., Mehrabian, R., and Nereo, G.E., Trans. Met. Soc. AIME , 1968, 242, 41.

5. Flemings, M.C., and Nereo, G.E., Trans. Met. Soc. AIME, 1968, 242, 50.

6. Youdelis, W.V., Ph.D. Thesis, McGill University, 1958.

7. Scheil, E., Metallforschung, 1942, 20, 69.

8. Kirkaldy, J.S., and Youdelis, W.V., Trans. Met. Soc. AIME, 1958, 58, 212.

9. Youdelis, W.V., The Solidification of Metals (Brighton Conference), The Iron and Steel Institute, London, p. 112.

10. Sauerwald, F., Metallwirtschaft, 1943, 22, 543.

11. Adams, D.E., Journal, Institute of Metals, 1948, 75, 809.

12. Youdelis, W.V., and Colton, D.R., Trans. Met. Soc. AIME, 1960, 218, 628.

13. Ball, L.S., and Youdelis, W.V., Journal, Institute of Metals, 1971, 99, 29.

14. Kaempffer, F.L., M.A.Sc. Thesis, University of British Columbia, 1970.

15. Szekeley, J., and Themelis, N.J., Rate Phenomena in Process Metallurgy, Wiley Interscience, 1971, p. 307.

16. Brody, H.D., and Flemings, M.C., Trans. Met. Soc. AIME, 1966, 236, 615.

17. Roth, von W., Z. Metallkunde, 1965, 56, 713.

18. Fricke, W.G., Trans. Met. Soc. AIME, 1969, 245, 1126.

19. Edwards, K.P., and Spittle, J.A., Metallurgical Transactions, 1972, 3, 1004.

20. Chase, G.D., and Rabinowitz, J.L., Principles of Radioisotope Methodology, Burgess Publishing Co., 1963.

21. Kohl, J., Zentner, R.D., and Lukens, H.R., Radioisotope Applications Engineering, Van Nostrand and Co., 1961

22. Leymonie, C., Radioactive Tracers in Physical Metallurgy, Chapman and Hall, London, 1963.

23. Mehrabian, R., Keane, M.A., and Flemings, M.C., Metallurgical Transactions, 1970, 1, 3238.